

April 1, 2011

Shell Deer Park Refining LP  
Deer Park Refinery  
East Property Flare  
Test Report



# Shell Deer Park Refining LP Deer Park Refinery East Property Flare Performance Test Report

by

Shell Global Solutions (US) Inc.

## Executive Summary

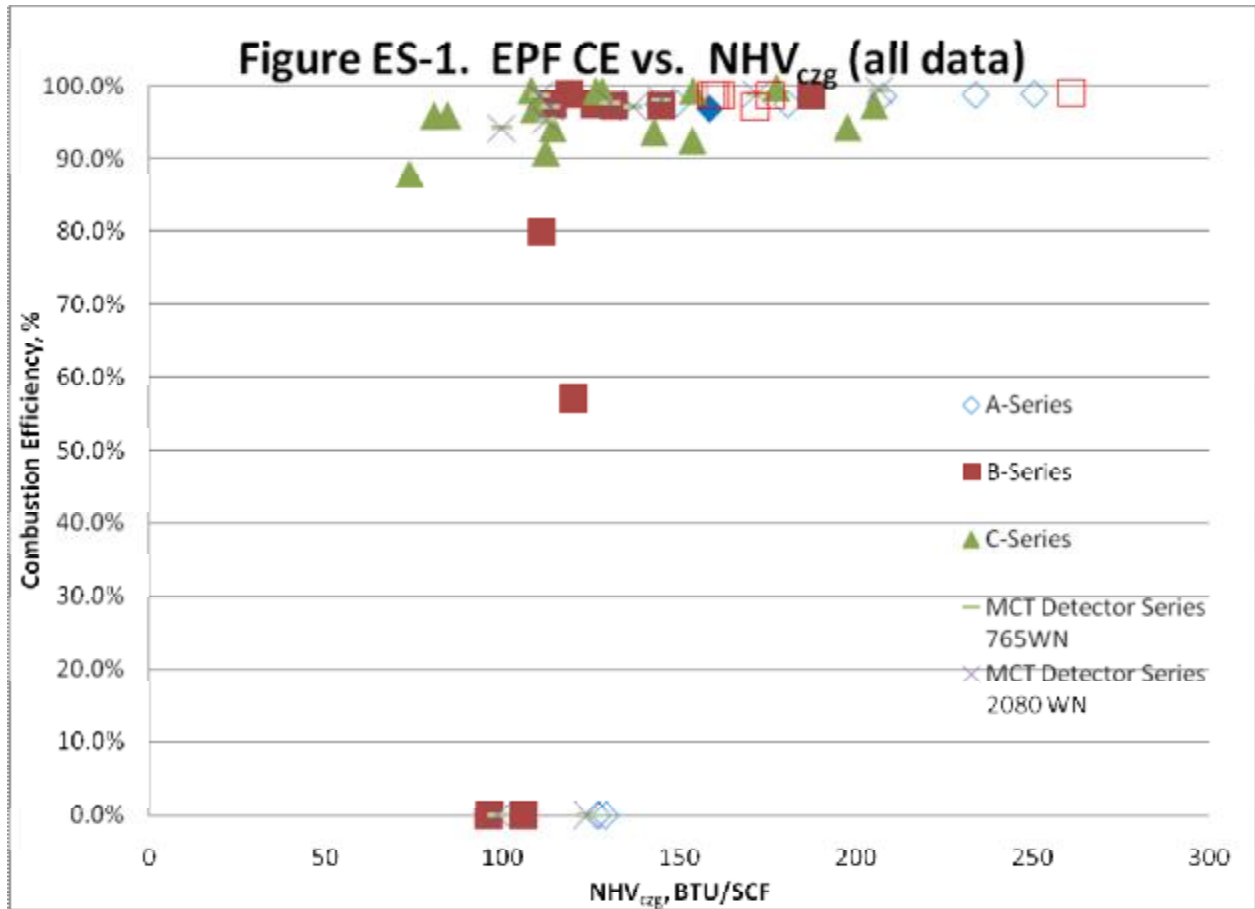
Shell Deer Park Site (SDP) received a letter, dated March 19, 2010, from the United States Environmental Protection Agency (EPA) requesting SDP to conduct a series of tests on the East Property Flare (EPF) and report the results. This report provides the EPF test results. The primary objective of the EPF testing was to obtain a better understanding of how the ratio of steam to vent gas (S/VG) at the flare combustion zone and the hydrogen content of the vent gas affect the combustion efficiency (CE).

The EPF, like many refinery flares, is a steam-assisted flare equipped with a steam injection system to inject high-pressure steam at the flare tip to aid combustion and reduce smoke formation. Steam injection reduces smoke formation by adding additional momentum to the low-pressure vent gas stream, educting additional air into the combustion zone, and participating in the combustion process. Too much steam can decrease CE. Accordingly, the Section 114 Request testing was intended to determine how the S/VG ratio and vent gas composition affect the CE achieved at the EPF.

To determine how the S/VG ratio and vent gas composition affect CE, the CE achieved during testing can be calculated from the composition of the flare plume. EPA directed SDP to utilize a Passive Fourier Transform Infrared (PFTIR) instrument to determine the composition of the flare gas plume. The PFTIR instrument analyzes the infrared signal from the hot gas plume from the flare. The infrared spectra emitted by individual gas species can be analyzed to identify the concentrations of the various gas species in the gas plume. The ratio of hot flare gas carbon dioxide to total flare gas carbon constituents was used to calculate CE.

SDP tested the EPF on several days in March and April, 2010. The data gathered during the testing provided useful insight into the factors that affect CE achieved by the EPF. The composition of the vent gas during this period was consistent with normal operation of the EPF, with the vent gas major constituents being hydrogen, nitrogen, and methane, with minor contributions from other low-molecular weight paraffinic, olefinic, and aromatic hydrocarbons.

The EPF exhibited high combustion efficiencies over a wide range of S/VG ratios. The EPF attained combustion efficiencies in excess of 98.0% up to S/VG ratios approaching 6 lb steam/lb vent gas. However, due to the large variation in vent gas composition observed at the EPF, poor combustion efficiencies were also seen at S/VG ratios as low as 1.2 lb steam/lb vent gas when the vent gas had high nitrogen contents and low heat content. While there was not a consistent relationship between CE and S/VG ratio due to significant changes in vent gas composition, a more consistent and predictable relationship was observed between CE and the net heating value of the combustion zone gas ( $NHV_{czg}$ ).  $NHV_{czg}$  is calculated as the volumetric dilution of all process gases going to the flare tip (e.g. vent gas, steam, and pilot gas). SDP observed high combustion efficiencies when the  $NHV_{czg}$  was above 200 BTU/SCF, as can be seen in Figure ES-1 which displays all observed  $NHV_{czg}$  and CE values from all of the Section 114 Request testing conducted on the SDP EPF.



A secondary objective of the EPF testing was to compare data gathered by the PTFIR instrument when using an Indium Antimonide (InSb) detector with data collected using a Mercury Cadmium Telluride (MCT) detector. Industrial Monitor and Control Corp. (IMACC) compared the InSb and MCT detectors and found that the CE data trends from each detector were indistinguishable. Since the MCT detector can analyze for the presence of CO<sub>2</sub> in multiple regions of the IR spectra, additional data on flare plume temperature can be obtained from the MCT detector, using a proprietary fitting algorithm developed by the PFTIR vendor IMACC. Due to the InSb detector's greater sensitivity in the 1-5.5 μm wavelength range, it remains the better detector to characterize unburned higher molecular weight hydrocarbons in the hot flare plume.

## Table of Contents

### Executive Summary

<b>1.</b>	<b>Introduction .....</b>	<b>1</b>
1.1	Background .....	1
1.2	Objectives of program.....	1
1.3	Testing Team.....	1
1.4	Flare System Components .....	1
1.4.1	Flare Purpose .....	1
1.4.2	Flare Tip.....	2
1.4.3	Flare Instrumentation and Control .....	2
1.4.3.1	Vent Gas Flow .....	2
1.4.3.2	Steam Flow and Control .....	2
1.4.3.3	Online Vent Gas Analyzer.....	3
1.5	Flare Test Equipment .....	3
1.5.1	Passive FTIR System .....	3
1.5.2	Online BTEX Gas Chromatograph (GC).....	3
1.5.3	Video Cameras .....	3
1.5.4	PFTIR Aiming Camera.....	4
1.5.5	FLIR GasFindIR Video Camera .....	4
1.6	Flare Test Program.....	4
1.6.1	Series A .....	4
1.6.2	Series B .....	5
1.6.3	Series C.....	6
1.6.4	Series D (Mercury Cadmium Telluride (MCT) Detector Comparison Series) .....	6
<b>2.</b>	<b>Summary of Results.....</b>	<b>8</b>
2.1	Summary and Key Data Trends by Test Series.....	8
2.1.1	Test Series A, Increasing Steam to Vent Gas (S/VG) Ratio at Low Hydrogen Content.....	8
2.1.2	Test Series B, Limiting S/VG Ratio with Variable Hydrogen Content.....	12
2.1.3	Test Series C, Increasing S/VG Ratio, Low Vent Gas Flow, Variable Hydrogen Content.....	16
2.1.4	Test Series D, Mercury Cadmium Telluride (MCT) Detector Comparison.....	19
2.2	Summary and Key Data Trends of Whole Data Set .....	23
2.2.1	Visible Emissions.....	23
2.2.2	CE vs. S/VG Ratio .....	25
2.2.3	CE vs. NHV <sub>czg</sub> .....	27
2.3	Factors Influencing Test Results .....	29
2.3.1	EPF Vent Gas Flow Measurements.....	29
2.3.1.1	EPF GE Panametric Flow Issues.....	29
2.3.1.2	Corrective Actions.....	30

2.3.1.3	Flow Validation from New Configuration/ Adjustment of Prior Data from Old Configuration .....	31
2.3.1.4	Adjustment of EPF flows during High N <sub>2</sub> Test Periods .....	36
2.3.2	Wind Effects and PFTIR Aiming Issues .....	36
2.3.3	PFTIR Variability - Confidence Intervals for Observed Combustion Efficiency Mean Values.....	37
2.3.4	PFTIR Component Errors .....	43
2.3.5	PFTIR Hot Cell Calibration.....	44
2.3.6	Validation of Online Gas Composition Analyzers.....	44
2.3.7	Potential Impacts of Integrated Sampling .....	50
2.3.8	Accuracy of Combustion Efficiency Measurements at Unstable Combustion Conditions .....	50
2.4	Conclusions .....	51
<b>3.</b>	<b>PFTIR Testing Methods and Procedures.....</b>	<b>52</b>
3.1	Description and Principles of Passive FTIR Measurements .....	52
3.2	PFTIR Siting Configuration .....	52
3.3	PFTIR Operation .....	54
3.4	PFTIR Data Reduction.....	54
<b>4.</b>	<b>Data Tables and Files.....</b>	<b>59</b>
4.1	Data Tables .....	59
4.2	Visible Video Files .....	59
4.3	GasFindIR Video Files.....	59
<b>5.</b>	<b>Appendices .....</b>	<b>60</b>
5.1	PFTIR Test Protocol (IMACC) .....	60
5.2	Weather Data .....	60
5.3	Summa Canister Sample Results.....	60
5.4	PFTIR Calibration Log .....	60
5.5	Master Data Workbook.....	60
5.6	Flare Testing Video Files.....	60
5.7	Flare Testing GasFindIR Video Files.....	60

## 1. Introduction

### 1.1 Background

Shell Deer Park Site (SDP) received a letter, dated March 19, 2010, from the United States Environmental Protection Agency (EPA) pursuant to Section 114 of the federal Clean Air Act (Section 114 Request) requesting SDP to conduct a series of tests and provide test results on the East Property Flare (EPF). This report provides the requested data and test results.

### 1.2 Objectives of program

The Section 114 Request defined the objectives of the EPF test program and required three test series. EPA subsequently added a fourth test series. The four test series are:

- A. Series A - Identify the relationship between Steam to Vent gas Ratio (S/VG) and combustion efficiency (CE) at the EPF when operating within a defined vent gas flow range and at a vent gas hydrogen composition below 30v%.
- B. Series B - Identify the relationship between hydrogen content of vent gas and CE at the EPF when operating within a defined vent gas flow range and at a S/VG ratio identified as resulting in a CE between 75% and 90% in Series A.
- C. Series C - During flare operating conditions that do not meet any of the test conditions specified for Series A or B, test at successive higher S/VG until the observed CE drops to below 75% in order to identify the relationship between S/VG ratio and CE.
- D. Series D (Mercury Cadmium Telluride Detector Comparison Series) - Compare the results from the Indium Antimonide (InSb) detector used in the other tests to a Mercury Cadmium Telluride (MCT) detector by obtaining CE data with the MCT detector under similar conditions used in testing with the InSb detector.

### 1.3 Testing Team

SDP conducted the tests responsive to the Section 114 Request in cooperation with Deer Park Operations, Maintenance, Engineering, and Environmental staff and with assistance from Shell Global Solutions (US) Inc. and Industrial Monitor and Control Corporation (IMACC) personnel (collectively, the "Testing Team").

Shell Global Solutions (US) Inc.  
3333 Hwy 6 South  
Houston, Texas 77082

IMACC  
800 Paloma, Suite 100  
Round Rock, Texas 78645

### 1.4 Flare System Components

#### 1.4.1 Flare Purpose

The EPF provides emergency relief capacity and waste gas destruction capability for nineteen process units in the Deer Park Refinery. The EPF flows range from 2,000 to 5,000 lb/hr at normal operating conditions to a maximum relief capacity of nominally 500,000 lb/hr. The EPF waste gas typically has high hydrogen content with periodic, limited instances of high nitrogen content.

The flare is operated within the maximum flare tip velocities and minimum net heating values as specified in 40 CFR 60.18. The Section 114 Request testing program specified test conditions at normal minimum flow conditions at the EPF.

#### 1.4.2 Flare Tip

The Deer Park Site East Property Flare is a 36" diameter, elevated, steam-assisted flare. The 36" diameter flare tip (model EEF-QA-36-C) was manufactured by the John Zink Company, Tulsa, OK, and was installed in May, 1990. The flare has provisions for steam addition from 21 upper steam ring flame shaping tips and from a center steam injection port.

**Table 1.4.2-1. Shell Deer Park Site East Property Flare Description**

Parameter	Value	Units
Pilot Gas	150	SCFH
Minimum Center Cooling Steam	1,500	lb/hr
Minimum Upper Cooling Steam	500	lb/hr
Maximum Hydraulic Capacity <sup>1</sup>	330,829-806,704	lb/hr
Maximum Smokeless Capacity <sup>2</sup>	105,000-140,000	lb/hr
Height of Flare Tip	60	ft above grade

Typical flows at the EPF are approximately 4% of the smokeless capacity of the flare and 1% of the maximum relief capacity. The EPF base load includes flare header sweep gas, seal purges from rotating equipment, flows from sample and analyzer stations, and process vents from the process units serviced by the EPF.

#### 1.4.3 Flare Instrumentation and Control

##### 1.4.3.1 Vent Gas Flow

SDP meters the waste gas flow to the EPF with a GE Panametric GF868 correlation transient line ultrasonic meter. The transducers are placed in a top down standard Midradius Bias 90 configuration with local temperature and pressure compensation installed as per manufacturer's specifications. The sensors are installed in a straight run configuration. The meter ID is FI30418. It is positioned between the final knock out vessel (V5086) and the flare. Signals from this analyzer are tied into the Deer Park Refinery Distributed Control System (DCS). Calibration is performed annually.

##### 1.4.3.2 Steam Flow and Control

The EPF steam control consists of a model 10" LVM-U Wyatt Venturi flow meter (FE-422), a model ED 1 ½" Fisher control valve (FV-422A), and a model ED 4" Fisher control valve (FV-422B). The control valves are operated in stages. An output between 0% and 50% operates the 1 ½" control valve, and an output between 51% to 100% operates the 4" control valve. When the output is above 50% the 1 ½" control valve is wide open while the 4" control valve begins to open. The flow meter is calibrated for a range of 0 to 100 inches of water column

<sup>1</sup> The maximum hydraulic capacity of the EPF varies from 330,829-806,704 lb/hr as the molecular weight of the vent gas varies from 7.4-44.

<sup>2</sup> The smokeless capacity of the EPF varies from 105,000-140,000 lb/hr as the molecular weight of the vent gas varies from 7.4-44.

which corresponds to a steam flow of 0 to 44,000 lb/hr. The steam to the East Property Flare is limited by upstream hydraulics to about 34,000 lb/hr. The steam addition to the flare is manually controlled by an operator who monitors the flare camera. The operator increases or decreases the control valve output in accordance with flare smoke observation.

#### 1.4.3.3 Online Vent Gas Analyzer

The online vent gas analyzer is a Siemens Maxum Edition II process analyzer with a full complement of modules to meet the TCEQ Chapter 115 HRVOC monitoring requirements. The analyzer cycle time is every 7 minutes. Quality Assurance and Quality Control programs meets all RATA and TCEQ HRVOC requirements including three point certified testing and  $R^2$  linearity requirements. The collected data is tied into the Deer Park Refinery LIMS system.

### 1.5 Flare Test Equipment

#### 1.5.1 Passive FTIR System

As directed, SDP used PFTIR spectroscopy to determine the gas composition of the hot flare gas plume. Chapter 3 and Appendix 5.1 describe the instrument and testing procedures.

PFTIR spectroscopy uses spectral analysis to detect individual compounds in the hot flare plume. Rather than using an active infrared (IR) source and detecting the energy adsorbed by the individual species from the active source, PFTIR analyzes the IR signal from the hot flare gas plume. The IR emission spectra emitted by individual species from a hot source is the same spectra or "fingerprint" as the absorption spectra being analyzed in an active FTIR system. The advantage of a PFTIR is that no active source is needed and no additional optics (retroreflectors) is needed to collect the active beam after it passes through the source plume. By observing the IR radiation emitted from the flare with an appropriate IR collection telescope and spectrometer, individual species can be detected and quantified, just as in active FTIR spectroscopy.

For this test program, the PFTIR operation and data analysis was overseen by Dr. Robert Spellicy and Dr. Curtis Laush of IMACC. The PFTIR instrumentation and software were developed by IMACC.

#### 1.5.2 Online BTEX Gas Chromatograph (GC)

EPA required measurement of the aromatics present in the EPF vent gas but SDP's vent gas GC does not speciate benzene, toluene, ethylbenzene, and xylenes (BTEX) because they historically make up less than one percent by volume of EPF waste gas. Therefore, these aromatic compounds have been grouped as a pseudo  $C_5^+$  compound by the existing GC. SDP installed a Photovac Voyager gas chromatograph with photo-ionization detection (PID) on the vent gas analyzer fast loop to measure BTEX components during the Section 114 Request testing. SDP used QA/QC programs in accordance with US EPA Method 18. Cycle time was at least as frequent as the process analyzer. SDP collected data from the BTEX device locally.

#### 1.5.3 Video Cameras

Two video cameras recorded the flare plume during the testing. The cameras are pan/tilt/zoom Pelco cameras fed to a Pelco DX4500 digital video recorder. Both cameras were mast mounted about 5 yards above grade and 100 yards from the flare on a similar vector as the PFTIR instrument.

#### 1.5.4 PFTIR Aiming Camera

The PFTIR Aiming Camera is an IR camera mounted on the PFTIR telescope. The PFTIR operator used the camera image to aim the PFTIR instrument. Images from this video stream give an indication of PFTIR aiming accuracy. An image from this camera is shown in Figure 1.4.5-1-1. The red square (added for this report) shows the area analyzed by the PFTIR. This red area completely fills the field of view of the PFTIR telescope during testing and indicates the area of the plume being sampled.



Figure 1.4.5-1. FTIR Aiming Camera

#### 1.5.5 FLIR GasFindIR Video Camera

A FLIR GasFindIR Model 25147-200 video camera recorded the thermal images of the flare tip during the Section 114 Request testing. The camera was tripod mounted adjacent to the IMACC FTIR and signal output was fed to a DVR recorder. A 50mm lens was used to optimize the field of view and default image settings gave the most consistent image. Those image settings were: (auto, histogram, and black polarity as hydrocarbon).

### 1.6 Flare Test Program

The Section 114 Request prescribed three test series, and EPA added a fourth test series. The procedures and conditions for each test series are discussed below.

#### 1.6.1 Series A

Series A was designed to identify the impact of the S/VG ratio on the CE of the EPF. As specified in the Section 114 Request, SDP was to conduct Series A testing at vent gas flows between 3,000 and 6,000 lb/hr, when the hydrogen content of the vent gas was less than 30v%. The Section 114 Request specified twelve S/VG values as listed in Table 1.6.1-1, below. SDP was to run each test for 30 minutes, except for those runs during which the preliminary CE was below 75%, in which case SDP could terminate the run after 10 minutes.

**Table 1.6.1-1. S/VG Ratios Requested for Series A**

Test EPA Test ID	S/VG (lb Steam/lb Vent Gas)
[EP-A-10.0]	10.0
[EP-A-9.0]	9.0
[EP-A-8.0]	8.0
[EP-A-7.0]	7.0
[EP-A-6.0]	6.0
[EP-A-5.0]	5.0

[EP-A-4.0]	4.0
[EP-A-3.0]	3.0
[EP-A-2.0]	2.0
[EP-A-1.0]	1.0
[EP-A-Minimum Cooling Steam]	0.33-0.67
[EP-A-API 521]	0.1-0.4

SDP deviated from the prescribed testing procedures and conditions in two ways. First, because the minimum manufacturer’s recommended cooling steam is 2,000 lb/hr for the EPF (1,500 lb/hr to the center steam port and 500 lb/hr to the upper steam ring), SDP could not operate at the API 521 suggested S/VG ratio at the flow rates requested in this series of tests (i.e., 3,000 to 6,000 lb/hr). Second, EPA requested that SDP begin Series A testing at the highest S/VG ratio and work back to the lower S/VG values. Because the EPF receives vent gas streams that have the potential to contain hydrogen sulfide (H<sub>2</sub>S), SDP, with EPA’s concurrence, started at lower S/VG ratios and incrementally increased the /VG to minimize the potential to extinguish the flare flame and release H<sub>2</sub>S to the environment.

### 1.6.2 Series B

Series B was designed to identify the impact of increasing hydrogen concentration in the vent gas on the CE of the EPF at a constant S/VG ratio. The Section 114 request set the S/VG ratio for this series as the lowest S/VG ratio at which SDP observed a CE between 75-90% during Series A testing. Table 1.6.2-1 depicts the vent gas hydrogen concentrations prescribed in the Section 114 Request for Series B testing.

**Table 1.6.2-1 Hydrogen Concentrations Requested for Series B Testing**

EPA Test ID	Vent Gas Hydrogen Concentration, v%
[EP-B-31]	31-40
[EP-B-41]	41-50
[EP-B-51]	51-60
[EP-B-61]	>60

Preliminary Series A test results indicated that CE deteriorated rapidly between an S/VG ratio of 4.0 to 5.0 lb steam/lb vent gas. Therefore, SDP conducted B Series tests starting at an /VG ratio of 4.0. Subsequently, SDP learned that the vent gas flow values obtained from the GE Panametrics flow meter during the Series A testing significantly under represented actual flows under the high nitrogen conditions present in the Series A tests. SDP adjusted the non-representative flows using other process instrumentation to better quantify actual flows during the Series A tests. The procedure to adjust the flows is explained in Section 2.3.1, but explains why the S/VG values presented in the Series B results section do not correspond to the S/VG values ultimately determined from the adjusted Series A test.

The impact of conducting the Series B tests at an S/VG ratio between 4.0 and 5.0, versus the value determined from the corrected flow data in Series A (~0.8 lb Steam/lb Vent Gas), was negligible. In fact, if Series B had been conducted at an S/VG ratio of 1.4, as indicated by the corrected Series A flow data, all CE results for Series B would have been above 98.0%, an area where little discernible impact of hydrogen would have been noticeable.

### 1.6.3 Series C

The EPF receives vent gas from a large number of units with limited ability to adjust flows or hydrogen concentrations to achieve the series A and B test criteria so there were numerous periods during the testing when SDP could not conduct Series A or Series B tests per the specified conditions. EPA asked SDP to use the available test time when process conditions were not within the Series A or B test conditions to conduct Series C tests at a broader range of operating conditions and obtain as much data as possible that may indicate how CE varies as a function of S/VG ratio. Series C flow rate ranges were 100-6,000 lb/hr with hydrogen concentrations above 30v%. SDP was to conduct each individual run for 10 minutes and, if possible, for an additional 10 minutes following the first 10-minute period. The Section 114 Request directed SDP to conduct the Series C testing from the highest achievable S/VG ratio to the lowest. However, as with the Series A tests, the Series C tests were run from lowest S/VG ratio to highest, to minimize the potential for H<sub>2</sub>S emissions. Table 1.6.3-1 describes the S/VG values EPA requested.

**Table 1.6.3-1. S/VG Ratios EPA Requested for Series C Testing**

EPA Test ID	S/VG (lb Steam/lb Vent Gas)
[EP-C-16.0]	16.0
[EP-C-15.0]	15.0
[EP-C-14.0]	14.0
[EP-C-13.0]	13.0
[EP-C-12.0]	12.0
[EP-C-11.0]	11.0
[EP-C-10.0]	10.0
[EP-C-9.0]	9.0
[EP-C-8.0]	8.0
[EP-C-7.0]	7.0
[EP-C-6.0]	6.0
[EP-C-5.0]	5.0
[EP-C-4.0]	4.0
[EP-C-3.0]	3.0

### 1.6.4 Series D (Mercury Cadmium Telluride (MCT) Detector Comparison Series)

SDP conducted Series A, B, and C testing using an Indium Antimonide (InSb) detector. The Testing Team believed that this detector had the best range of sensitivities for the detection of a broad range of hydrocarbons, methane, and carbon monoxide (CO), although it is less sensitive with respect to carbon dioxide (CO<sub>2</sub>). This is because the InSb detector cannot detect signals below a wavenumber of 2000 cm<sup>-1</sup>, which is where the strongest CO<sub>2</sub> absorption band falls. Although the Testing Team did not expect this lack of CO<sub>2</sub> absorption sensitivity to be problematic for robust flames, the Testing Team was uncertain about the InSb detector's ability to detect CO<sub>2</sub> in unstable combustion situations where low CO<sub>2</sub> concentrations might be encountered.

The MCT detector is capable of detecting CO<sub>2</sub> in three different wave number regions: 2080 cm<sup>-1</sup>, 1000 cm<sup>-1</sup>, and 765 cm<sup>-1</sup>. Therefore, the Testing Team hypothesized that the MCT detector might provide more accurate CO<sub>2</sub> measurements at low CO<sub>2</sub> concentrations.

Because IMACC did not have a beam splitter during the test, it was not possible to utilize both the InSb and MCT detectors at the same time to detect the same flare IR signature. Therefore,

for the last two test days (April 15<sup>th</sup> and 16<sup>th</sup>), IMACC replaced the InSb detector with the MCT detector and SDP conducted a series of tests at conditions similar to those encountered using the InSb detector on previous days. IMACC analyzed the CO<sub>2</sub> data at both the 765 cm<sup>-1</sup> and 2080 cm<sup>-1</sup> wavenumber with the MCT detector. IMACC used its proprietary iterative comparison technique to estimate the temperature of the hot flare plume. The temperature determined from this iterative process was then used to reduce the data obtained from other species detected in the hot gas plume. Although it was not possible to directly compare the data gathered by the InSb detector and the MCT detector, test conditions with the MCT detector were matched as closely as possible to the conditions at which the InSb detector was utilized. Table 1.6.4-1 illustrates the test conditions selected for the MCT detector comparison testing.

**Table 1.6.4-1. S/VG Ratios Selected for MCT Detector Testing**

<b>EPA Test ID</b>	<b>S/VG (lb Steam/lb Vent Gas)</b>
EP-D-2.0(MCT2)	2.0
EP-D-3.0(MCT2)	3.0
EP-D-4.0(MCT2)	4.0
EP-D-5.0(MCT1)	5.0
EP-A-5.0(MCT3)	5.0
EP-D-6.0(MCT'1)	6.0
EP-D-2.0(MCT1)	2.0
EP-D-3.0(MCT1)	3.0
EP-D-4.0(MCT1)	4.0
EP-D-6.0-1 MCT	6.0
EP-D-4.5(MCT1)	4.5

## 2. Summary of Results

### 2.1 Summary and Key Data Trends by Test Series

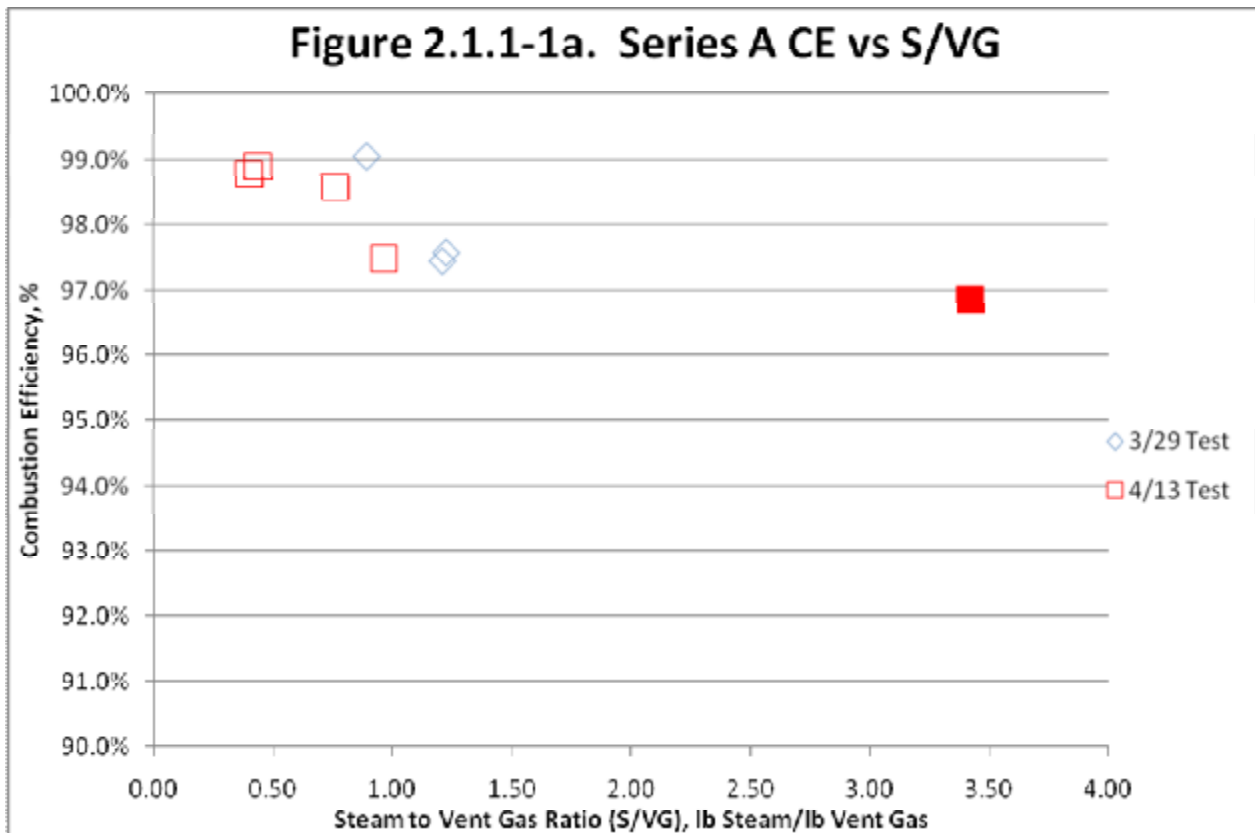
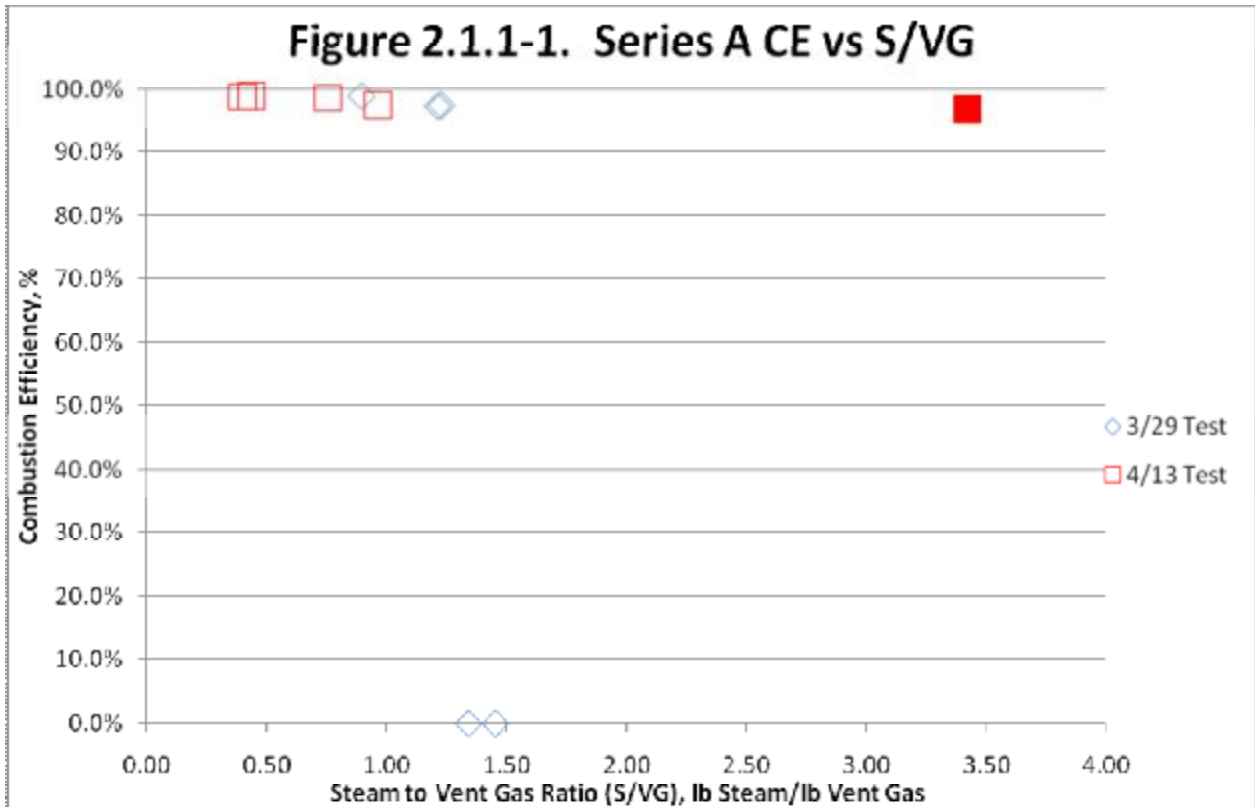
#### 2.1.1 Test Series A, Increasing Steam to Vent Gas (S/VG) Ratio at Low Hydrogen Content

EPA instructed SDP to conduct Series A testing when the hydrogen composition of the stream was less than 30v%. However, historic EPF composition data indicated that the vent gas hydrogen content is not normally below 30v% except during the nitrogen purge cycle of the Catalytic Reformer-3 (CR-3) regeneration. This purge cycle occurs every 30-36 hours, so SDP had a limited number of daylight opportunities to test with hydrogen below 30v% during the Section 114 Request test period. SDP conducted Series A tests on March 29 and April 13, 2010. Figure 2.1.1-1 and Figure 2.1.1-1a illustrate the CE results from this series of tests. Tabulated data from this test series are presented in Table 2.1.1-1.

During the Series A testing, the vent gas flow readings from the GE Panametric GF868 flow meter during the CR-3 nitrogen purge cycle were not representative of the anticipated flows based on process knowledge (i.e., extremely low measured vent gas flows, when based on other process data the flow was known to be much higher). The flare exhibited visually stable combustion and high measured CE with the PFTIR at S/VG ratios in excess of 30, as calculated using indicated flows from the GE flow meter. Further investigation of the flow meter response at high nitrogen concentrations led SDP, in consultation with EPA, to adjust the flow meter results, using other plant instrumentation, to provide representative flows during the high nitrogen flow conditions. Section 2.3.1 provides a detailed discussion of the procedures used to make the flow adjustments.

SDP adjusted all vent gas flow data during the CR-3 nitrogen purge including data gathered during the Series A testing conducted on March 29. Accordingly, all but one of the Series A S/VG ratios reported and displayed in Figure 2.1.1-1 are based upon adjusted flow data, which varied considerably from the values computed from the vent gas flow numbers obtained during the test period. Data points calculated from adjusted flows are shown as open symbols in the graphs in this report, while data calculated from the unadjusted vent gas flow meter values are shown as closed symbols. Data calculated from adjusted vent gas flows in the tables in this report are printed in **red**, while data calculated from the existing EPF vent gas flow meter are printed in black.

At constant vent gas composition, CE is relatively constant with increasing S/VG ratios until a critical S/VG value is reached, at which point there is a very rapid drop in the observed CE. For the Series A tests this breakpoint in CE occurred at a S/VG ratio of approximately 1.2 lb sSteam/lb vent gas. As will be seen in later results, the S/VG ratio at which this drop in CE occurs is a function of the vent gas composition and the combustion properties of the vent gas.



\* The expanded scale graphs in this report depict the high combustion efficiency data at a larger scale to facilitate visual data analysis. However, the expanded scale graph excludes any CE data below 90%. The expanded scale graph should be used in conjunction with the full scale graphs for a full representation of the subject data sets.

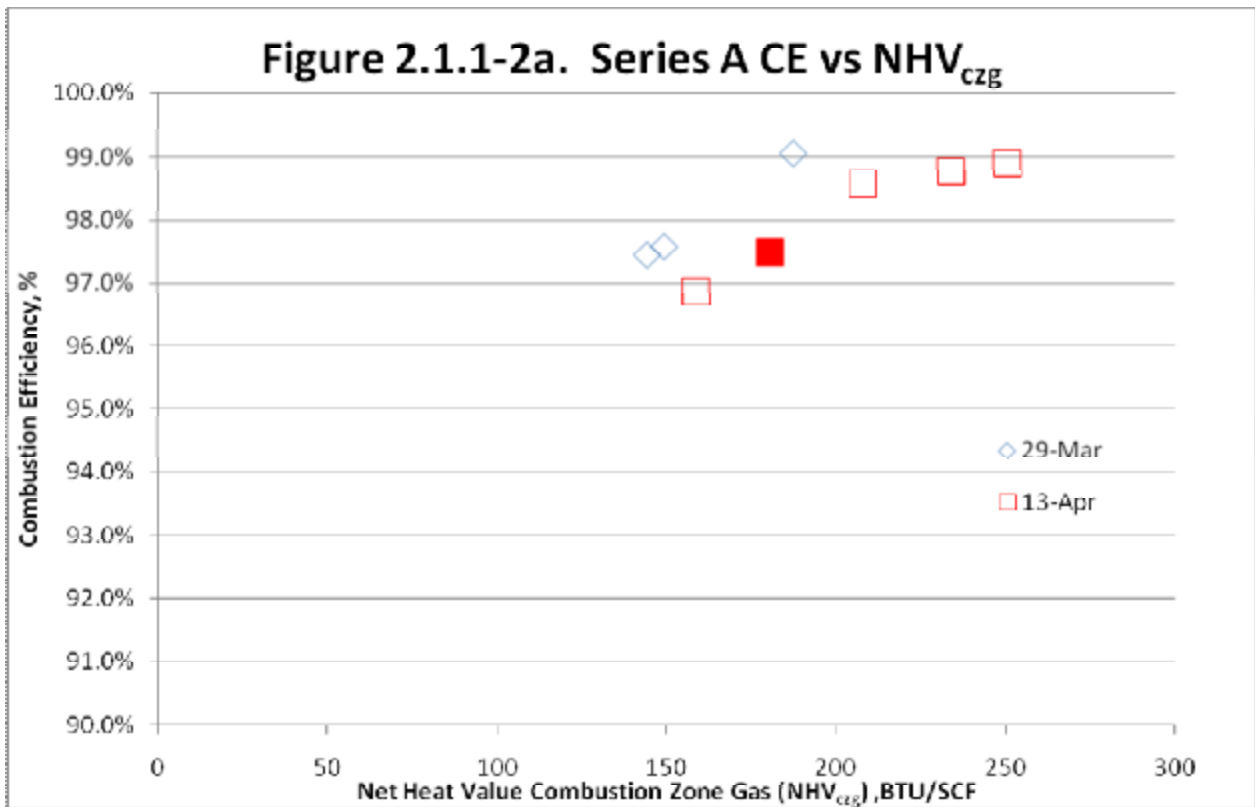
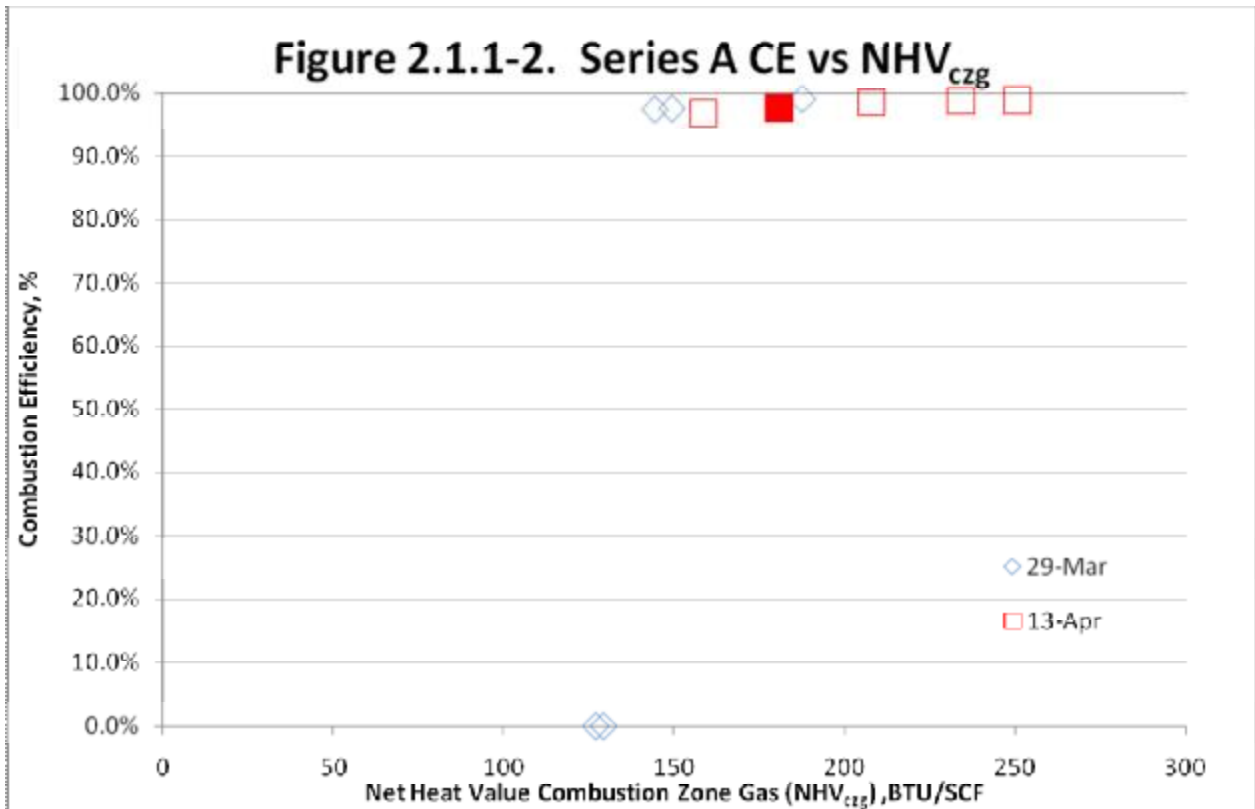
Table 2.1.1-1 Series A Test Results Summary

Test Number	Start Time	End Time	Min	# PFTIR scan avg.	NHV <sub>czg</sub> (BTU/SCF)	CE (%)	H <sub>2</sub> (v%)	THC (v%)	N <sub>2</sub> (v%)	S/VG (lb/lb)
[EP-A-2.0(1)] *	3/29/2010 13:30	3/29/2010 14:23	53	13	188	99.1	29.6	16.1	53.4	0.90
[EP-A-3.0(1)] *	3/29/2010 11:37	3/29/2010 12:20	43	10	144	97.4	27.3	15.3	56.7	1.21
[EP-A-4.0(1)] *	3/29/2010 12:21	3/29/2010 12:51	30	8	149	97.6	28.2	15.3	55.7	1.23
[EP-A-5.0(1)] *	3/29/2010 13:10	3/29/2010 13:15	05	1	129	0.0	27.5	14.0	57.6	1.34
[EP-A-5.0(2)] *	3/29/2010 13:16	3/29/2010 13:22	06	1	127	0.0	27.8	14.4	56.9	1.45
[EP-A-6,000(1)] *	4/13/2010 9:30	4/13/2010 10:04	34	16	251	98.9	25.9	24.4	48.4	0.44
[EP-A-5,500(1)] *	4/13/2010 10:07	4/13/2010 10:39	32	15	234	98.8	24.2	22.5	52.0	0.40
[EP-A-10,000(1)] *	4/13/2010 10:51	4/13/2010 11:22	31	16	208	98.6	20.5	30.1	48.1	0.76
[EP-A-12,500(1)] *	4/13/2010 11:32	4/13/2010 12:03	31	16	181	0.00	20.4	30.2	48.1	0.97
[EP-A-10,000(1)]	4/13/2010 12:51	4/13/2010 13:11	20	10	159	96.9	48.4	34.0	14.1	3.42

<sup>1</sup>EPA test number nomenclature identified Series A tests by the intended S/VG. This nomenclature was used for the March 29 testing. However, after determining that vent gas flow readings, and thus the S/VG, were not representative of process conditions, the April 13 test runs were named by the total steam (lb/hr) going to the flare.

\* Measured vent gas flow was adjusted for this test. Results presented are based on the adjusted vent gas flow values, not the incorrect measured values. See discussion in Section 2.3.1.

Because the S/VG at which CE rapidly declines may vary drastically as a function of vent gas composition, EPA proposed an alternate parameter to account for the impacts of both the vent gas composition and S/VG ratio on CE: the net heating value in the combustion zone (NHV<sub>czg</sub>). The NHV<sub>czg</sub> is calculated as the volumetric dilution of the gas components entering the flame zone (e.g. vent gas, pilot gas, and steam). Figure 2.1.1-2 and Figure 2.1.1-2a illustrate the Series A CEs as a function of NHV<sub>czg</sub>. Based on the data displayed in Figure 2.1.1-2, SDP believes that the NHV<sub>czg</sub> may be a suitable control parameter to predict expected CEs at varying vent gas compositions and S/VG ratios. For the Series A tests the CE was always above 98.0% when the NHV<sub>czg</sub> was above 200 BTU/SCF.



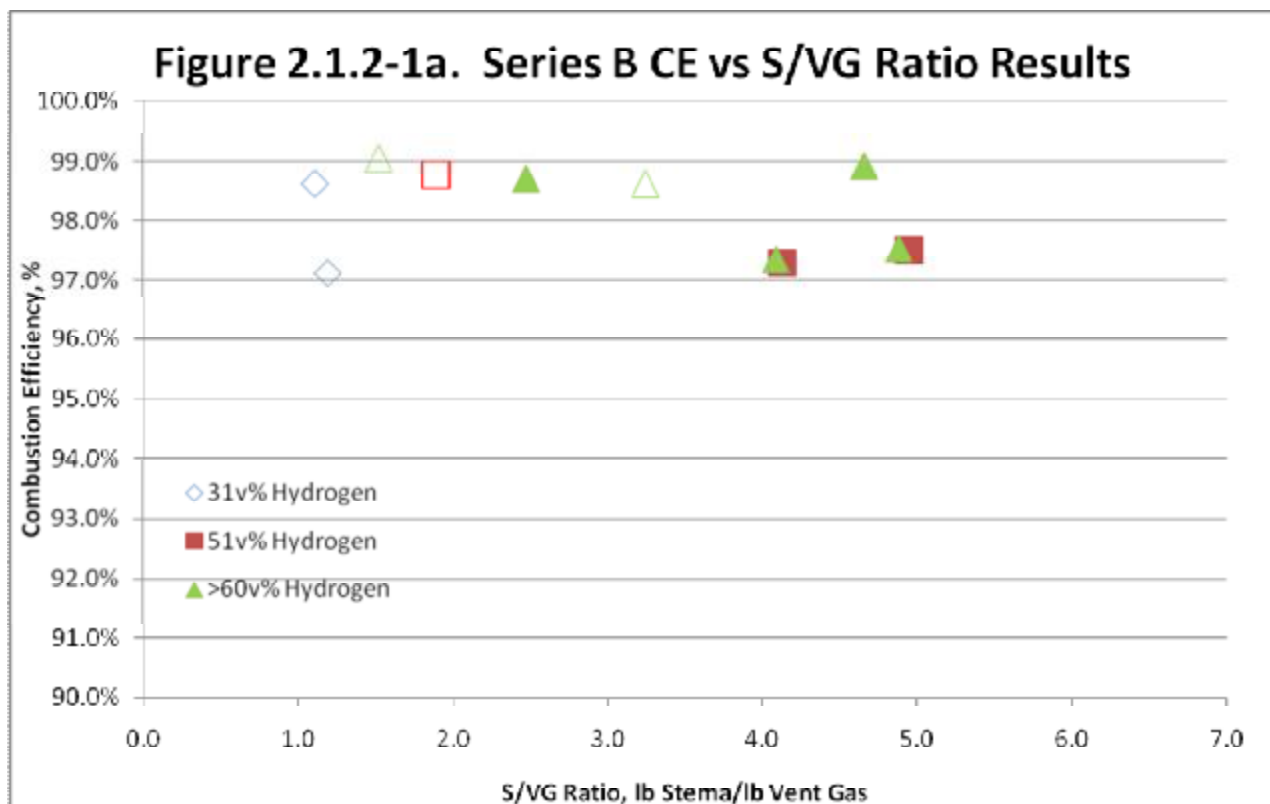
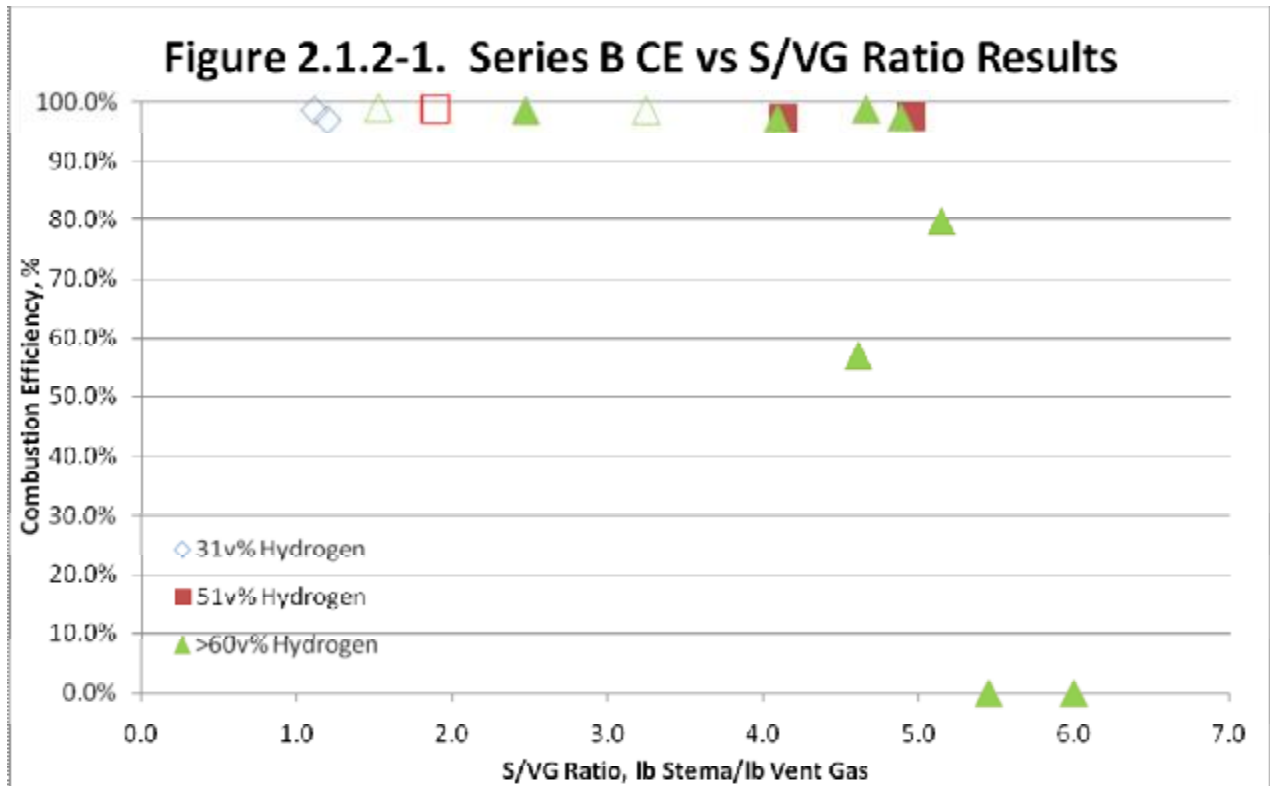
\* The expanded scale graphs in this report depict the high combustion efficiency data at a larger scale to facilitate visual data analysis. However, the expanded scale graph excludes any CE data below 90%. The expanded scale graph should be used in conjunction with the full scale graphs for a full representation of the subject data sets.

### 2.1.2 Test Series B, Limiting S/VG Ratio with Variable Hydrogen Content

One objective of the Series A tests was to determine the S/VG ratio that yielded a CE between 75-90%. Based upon the unadjusted March 29 test flow data this CE was observed at an S/VG between 4 and 5. Therefore, SDP attempted to conduct Series B tests at a S/VG ratio between 4 and 5. SDP did not discover that the flow readings observed from the vent gas flow meter during periods of elevated nitrogen concentrations were not representative of actual flows until after Series B testing was completed. The impact of conducting the Series B tests at an S/VG ratio of between 4.0 and 5.0, versus the value determined from the corrected flow data in Series A (~1.2-1.4 lb Steam/lb Vent Gas), was negligible. In fact, if Series B had been conducted at a S/VG ratio of 1.2, as indicated by the corrected Series A flow data, all CE results for Series B would have been above 98.0%, an area where little discernible impact of hydrogen would have been noticeable.

SDP conducted Series B testing on March 30, April 1, and April 6, 2010. Figures 2.1.2-1 and 2.1.2-2a depict the results from the Series B tests, and Table 2.1.2-1 presents the tabulated data from this test series. Figure 2.1.2-1 shows that under typical gas compositions, outside the CR-3 nitrogen purge window, high CEs were observed up to a S/VG ratio of near 5, with extinction of the flame observed at a S/VG ratio between 5 and 6. As observed during Series A testing, when the nitrogen concentration increases, such as during CR-3 nitrogen purges, the breakpoint in the CE curve versus S/VG will be pushed to lower S/VG ratios. Conversely, at constant nitrogen concentrations, as the ratio of hydrogen to total hydrocarbon increases, the breakpoint in the CE versus S/VG relationship will be pushed to higher S/VG ratios. This trend is somewhat obscured in the data, as SDP does not have the ability to independently manipulate the hydrogen concentration without impacting the resulting hydrocarbon and nitrogen concentrations.

Figure 2.1.2-2 and Figure 2.1.2-2a display the CEs measured during Series B testing as a function of  $NHV_{czg}$ . These Series B tests display high observed combustion efficiencies (>98.0%) when the  $NHV_{czg}$  is above 150 BTU/SCF. This breakpoint in combustion efficiency versus  $NHV_{czg}$  is about 50 BTU/SCF lower than that observed in the Series A testing, which is believed to be a result of the higher hydrogen content of the vent gas during the Series B tests. Consistent with Series A results,  $NHV_{czg}$  appears to have a more consistent correlation with CE than S/VG ratio.

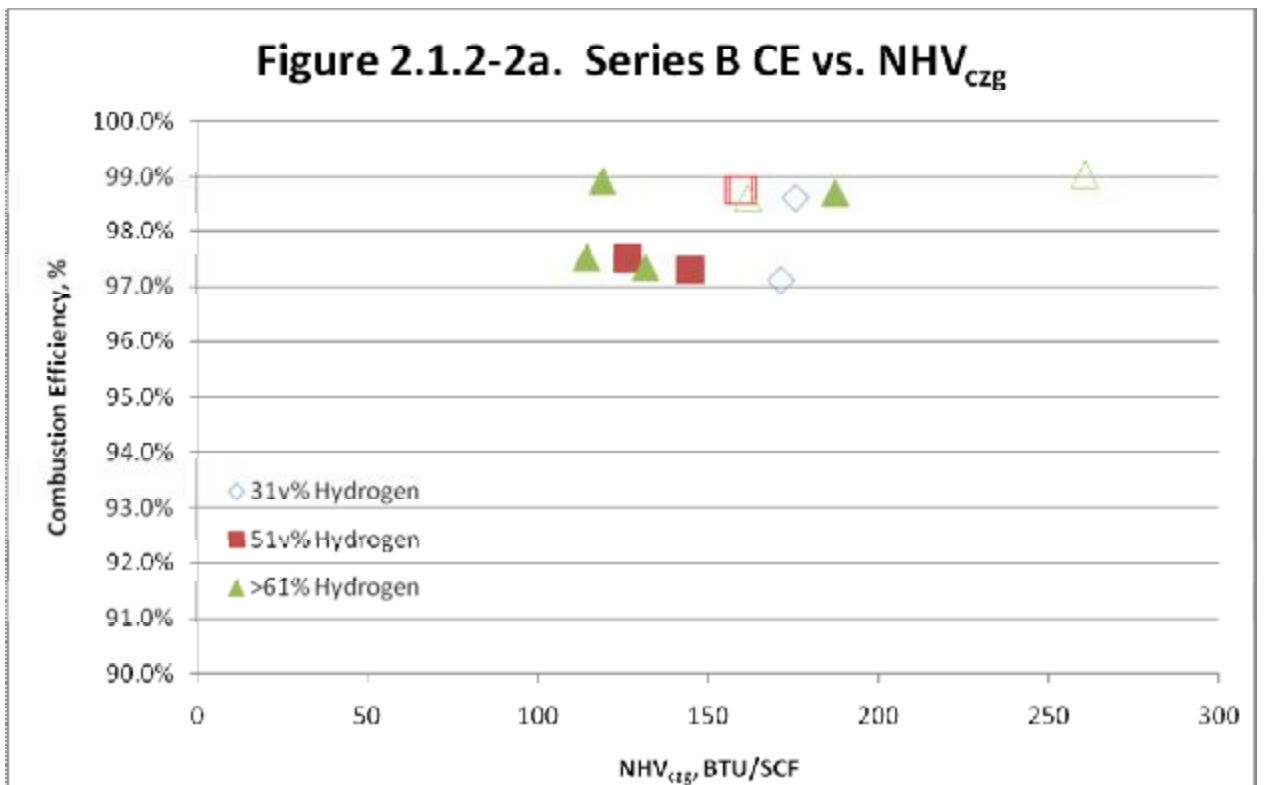
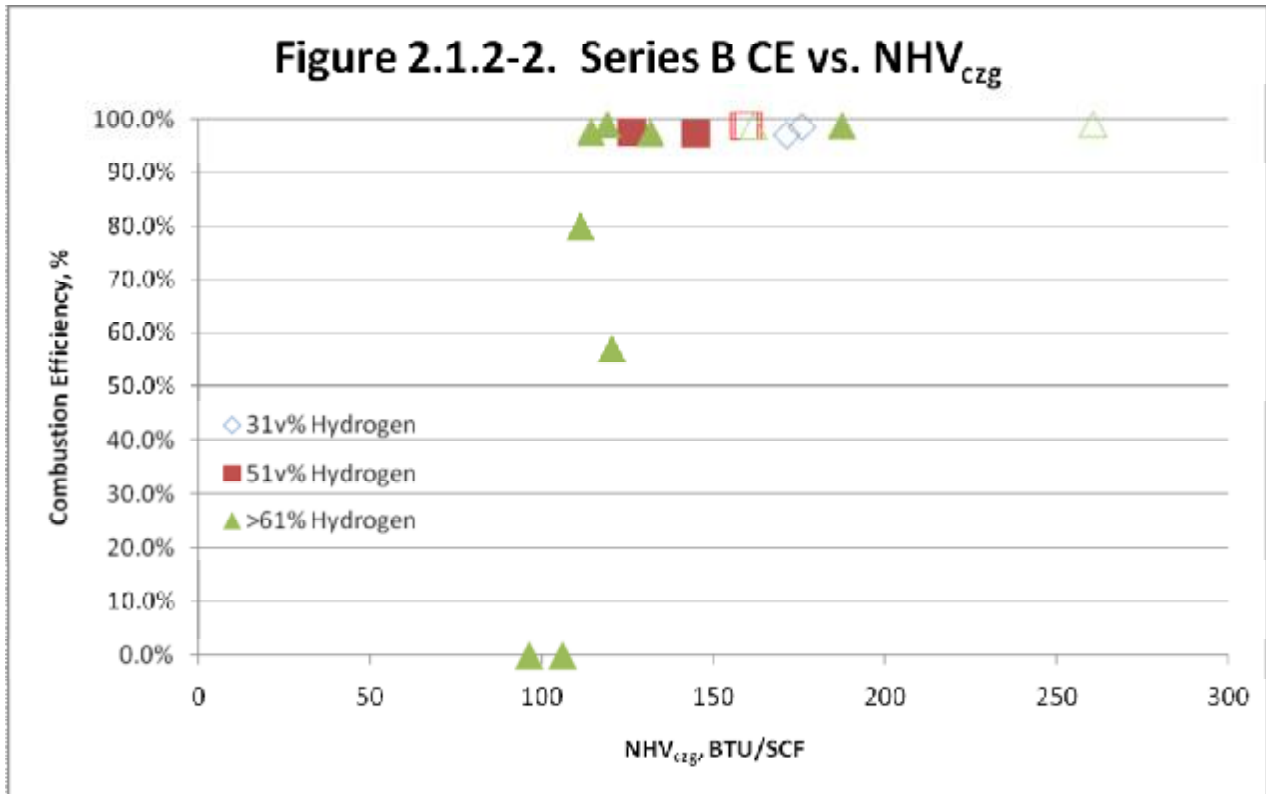


\* The expanded scale graphs in this report depict the high combustion efficiency data at a larger scale to facilitate visual data analysis. However, the expanded scale graph excludes any CE data below 90%. The expanded scale graph should be used in conjunction with the full scale graphs for a full representation of the subject data sets.

Table 2.1.2-1. Series B Test Results Summary

Test Number	Start Time	End Time	Min	# PFTIR scan avg.	NHV <sub>czg</sub> (BTU/SCF)	CE (%)	H2 (v%)	THC (v%)	N2 (v%)	S/VG (lb/lb)
[EP-B-51(1)]	3/30/2010 9:55	3/30/2010 10:38	43	18	145	97.3	57.1	27.1	13.4	4.13
[EP-B-51(2)]	3/30/2010 10:40	3/30/2010 11:30	50	18	126	97.5	57.0	27.4	13.3	4.95
[EP-B-61(1)] *	4/1/2010 8:48	4/1/2010 9:16	28	13	162	98.6	60.4	23.8	14.3	3.25
[EP-B-61(2)] *	4/1/2010 9:17	4/1/2010 9:46	29	15	261	99.0	61.9	23.7	12.9	1.53
[EP-B-31(3)] *	4/1/2010 10:17	4/1/2010 10:50	33	16	171	97.1	37.1	16.5	45.3	1.20
[EP-B-31(2)] *	4/1/2010 10:51	4/1/2010 11:28	37	19	176	98.6	35.7	16.0	47.0	1.12
[EP-B-51(HiFlo1)] *	4/1/2010 12:32	4/1/2010 13:16	44	22	160	98.8	50.8	15.4	32.7	1.91
[EP-B-51(HiFlo2)] *	4/1/2010 13:17	4/1/2010 13:53	36	18	159	98.8	51.0	15.0	32.9	1.90
[EP-B-61-2i]	4/6/2010 10:00	4/6/2010 10:16	16	8	132	97.3	61.2	21.4	14.6	4.09
[EP-B-61-2ii]	4/6/2010 10:17	4/6/2010 10:42	25	13	120	57.1	61.0	21.5	14.8	4.61
[EP-B-61-2iii]	4/6/2010 10:43	4/6/2010 10:53	10	6	111	79.8	61.1	21.6	14.4	5.15
[EP-B-61-2iv]	4/6/2010 10:54	4/6/2010 11:14	20	10	106	0.0	61.1	21.7	14.5	5.45
[EP-B-61-3i]	4/6/2010 11:16	4/6/2010 11:24	08	3	187	98.7	61.0	21.7	14.8	2.47
[EP-B-61-3ii]	4/6/2010 11:32	4/6/2010 11:49	17	1	119	98.9	60.6	21.7	14.9	4.66
[EP-B-61-3iii]	4/6/2010 11:50	4/6/2010 11:58	08	4	114	97.5	59.8	22.1	15.2	4.89
[EP-B-61-3iv]	4/6/2010 11:59	4/6/2010 12:09	10	5	130	0.0	59.9	21.8	15.5	6.01

\* Vent gas flow was adjusted for these tests. See discussion in Section 2.3.1.



\* The expanded scale graphs in this report depict the high combustion efficiency data at a larger scale to facilitate visual data analysis. However, the expanded scale graph excludes any CE data below 90%. The expanded scale graph should be used in conjunction with the full scale graphs for a full representation of the subject data sets.

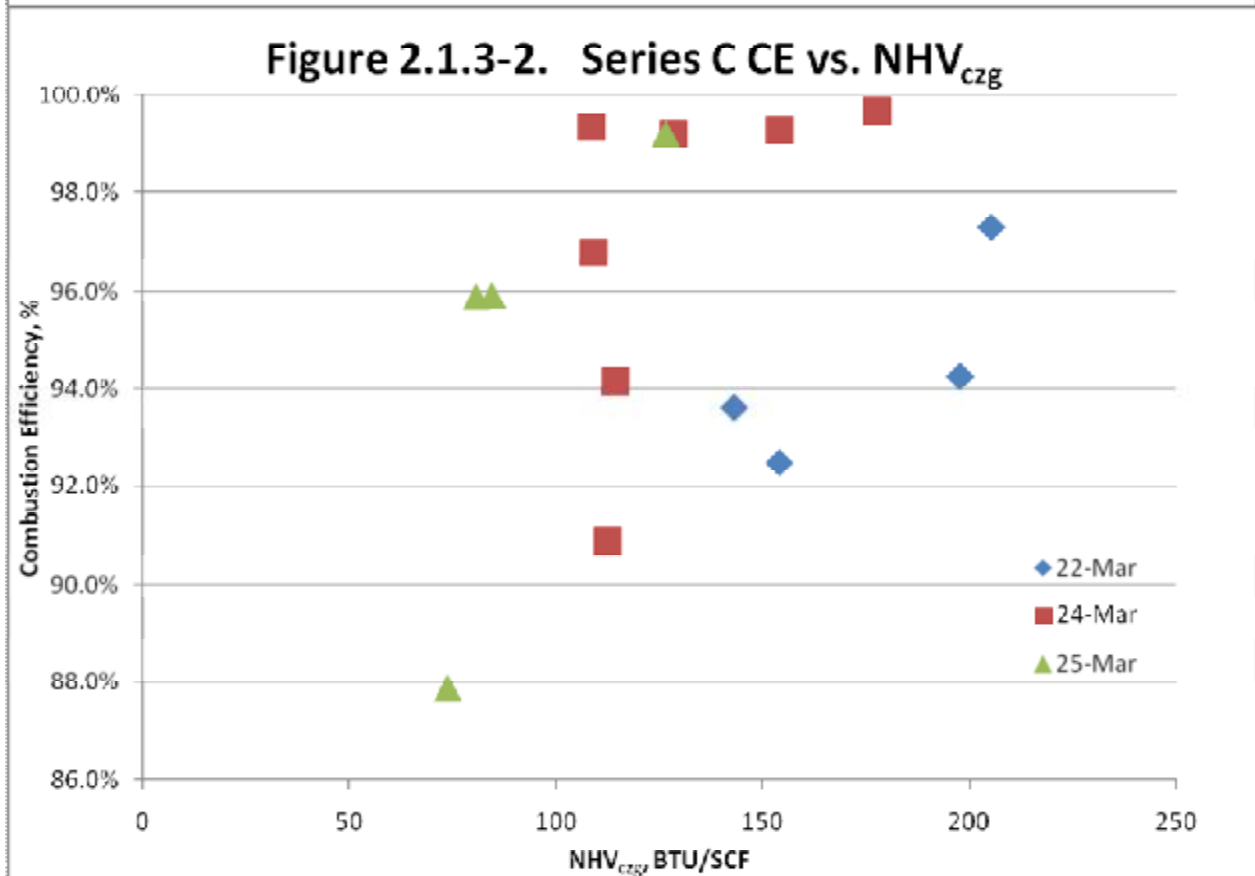
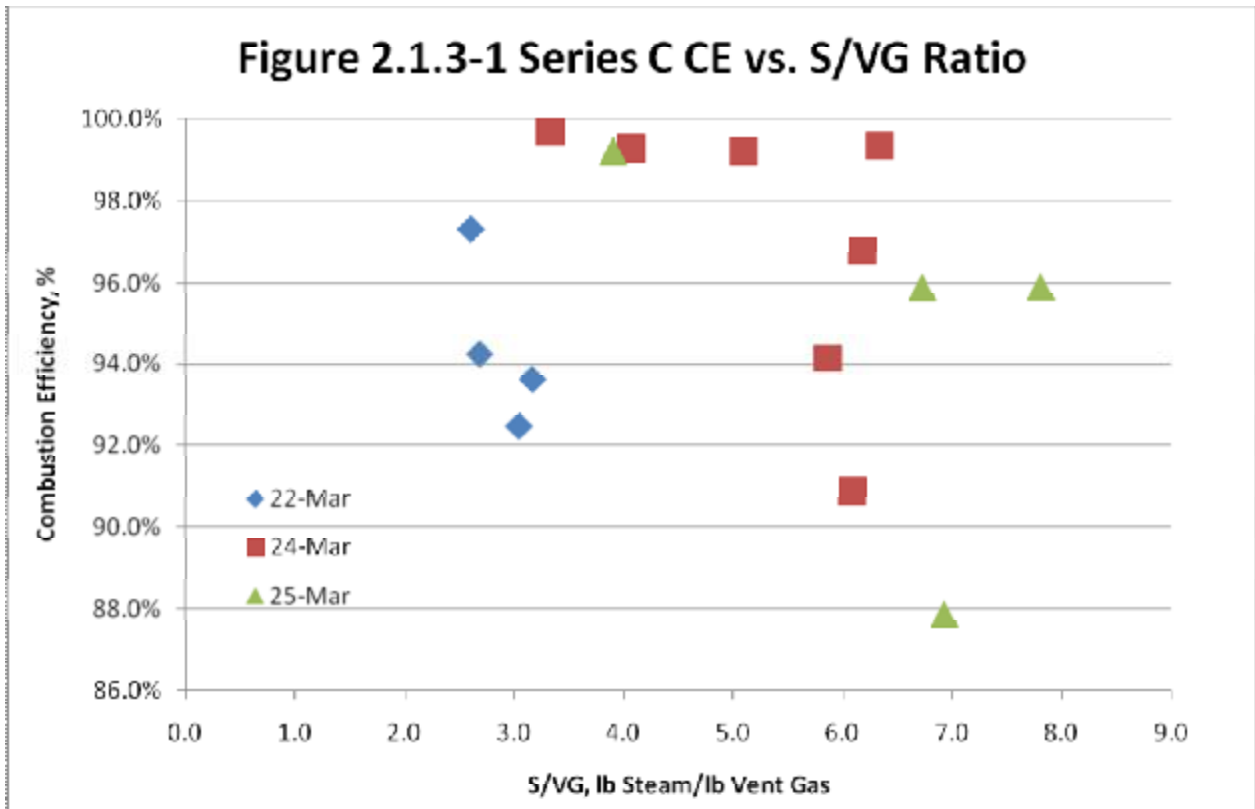
### 2.1.3 Test Series C, Increasing S/VG Ratio, Low Vent Gas Flow, Variable Hydrogen Content

SDP conducted Series C testing on March 22, 24, and 25, 2010. SDP started the C Series test at an S/VG ratio of approximately 2.5 and incrementally increased the S/VG ratio. The results for these tests are illustrated in Figure 2.1.3-1, and the numerical results are tabulated in Table 2.1.3-1. As in the Series B tests, the CE started above 98.0%, but decreased as the S/VG ratio increased. However, depending upon the composition of the gas (hydrogen, nitrogen, and total hydrocarbon concentrations being the key parameters of interest), the breakpoint in CE performance occurred anywhere between a S/VG ratio of slightly less than 3 lb steam/lb vent gas to almost 6 lb steam/lb vent gas. This reinforces the previous observation that the CE breakpoint with respect to S/VG is strongly influenced by the concentrations of hydrogen, nitrogen, and total hydrocarbon in the vent gas.

Displaying the combustion data versus the net heating value of the combustion zone gas ( $NHV_{czg}$ ) collapsed the data from the individual days and vent gas compositions to a reasonably consistent relationship. See Figure 2.1.3-2. There are still some minor differences in the shape of the combustion efficiency versus  $NHV_{czg}$  relationship between the different test days that cannot be completely explained by the observed composition changes observed in the vent gas. The observed combustion efficiencies for the Series C tests also exhibit an increase in combustion efficiency as the  $NHV_{czg}$  increases. While the data from the first day of testing, March 22<sup>nd</sup>, also exhibits this trend the observed combustion efficiencies were somewhat lower than would have been predicted by the trend presented by the rest of the data. Conditions during this test run were dissimilar from most of the other test conditions in that these runs were characterized by high hydrogen, relatively high nitrogen (approaching the 30% that was observed to cause issues with the vent gas flow meter previously), but low THC content in the vent gas (leading to lower  $CO_2$  concentrations in the hot flare plume). None of these observations necessarily invalidate the data, but they are believed to have contributed to the broader than expected scatter in the data. This scatter aside, combustion efficiencies of greater than 98% were still observed for test runs with combustion zone gas net heating values above 200 BTU/SCF.

Table 2.1.3-1. Series C Test Results Summary

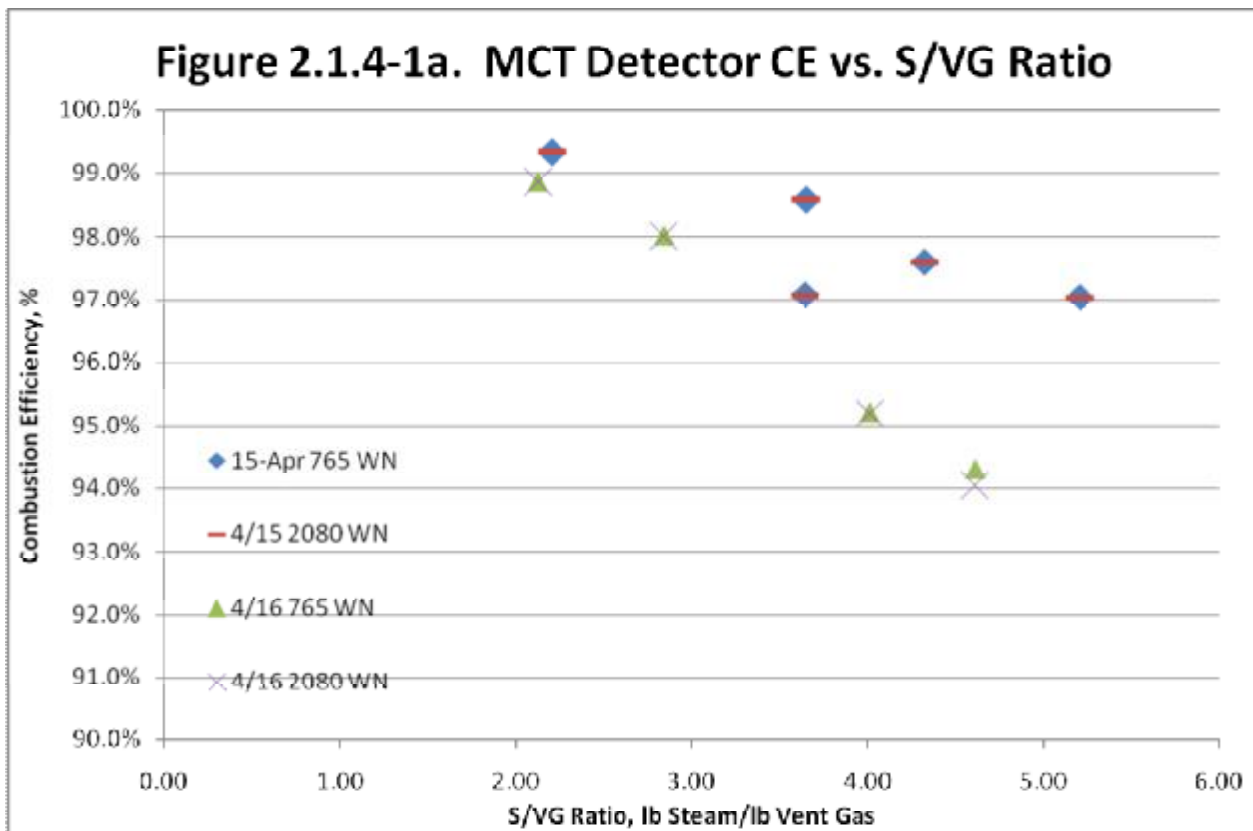
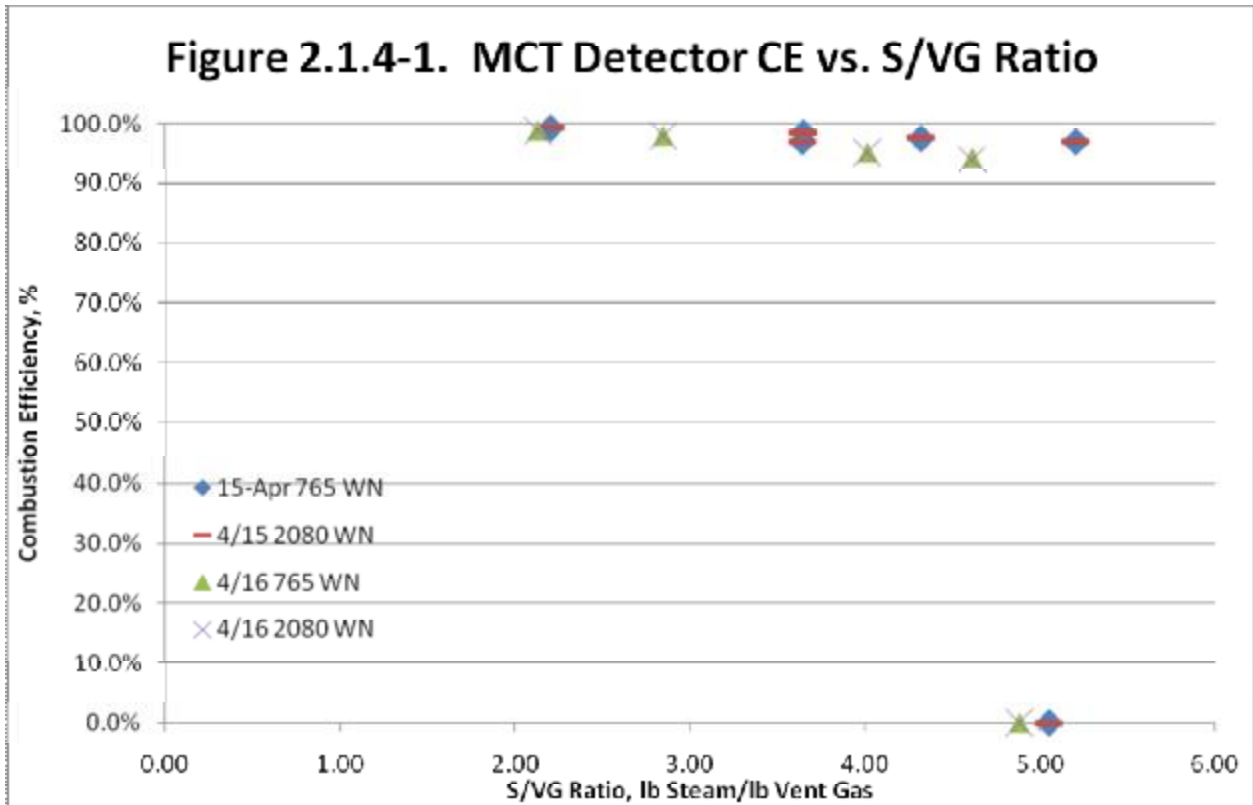
Test Number	Start Time	End Time	Min	# PFTIR scan avg.	NHV <sub>czg</sub> (BTU/SCF)	CE (%)	H2 (v%)	THC (v%)	N2 (v%)	S/VG (lb/lb)
[EP-C-2.5(1)]	3/22/2010 17:14	3/22/2010 17:38	24	9	205	97.3	53.2	27.5	17.1	2.60
[EP-C-2.5(2)]	3/22/2010 17:39	3/22/2010 19:16	37	28	198	94.3	54.0	26.6	17.0	2.69
[EP-C-3.0(1)]	3/22/2010 19:17	3/22/2010 20:08	51	18	154	92.5	47.1	23.9	26.9	3.05
[EP-C-3.0(2)]	3/22/2010 20:09	3/22/2010 20:39	30	9	143	93.6	45.1	26.1	26.7	3.17
[EP-C-3.0(3)]	3/24/2010 14:08	3/24/2010 14:18	10	2	178	99.7	44.4	41.8	11.4	3.33
[EP-C-4.0(1)]	3/24/2010 14:26	3/24/2010 14:35	09	2	154	99.3	43.2	43.2	11.3	4.06
[EP-C-4.0(2)]	3/25/2010 15:55	3/25/2010 16:16	21	5	127	99.2	36.9	36.0	25.4	3.90
[EP-C-5.0(1)]	3/24/2010 16:01	3/24/2010 16:11	10	5	128	99.2	44.1	42.4	11.0	5.09
[EP-C-6.0(1)]	3/24/2010 15:47	3/24/2010 15:58	11	5	109	96.8	44.8	41.7	10.8	6.19
[EP-C-6.0(2)]	3/24/2010 16:20	3/24/2010 16:31	11	4	114	94.1	44.5	42.0	10.7	5.87
[EP-C-6.0(3)]	3/24/2010 16:41	3/24/2010 16:52	11	5	112	90.9	44.6	42.2	10.3	6.09
[EP-C-6.0(4)]	3/24/2010 16:56	3/24/2010 17:07	11	3	108	99.3	44.5	42.6	10.3	6.34
[EP-C-7.0(1)]	3/25/2010 10:02	3/25/2010 10:16	14	3	74	87.9	46.9	26.4	25.0	6.92
[EP-C-7.0(2)]	3/25/2010 10:20	3/25/2010 10:32	12	4	81	95.9	48.0	28.4	22.0	6.72
[EP-C-8.0(1)]	3/25/2010 11:28	3/25/2010 11:37	9	3	85	95.9	51.7	33.1	13.7	7.81



#### 2.1.4 Test Series D, Mercury Cadmium Telluride (MCT) Detector Comparison

Without a beam splitter IMACC could not use a MCT detector and an InSb detector at the same time. Since SDP has very limited means to control the composition of the EPF vent gas, it was also impractical to recreate test conditions identical to those that occurred when SDP collected data with the InSb detector. Given these constraints, the only way to compare the MCT detector to the InSb detector was to gather as many data points as practical with the MCT detector at similar, but not identical, conditions as occurred when data were gathered with the InSb detector, and then compare the two data sets. Figure 2.1.4-1 and Figure 2.1.4-1a depict the CE versus S/VG ratio data obtained during the detector comparison testing. These data are tabulated in Table 2.1.4-1. Figure 2.1.4-2 and Figure 2.1.4-2a depict the relationship between CE and  $NHV_{czg}$  observed during Series D testing. Combustion efficiency data were calculated from the PFTIR data using the CO<sub>2</sub> results from both the 765 cm<sup>-1</sup> wave number and the 2080 cm<sup>-1</sup> wave number. Results at the 2080 wave number would be indicative of results achieved when the InSb detector was being used. Results at a wavenumber of 765 are indicative of the MCT detector.

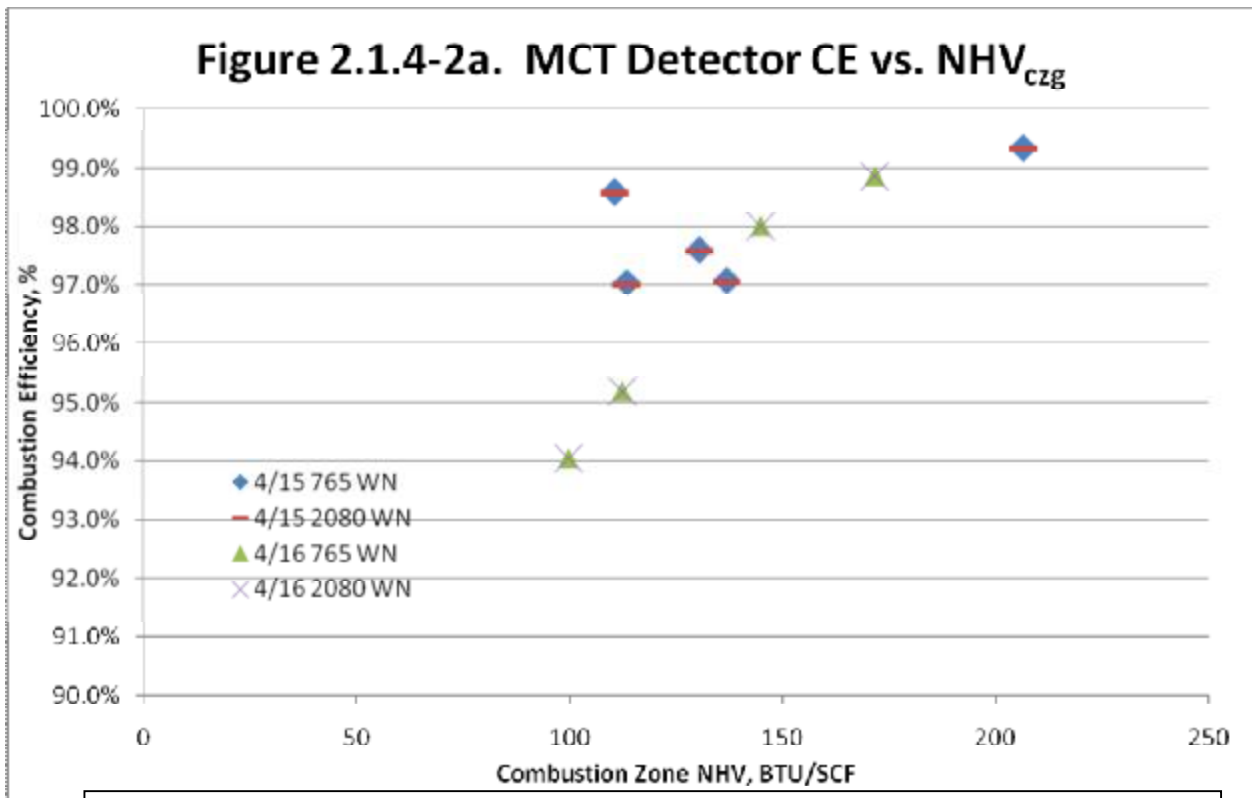
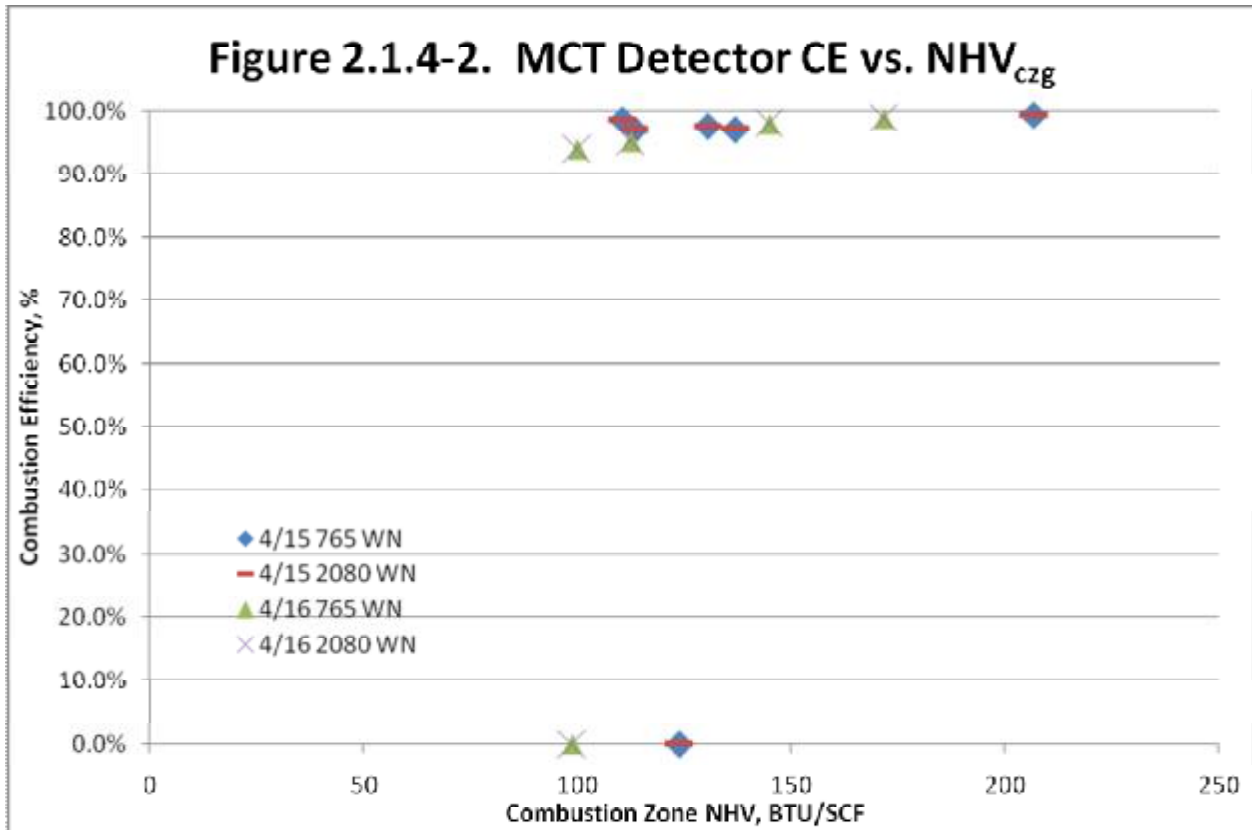
SDP conducted Series D testing on April 15 and 16, 2010. During the two MCT detector test days the range of measured vent gas compositions did not vary as much as during the longer InSb test campaigns (i.e., Series A, B, and C). However, the CE data obtained with the MCT detector exhibited a similar functional relationship versus both S/VG and  $NHV_{czg}$ . The breakpoint where CE started to decline was at a S/VG ratio of approximately 4.0 and the flare was extinguished at a S/VG ratio of 5.0. The  $NHV_{czg}$  required to achieve a CE greater than 98.0% was approximately 150 BTU/SCF. These data are very consistent with data collected at high hydrogen and low nitrogen concentrations with the InSb detector.



\* The expanded scale graphs in this report depict the high combustion efficiency data at a larger scale to facilitate visual data analysis. However, the expanded scale graph excludes any CE data below 90%. The expanded scale graph should be used in conjunction with the full scale graphs for a full representation of the subject data sets.

Table 2.1.4-1. MCT Detector Comparison Series Test Result Summary

Test Number	Start Time	End Time	Mins	# PFTIR scan avg.	NHV <sub>czg</sub> (BTU/SCF)	CE % @ 765 (cm-1)	CE % @ 2080 (cm-1)	H2 (v%)	THC (v%)	N2 (v%)	S/V G
[EP-D-2.0(MCT1)]	4/15 12:44	4/15 13:15	31	14	207	99.3%	99.3%	62.30	21.20	12.77	2.21
[EP-D-3.0(MCT1)]	4/15 10:28	4/15 10:59	31	14	111	98.6%	98.6%	61.68	20.97	13.29	3.65
[EP-D-4.0(MCT1)]	4/15 11:09	4/15 11:39	30	14	131	97.6%	97.6%	63.05	21.11	12.34	4.32
[EP-D-5.0(MCT1)]	4/15 11:46	4/15 12:17	31	14	113	97.0%	97.0%	63.06	21.15	12.05	5.21
[EP-D-4.0(MCT2)]	4/15 13:34	4/15 14:05	31	15	137	97.1%	97.1%	55.30	22.71	18.90	3.64
[EP-D-5.0(MCT2)]	4/15 12:22	4/15 12:32	10	0	124	0.00%	0.0%	63.39	21.05	11.78	5.06
[EP-D-2.0(MCT2)]	4/16 10:28	4/16 11:01	33	16	199	98.9%	98.9%	52.95	19.38	24.37	2.13
[EP-D-3.0(MCT2)]	4/16 11:09	4/16 11:46	37	18	160	98.0%	98.0%	54.92	19.56	22.52	2.85
[EP-D-4.0(MCT3)]	4/16 11:58	4/16 12:29	31	15	132	95.2%	95.2%	55.70	19.28	22.13	4.01
[EP-D-5.0(MCT3)]	4/16 12:58	4/16 13:07	9	0	119	0.0%	0.00%	55.21	20.07	21.77	4.88
[EP-D-4.5(MCT)]	4/16 13:43	4/16 14:20	37	15	100	94.3%	94.0%	55.23	19.28	22.25	4.61



\* The expanded scale graphs in this report depict the high combustion efficiency data at a larger scale to facilitate visual data analysis. However, the expanded scale graph excludes any CE data below 90%. The expanded scale graph should be used in conjunction with the full scale graphs for a full representation of the subject data sets.

## 2.2 Summary and Key Data Trends of Whole Data Set

### 2.2.1 Visible Emissions

The principal reason steam is added to the flare is to prevent visible emissions (e.g. smoking). The American Petroleum Institute (API) has developed suggested minimum values of steam to vent gas ratios needed to prevent smoking for various classes of vent gas compounds. These minimum suggested steam values have been published as part of API Standard 521, *Pressure-Relieving and Depressuring Systems*. Table 11 from API 521 has been reproduced as Table 2.2.1-1 in this report.

**Table 2.2.1-1 Table 11 from API 521 – Suggested Steam Injection Rates**

**Table 11 — Suggested injection steam rates**

Gases being flared	Steam required <sup>a</sup>
	kg (lb) of steam per kg (lb) of hydrocarbon gas
Paraffins	
Ethane	0,10 to 0,15
Propane	0,25 to 0,30
Butane	0,30 to 0,35
Pentane plus	0,40 to 0,45
Olefins	
Ethylene	0,40 to 0,50
Propylene	0,50 to 0,60
Butene	0,60 to 0,70
Diolefins	
Propadiene	0,70 to 0,80
Butadiene	0,90 to 1,00
Pentadiene	1,10 to 1,20
Acetylenes	
Acetylene	0,50 to 0,60
Aromatics	
Benzene	0,80 to 0,90
Toluene	0,85 to 0,95
Xylene	0,90 to 1,00

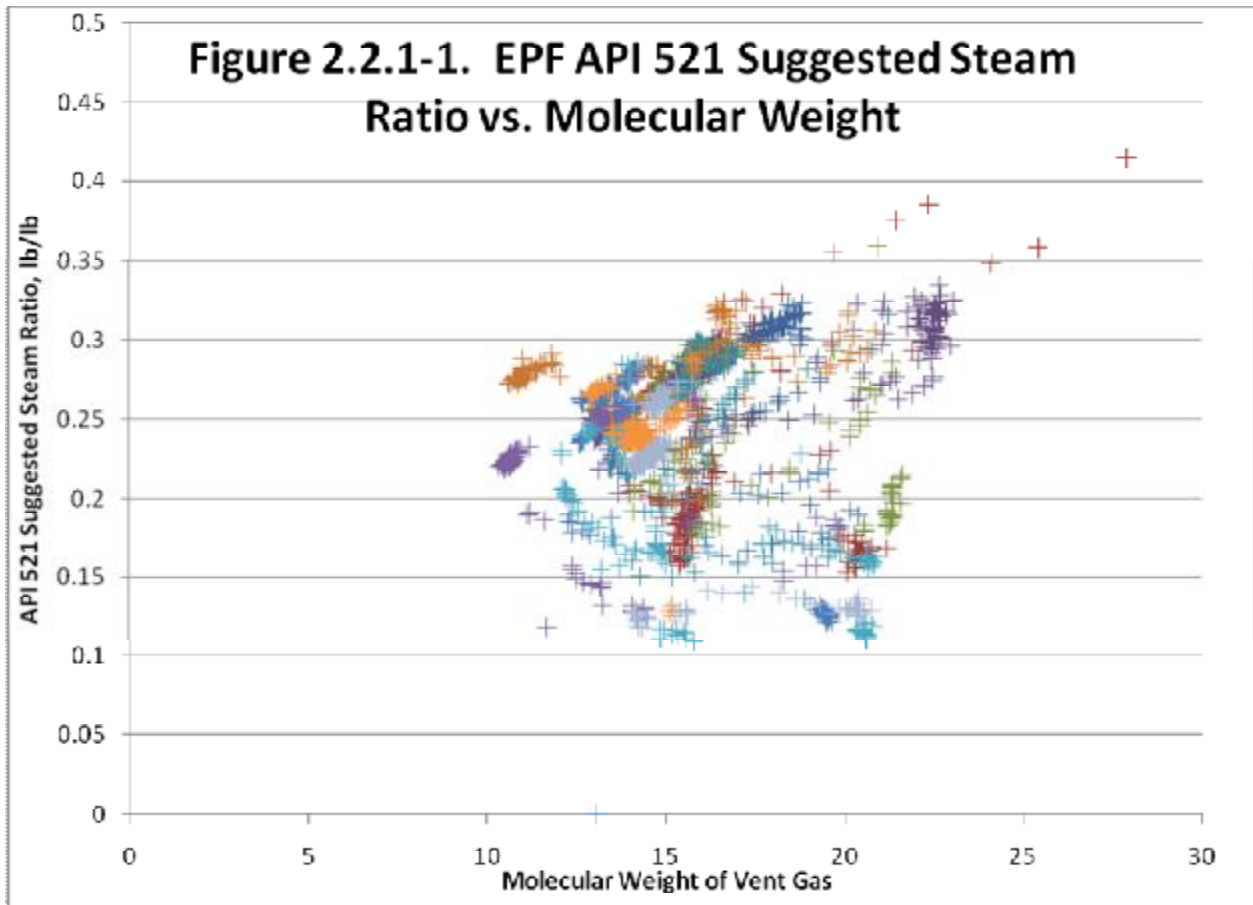
<sup>a</sup> The suggested amount of steam that should be injected into the gases being flared in order to promote smokeless burning (Ringlemann 0) can be determined from this table. The given values provide a general guideline for the quantity of steam required. Consult the flare vendor for detailed steam requirements.

The composition of the EPF vent gas is primarily low molecular weight paraffinic hydrocarbons and hydrogen. There are few olefinic compounds in the EPF vent gas and generally less than 1v% of aromatic compounds. As such, this flare typically does not exhibit a high tendency to smoke. Since this flare has an online GC, as required by the Texas Commission on Environmental Quality (TCEQ) Highly Reactive Volatile Organic Compound (HRVOC) rule (30 TAC 115, Subchapter H), API 521 suggested steam rates can be calculated directly from the online GC data, per Table 11 from API 521. The values for individual compounds in this table are listed as mass of steam per mass of hydrocarbon. API 521 ratios values for this study were

computed by using Equation (1), which appropriately adjusts each ratio value for the total hydrocarbon content of the vent gas.

$$\text{API 521 Suggest Steam Value} = \frac{\sum_{i=1}^N \text{wgt. fraction}(i) \cdot \text{API 521}(i)}{\text{(hydrocarbon wgt. fraction of vent gas)}} \quad \text{(Equation 1)}$$

Figure 2.2.1-1 illustrates the range of API 521 ratios values encountered at the EPF during the Section 114 Request testing.

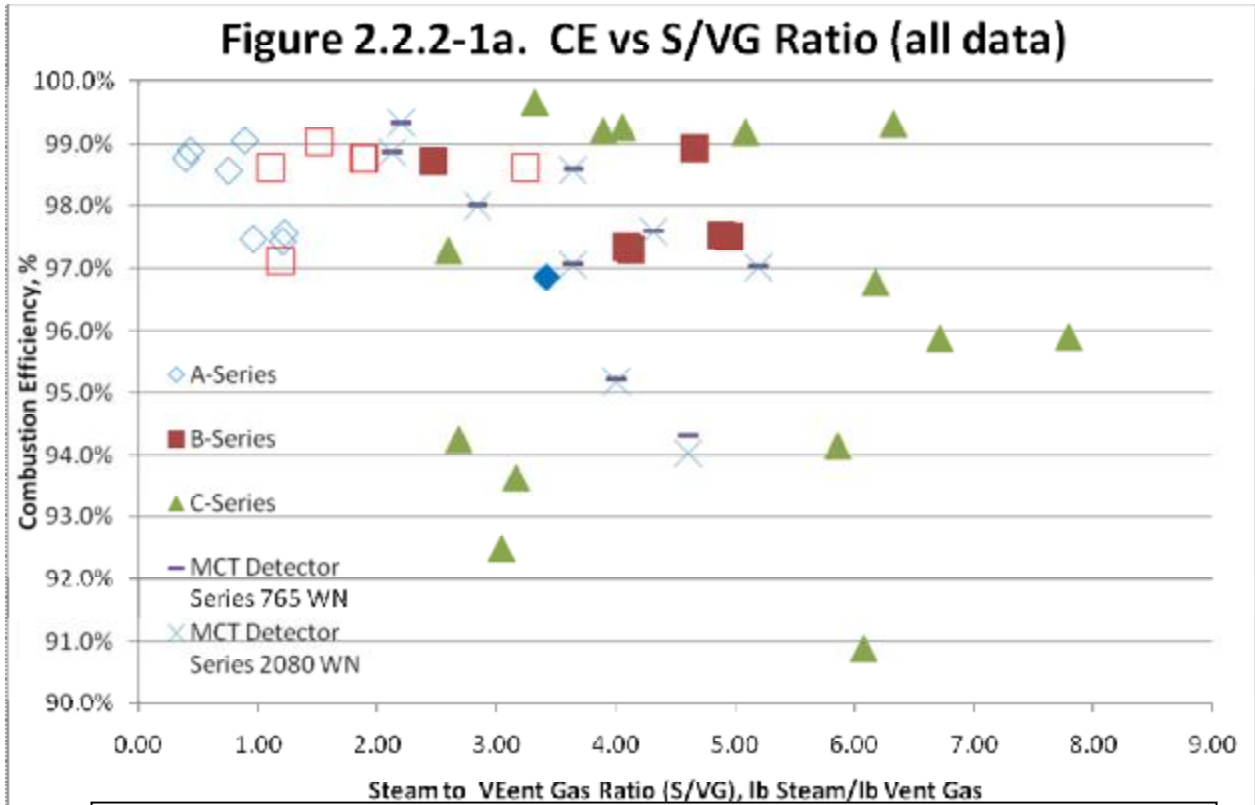
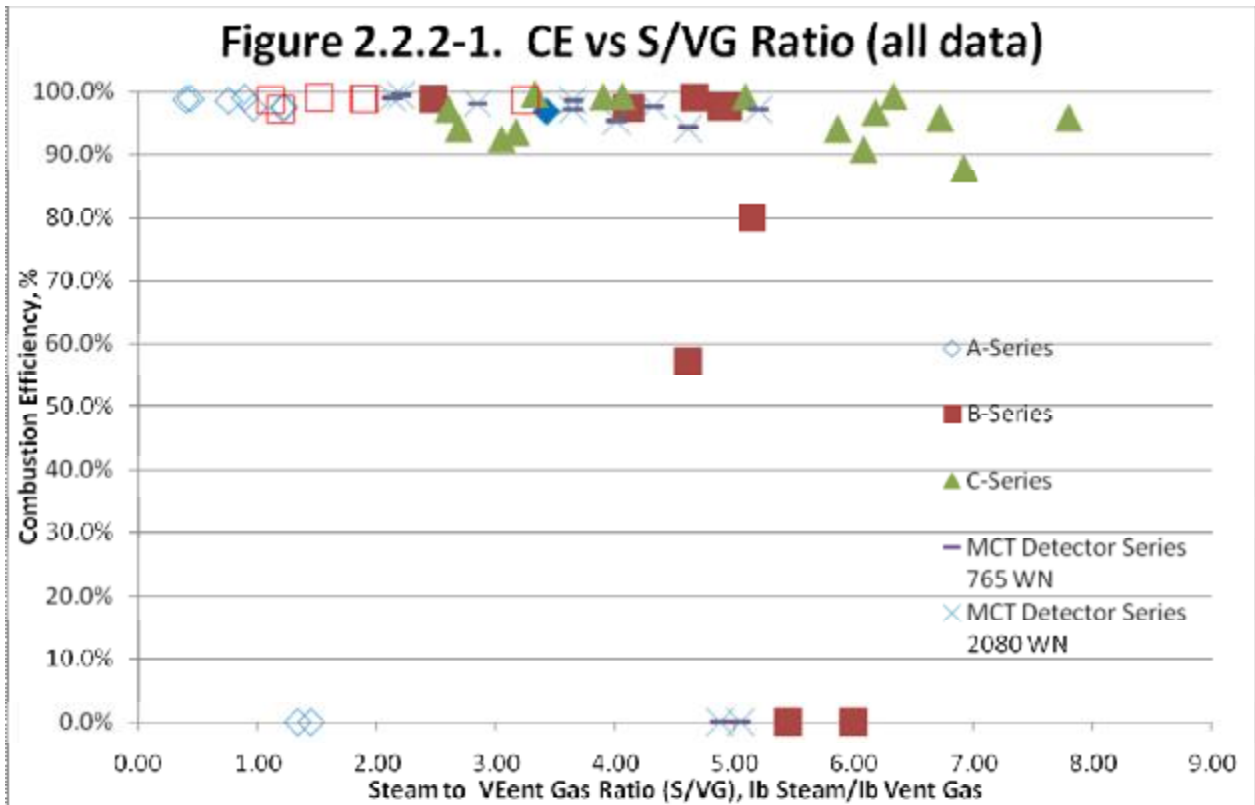


While there is some variability in the computed API 521 suggested steam ratio values, for the entire test period, the suggested API 521 steam ratios value ranged only from 0.1 -0.4 lb steam/lb vent gas.

The lowest S/VG ratio achieved during the testing was a value of 0.33 lb steam/lb of vent gas, and the test S/VG ratios were always above the suggested API 521 ratio. As would be expected from Figure 2.2.1-1, at no point during the testing were visible emissions observed from the EPF.

### 2.2.2 CE vs. S/VG Ratio

Figure 2.2.2-1 and Figure 2.2.2-1a display the CE data as a function of S/VG ratio for all test points during the EPF Section 114 Request testing. While high CEs were observed at S/VG ratios of 1.0 lb steam/lb vent gas up to almost 6.0 lb/lb, significant deterioration of observed CE was also observed at S/VG ratios as low as 1.2-1.4 lb steam/lb vent gas. These data indicate that the composition of the vent gas (principally hydrogen, nitrogen, and total hydrocarbons concentrations) also significantly affect the S/VG ratio at which CE starts to decline. The following subsection addresses a parameter that accounts for both S/VG and vent gas composition, the combustion zone net heating value, and therefore, exhibits a more consistent correlation with CE than either S/VG ratio or vent gas composition alone.

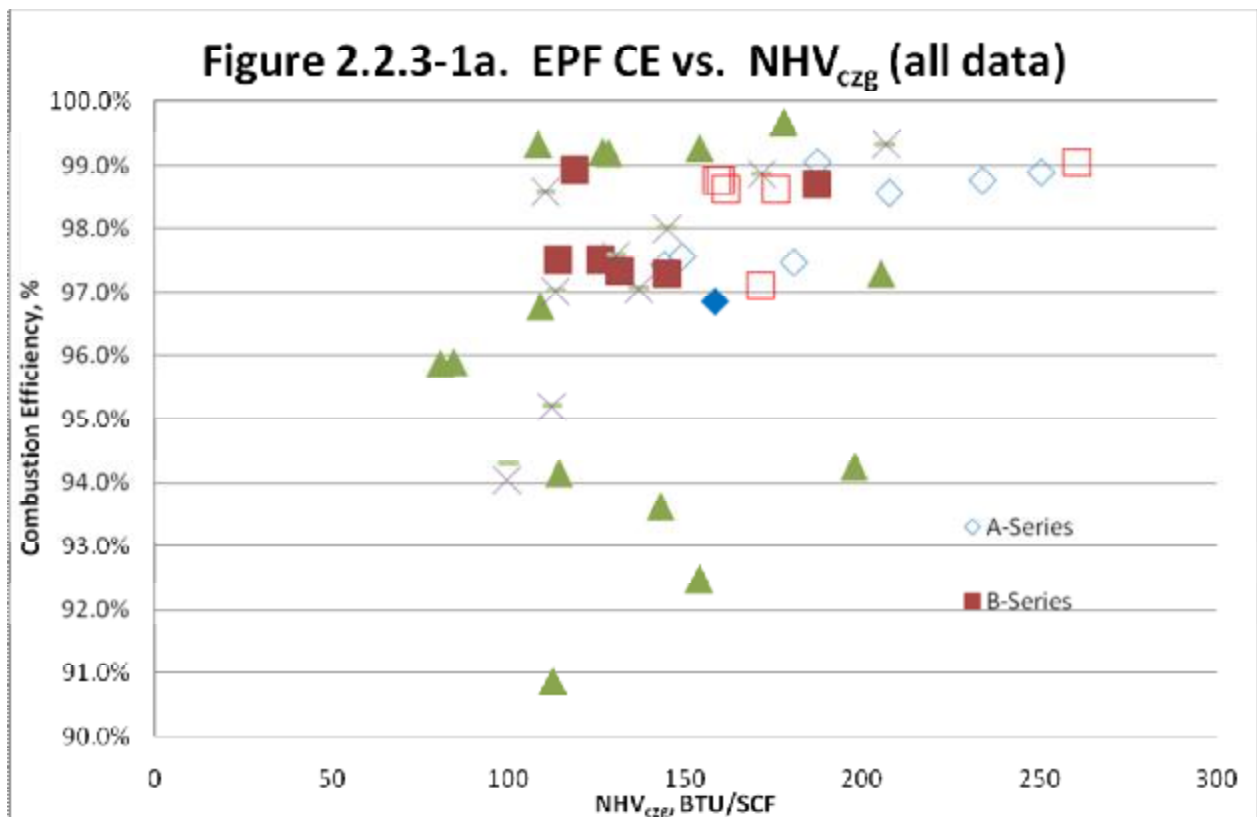
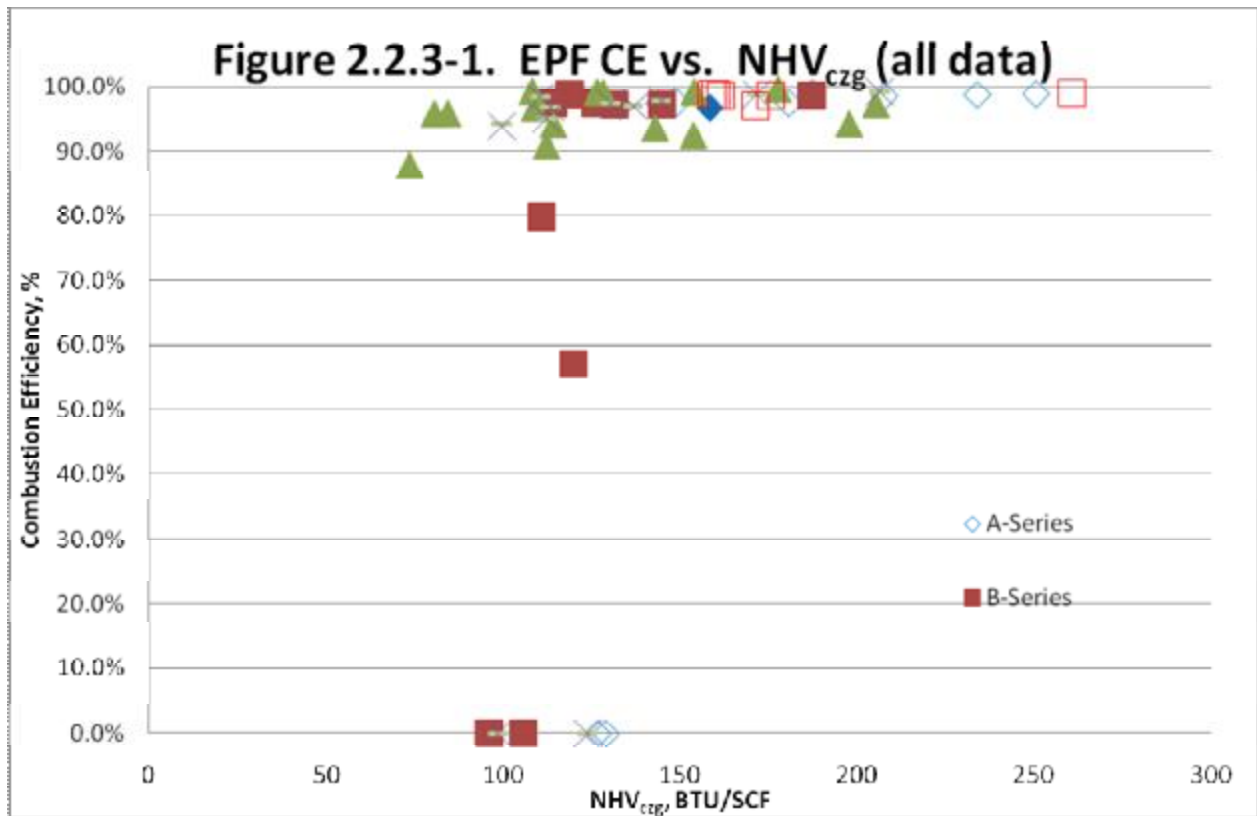


\* The expanded scale graphs in this report depict the high combustion efficiency data at a larger scale to facilitate visual data analysis. However, the expanded scale graph excludes any CE data below 90%. The expanded scale graph should be used in conjunction with the full scale graphs for a full representation of the subject data sets.

### 2.2.3 CE vs. $NHV_{czg}$

EPA suggested using the  $NHV_{czg}$  parameter as a potential means to assess the impact of gas composition on the observed CE. Figure 2.2.3-1 and Figure 2.2.3-1a depict all calculated  $NHV_{czg}$  values versus CE data from the EPF Section 114 Request testing in one graph. This figure illustrates that  $NHV_{czg}$  exhibits a far more consistent relationship with CE than either the S/VG ratio or vent gas composition alone.

These data indicate that a significant decline in CE occurs at a  $NHV_{czg}$  between 100 and 150 BTU/SCF at typical vent gas compositions ( $H_2 > 40v\%$ ). However, during the nitrogen purge portion of the CR-3 regeneration, when the nitrogen content of the vent gas can exceed 50v%, and the hydrogen content falls below 30v%, a significant decline in CE occurred at  $NHV_{czg}$  values between 150 and 200 BTU/SCF. Qualitatively, higher nitrogen concentrations will increase the  $NHV_{czg}$  required to achieve a CE of greater than 98.0%, and higher hydrogen concentrations will tend to lower the  $NHV_{czg}$  required to achieve a CE of 98.0%. However, within the relatively wide range of nitrogen and hydrogen concentrations encountered in these tests the  $NHV_{czg}$  required to achieve a CE of 98.0% varied between 150-200 BTU/SCF.



\* The expanded scale graphs in this report depict the high combustion efficiency data at a larger scale to facilitate visual data analysis. However, the expanded scale graph excludes any CE data below 90%. The expanded scale graph should be used in conjunction with the full scale graphs for a full representation of the subject data sets.

## 2.3 Factors Influencing Test Results

### 2.3.1 EPF Vent Gas Flow Measurements

#### 2.3.1.1 EPF GE Panametric Flow Issues

Prior to beginning the EPA 114 Request testing, a GE Field Service Technician made a site visit to Deer Park and verified that the GE Panametric GF 868 flow meter was responding correctly and that all flow meter parameters were within acceptable ranges. Further, SDP had discussions with senior GE technical support for these meters to discuss the impact of high nitrogen content on observed results from the meter. Although GE mentioned that the algorithm used to convert volumetric flow to mass flow is impacted by variable nitrogen conditions, GE asserted that the volumetric flows determined from the flow meter should be accurate and unaffected by high nitrogen contents. Since Deer Park uses the data from the online HRVOC GC to convert the volumetric flows into mass flows, the existing GE flow meter installation was deemed fit for purpose for the upcoming tests.

To achieve the hydrogen concentrations in the EPF vent gas specified for the Series A tests, SDP had to conduct EPF Series A testing during the nitrogen purge portion of the CR-3 regeneration cycle. The high nitrogen flow from the CR-3 regen cycle dilutes the hydrogen in the EPF vent gas stream sufficiently to meet the hydrogen concentration requirements for the Series A tests. SDP conducted the first Series A test on March 29, 2010. The measured EPF mass flows during this test remained relatively constant during the nitrogen purge cycle, and did not exhibit the flow increase that was expected based on readings from CR-3 unit instrumentation. Standard operating procedure at the CR-3 unit is to establish a nitrogen purge flow of 3-4 MMSCFD (~9,000-12,000 lb/hr N<sub>2</sub>), which is routed to the EPF.

The next Series A test did not occur until April 13, 2010. During the CR-3 nitrogen purge that day, the Panametrics flow meter indicated a very low flow to the EPF (100-500 lb/hr), yet CEs of greater than 98% were observed at apparent S/VG ratios in excess of 30:1. SDP concluded from these instrument readings that the GE Panametric flow readings must be in error when nitrogen concentrations in the EPF line were greater than 30v%.

For the high nitrogen test cases encountered during CR-3 regenerations (N<sub>2</sub> concentrations >30%v), vent gas flow estimates generated by using EPF baseline flow estimates and measured flows to the flare from the CR-3 unit were used in the resulting data analysis (S/VG and CZG<sub>NHV</sub> calculations). These flow estimates yielded results that were 1) consistent with the amount of nitrogen used in the CR-3 regeneration process, 2) yielded S/VG ratio when the flare was extinguished that were consistent with theoretical calculation of the onset of an incombustible mixture, and 3) were also in line with flows measured with the subsequently installed 22" flow sensors. Based upon the agreement of this method with the newly installed longer flow sensor, the process instrumentation at CR-3, and the fact that S/VG ratios calculated from this method were consistent with when combustion theory would predict the flare to be extinguished, SDP believes that flows adjusted using the CR-3 Instrumentation Method are a reasonably accurate representation of the flow to the EPF when the nitrogen concentration in the vent gas exceeded 30%v. Therefore, when the nitrogen concentration in the EPF vent gas was under 30% the flows from the existing EPF flow sensors were used. When the nitrogen concentration was above 30%, flows were adjusted by using estimates of the EPF baseline flow and adding measured flows from the CR-3 unit to the EPF header. Sections 2.3.1.2-4 describe the analysis methods used to arrive at this conclusion. As previously mentioned all data points calculated from adjusted flows are depicted as open symbols in this report. Data points calculated using the existing ultrasonic time of flight flow sensors are represented as solid symbols. Similarly,

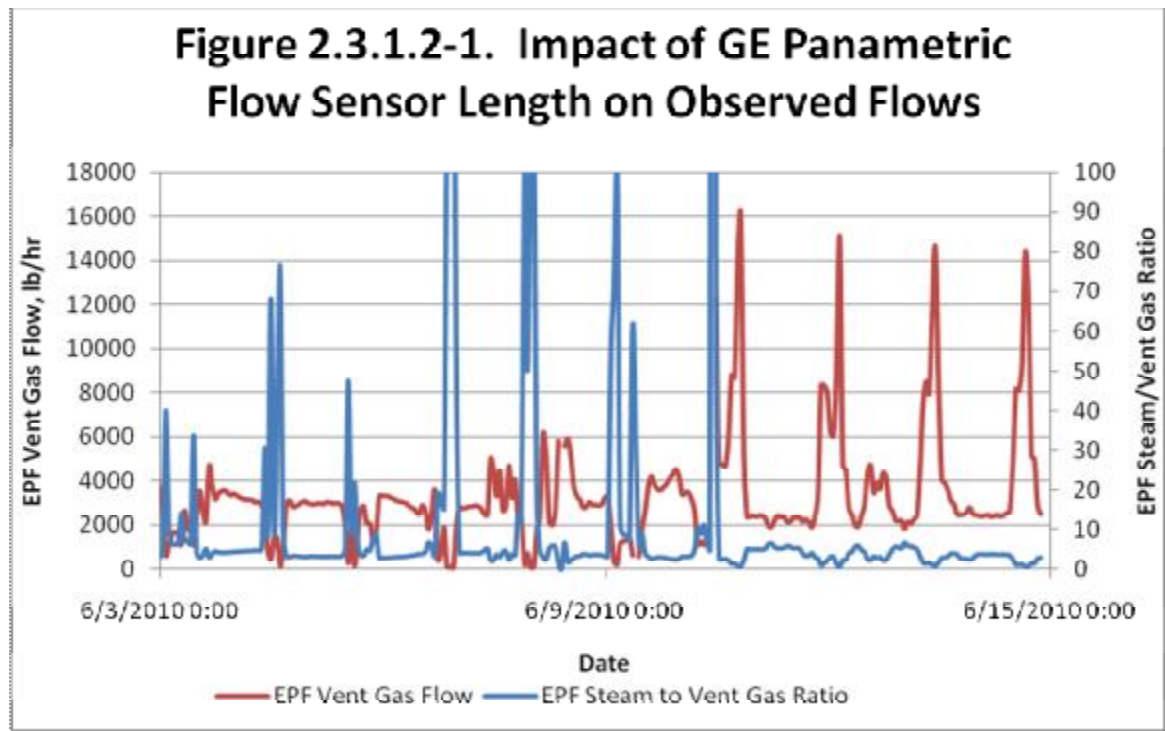
data generated from estimated flows are tabulated in red, while data calculated from the existing flow meters are tabulated in black.

2.3.1.2 Corrective Actions

Once SDP determined that the flow meter was not providing accurate flow rate data at vent gas nitrogen concentrations greater than 30v%, SDP investigated and implemented corrective actions. GE technical support personnel informed SDP that “stratification” of vent gas components had been observed in a limited number of prior applications where there were large differences in the molecular weight of component gases.

The Deer Park GE Panametric Model GF868 installation is a standard “Bias 90” configuration. In this configuration the sensors are positioned in the top quadrant of the pipe flow (e.g. top insertion to a depth of 9” in a total pipe diameter of 36”). GE suggested building longer flow sensors and to installing them in the bottom quadrant of the EPF vent header (e.g. sensor inserted from the top to a depth of 22” out of total pipe diameter of 36”). SDP installed the longer sensors on June 10, 2010.

Figure 2.3.1.2-1 depicts hourly average plant data from the process computers for a 12-day period from June 3<sup>rd</sup> to June 12<sup>th</sup>. Ten CR-3 regeneration cycles occurred over these 12 days. The flow response differences between the 9” sensor insertion and 22” sensor insertion configurations are apparent in the data. Prior to the June 10<sup>th</sup> sensor installation, observed flows during the N<sub>2</sub> purge portion of the CR-3 regeneration cycle could be characterized by either constant flow or in some cases diminishing flows. After installing the longer flow sensor, SDP observed the expected increase in flow during CR-3 N<sub>2</sub> purge cycles. The apparent spikes in S/VG ratio observed during virtually every CR-3 regeneration cycle with the old sensor were also absent after installation of the new longer flow sensor.



### 2.3.1.3 Flow Validation from New Configuration/ Adjustment of Prior Data from Old Configuration

While Figure 2.3.1.2-1 illustrates the apparent differences in the responses observed from the two different flow sensors, it does not speak to the accuracy of one flow sensor configuration versus the other. To validate the flow response of the new longer sensor and develop a basis for adjusting flow measurements during the test to reflect flow conditions, SDP considered two alternate methods of determining flow to the EPF to estimate flows in the EPF vent gas line during high N<sub>2</sub> periods.

**N<sub>2</sub> Material Balance.** Assuming the baseline flow to the EPF (all flow to the EPF header except that from the CR-3 unit) varies on a longer time scale than the typical CR-3 N<sub>2</sub> purge cycle (3-4 hours), then both the baseline flow to the flare and the N<sub>2</sub> concentration of that baseline flow can be approximated by a linear interpolation of the values of each of these parameters at the beginning and end of the CR-3 N<sub>2</sub> purge cycle. Since the gas from the CR-3 during the N<sub>2</sub> purges is 100v% N<sub>2</sub>, and the N<sub>2</sub> concentration of the combined flow to the EPF is measured by the online HRVOC GC, the volume of N<sub>2</sub> coming from CR-3 to the EPF header, and therefore the total flow to the EPF header, can be calculated from a system of two equations with two unknowns (CR-3 N<sub>2</sub> flow and Total EPF Flow) constructed from a material balance around this system.

Figures 2.3.1.3-2, 2.3.1.3-3, and 2.3.1.3-4 compare the results from the N<sub>2</sub> Material Balance to the flow rate measured by the longer sensor for first three successive CR-3 regeneration cycles after the installation of the longer sensors.

The shape of the curve of the EPF flow calculated from the N<sub>2</sub> Material Balance over time very closely matches the shape of the curve of the flow measured by the longer 22" flow sensor over time. However, the amplitude of the N<sub>2</sub> Material Balance flow rate curve is somewhat higher than the flow rate curve measured by the 22" probe. To quantify the magnitude of this variation, SDP performed a minute by minute integration of the area under the two curves. The integrated flow for the N<sub>2</sub> Material Balance was 105.9%, 98.4% and 109.8% of the integrated flow measured by the 22" sensor, respectively, for each of the examples shown.

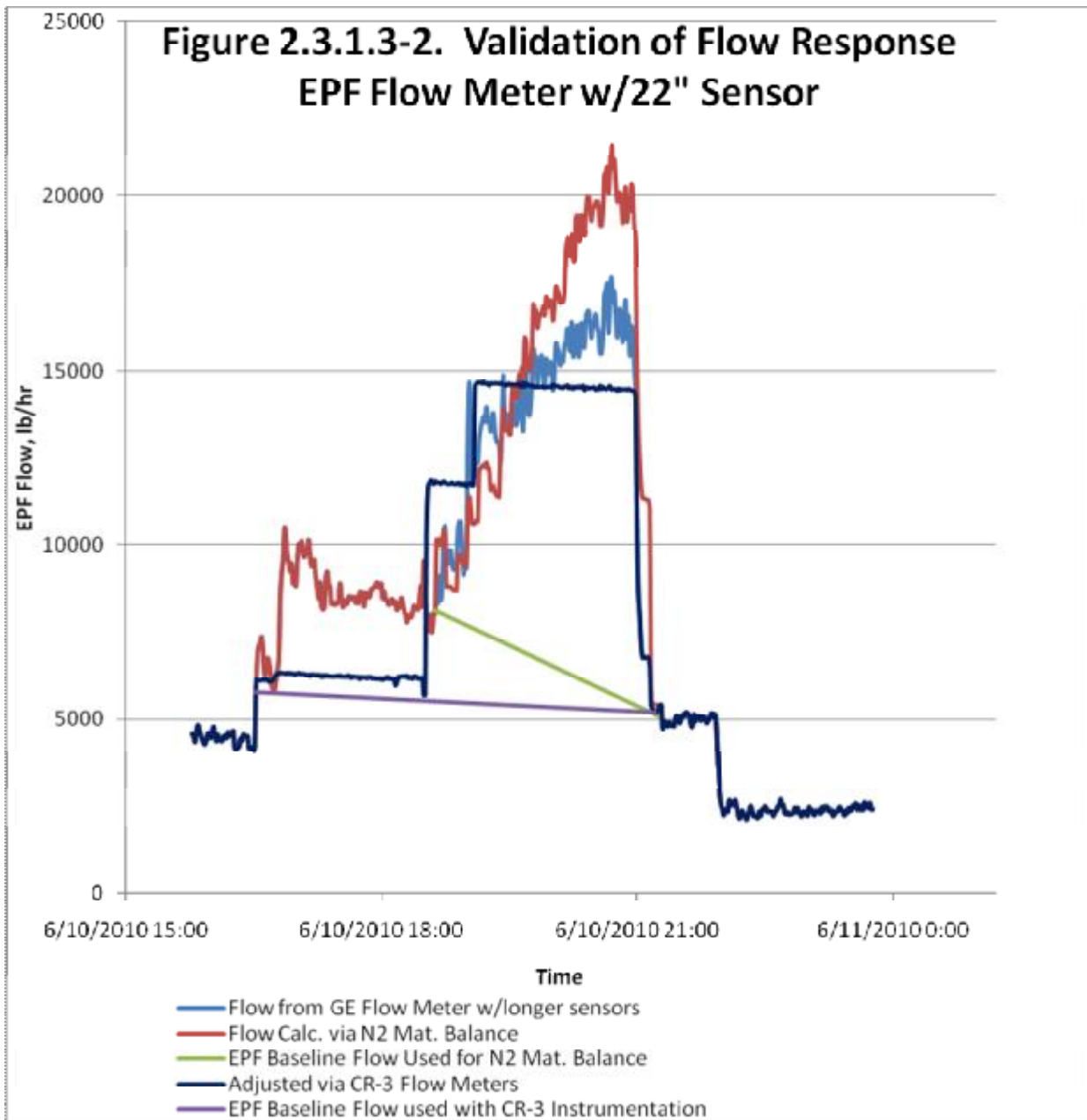
**CR-3 Process Instrumentation.** Alternatively, SDP estimated EPF flows using the same EPF baseline flow assumption -- that the base load flow remains constant or changes linearly during the N<sub>2</sub> purge cycle. Adding the N<sub>2</sub> flow add to the EPF, as measured from the CR-3 instrumentation, to the EPF estimated base flow resulted in the total vent gas flow to the EPF.

During the CR-3 regeneration cycle, flow from the CR-3 Caustic Water Wash Column (CWWC) is routed to the EPF header. This part of the regeneration cycle commences with a hydrogen purge and finishes with a nitrogen purge. The flow of H<sub>2</sub> and N<sub>2</sub> to the regeneration loop is continuously monitored by CR-3 instrumentation. Because the regeneration loop is a closed system, the amount of H<sub>2</sub> and N<sub>2</sub> being added to the loop is equivalent to the amount of gas exiting the loop to the EPF header. These flows determined from CR-3 instrumentation were used to estimate the flow from CR-3 to the EPF header.

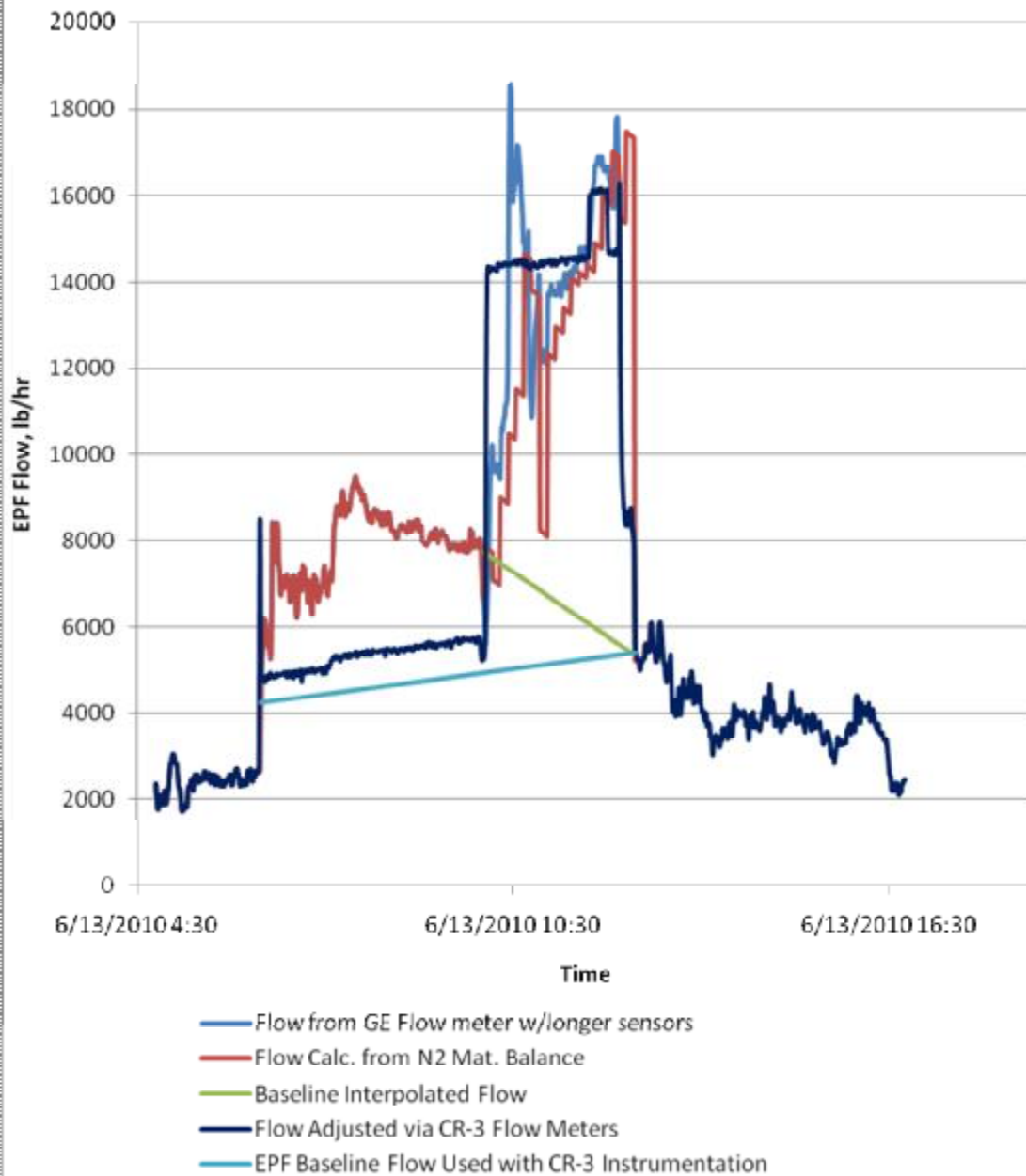
After evaluating process data for flare flows outside the purge cycle, SDP assumed that the baseline flow to the EPF header from other units varied linearly during the CR-3 regeneration cycle. SDP estimated the baseline by taking the last Panametrics flow value prior to the CWWC being opened to the flare and the flow value point after flow from the CR-3 CWWC was stopped. SDP used a linear interpolation for all intermediate baseline flow values between these two points. The total flow to the EPF was then estimated as the baseline flow plus the measured flows from the CR-3 CWWC. The flows calculated from this procedure are also illustrated on Figures 2.3.1.3-2, 2.3.1.3-3, and 2.3.1.3-4.

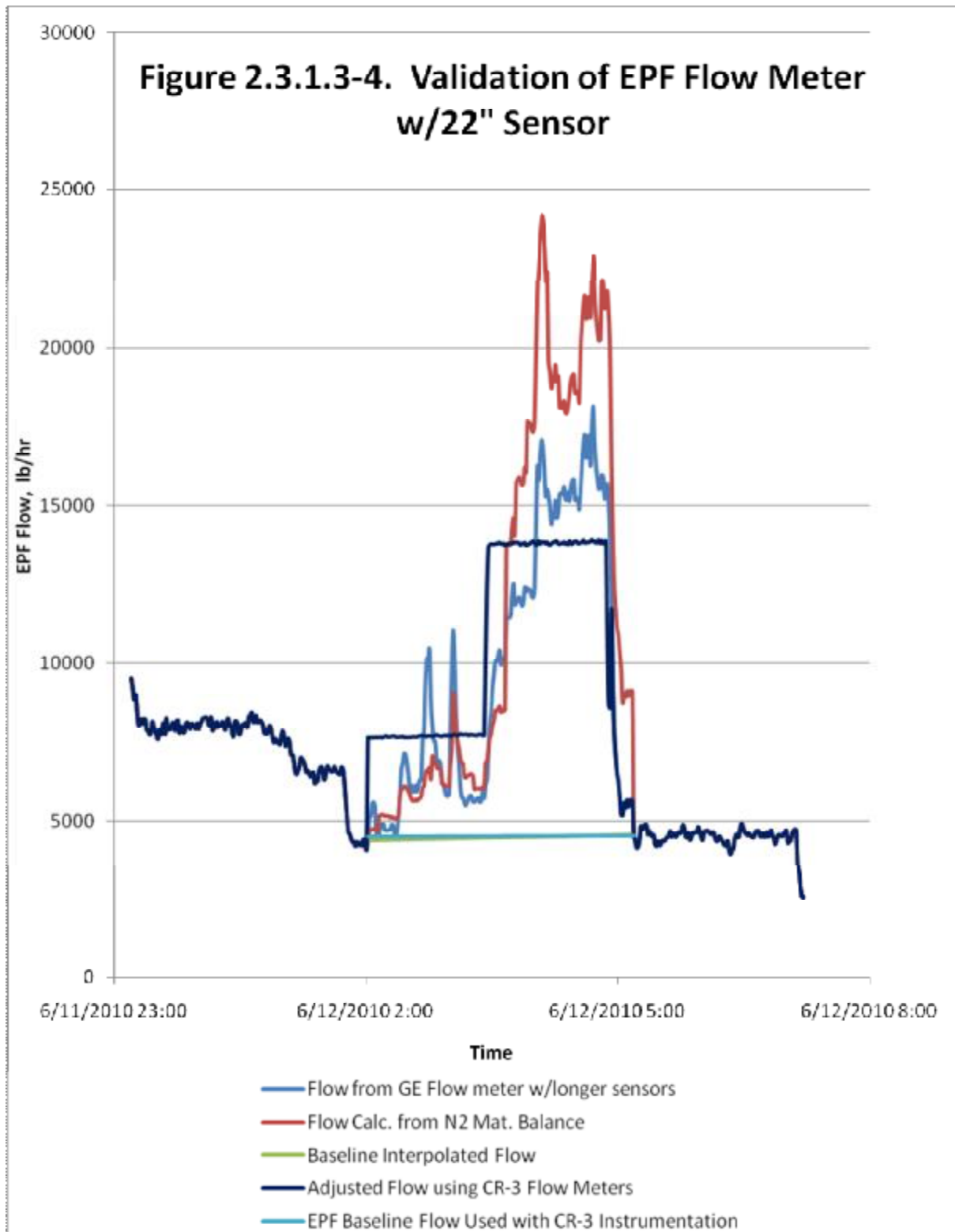
Figures 2.3.1.3-2, 2.3.1.3-3, and 2.3.1.3-4 illustrate that the EPF flows determined from the CR-3 flow instrumentation estimation are consistent with the values measured by the longer GE Panametric flow sensors. The shape of the flow curve determined from the CR-3 instrumentation is slightly more square than that observed at the sensor, and exhibits a slight time lag. This is to be expected because of the difference in measurement points. SDP also did a minute-by-minute integration for the CR-3 Instrumentation EPF flow validation method. The integrated flows were 100.2%, 101.2% and 105.6% of the flow measured by the newly installed 22" GE Panametric flow sensors.

These data indicate that the flows measured by the new sensor positioned at 22" from the top of the 36" EPF header are consistent with the flows calculated using two independent methods of estimating the EPF vent gas flow when high N<sub>2</sub> concentration are present. The EPF flow instrumentation configuration utilizing the longer sensors appears to provide representative flows in the EPF header, even under high nitrogen conditions, with acceptable accuracy (e.g. estimated to be better than  $\pm 5\%$ ).



**Figure 2.3.1.3-3. Validation of Flow Response  
EPF Flow Meter w/22" Sensor**





#### 2.3.1.4 Adjustment of EPF flows during High N<sub>2</sub> Test Periods

SDP calculated adjusted values for the test data when the nitrogen concentration in the vent gas exceeded 30v% using both the N<sub>2</sub> Material Balance method and the CR-3 Process Instrumentation method, discussed above. The N<sub>2</sub> Material Balance method gave results that were inconsistent with other measurements. During both the March 29 and April 13 tests, the average N<sub>2</sub> flow determined from the material balance method was below the flow expected based on the rate of nitrogen addition to the CR-3 process. In addition, the dilution calculated from the flows adjusted via the N<sub>2</sub> Material Balance method would have yielded incombustible mixtures, as calculated from standard mixing rules for combustible mixtures, yet the PFTIR instrumentation measured high CE values for these tests. While there is a modest level of uncertainty associated with the mixing constants used to calculate the combustion envelope for the mixture of a combustible gas with a incombustible diluent (steam), it is unlikely that the S/VG ratios and NHV<sub>CZG</sub> calculated from EPF flows calculated from the N<sub>2</sub> Material Balance method are accurate for the high nitrogen concentration tests.

For the high nitrogen cases encountered during CR-3 regenerations, using EPF flows estimated from the estimated EPF baseline flow and measured flows to the flare from the CR-3 unit yielded results that were 1) consistent with the amount of nitrogen used in the CR-3 regeneration process, 2) yielded steam to vent gas ratio when the flare was extinguished that were consistent with theoretical calculation of the onset of an incombustible mixture, and 3) were also in line with flows measured with the newly installed 22" flow sensors. SDP determined EPF flows for periods when the nitrogen concentration exceeded 30v% by adding the estimated EPF baseline flow to the flows from the CR-3 unit to the EPF, determined from CR-3 instrumentation, to determine the total flow to the EPF. Based upon the agreement of this method with the newly installed longer flow sensor, the process instrumentation at CR-3, and the fact that steam to vent gas ratios calculated from this method were consistent with when combustion theory would predict the flare to be extinguished, SDP believes that flows adjusted using the CR-3 Instrumentation Method are a reasonably accurate representation of the flow to the EPF when the nitrogen concentration in the vent gas exceeded 30%v. When the nitrogen concentration was under 30% the flows from the existing EPF flow sensor were used.

#### 2.3.2 Wind Effects and PFTIR Aiming Issues

SDP obtained 5-minute average weather data (temperature, pressure, dew point, wind direction, wind speed, relative humidity, and rainfall) from a local weather station. For each day the prevailing wind direction has been characterized by producing a wind rose for that day. These figures are presented in Appendix 5.2 along with the tabulated 5-minute average data. Recently, another refiner conducting similar PFTIR testing on another flare reported significant issues positioning the PFTIR telescope in the appropriate position to collect representative data.<sup>3</sup> These aiming issues were in large part a function of prevailing wind conditions with respect to where the PFTIR telescope could be sited. While prevailing winds and siting criteria are important considerations in developing the PFTIR test plan for conducting CE measurements of a flare, SDP encountered few problems during the testing of the EPF in positioning the PFTIR telescope to collect representative data. SDP was able to regularly aim the PFTIR telescope at a point approximately one flame length from the flare flame.

---

<sup>3</sup> *"Performance Test of a Steam-Assisted Elevated Flare with Passive FTIR,"* Marathon Petroleum Company, LLC, Texas Refining Division, 502 10<sup>th</sup> Street South, Texas City, Texas 77590, prepared by Clean Air Engineering, Inc. Project No. 10810.

Problems were reported in other studies when strong winds were directly aligned with the relative positioning of the PFTIR telescope. During the EPF tests, winds aligned with the PFTIR telescope and the EPF on only a few occasions, and on each of these occasions, winds were very light. Therefore, IMACC did not report problems aiming the telescope at the desired location in the flare plume.

### 2.3.3 PFTIR Variability - Confidence Intervals for Observed Combustion Efficiency Mean Values

SDP calculated the 95<sup>th</sup> and 99<sup>th</sup> percentile confidence intervals for the mean CE of each test. See Figures 2.3.3-1, 2.3.3-2, 2.3.3-3, 2.3.3-4 and Table 2.3.3-1, 2.3.3-2, 2.3.3-3, 2.3.3-4. These data illustrate that the variability in the observed CEs tends to be less at stable combustion conditions and high CEs, but the variability increases as combustion conditions become more unstable. At high CEs the confidence interval is generally within  $\pm 0.5\%$ , but as combustion conditions becomes more unstable the confidence interval increases up to  $\pm 50\%$ . This high degree of variability is both a function of the high degree of variability in the combustion process at these conditions and the higher degree of uncertainty in the PFTIR technique under these conditions.

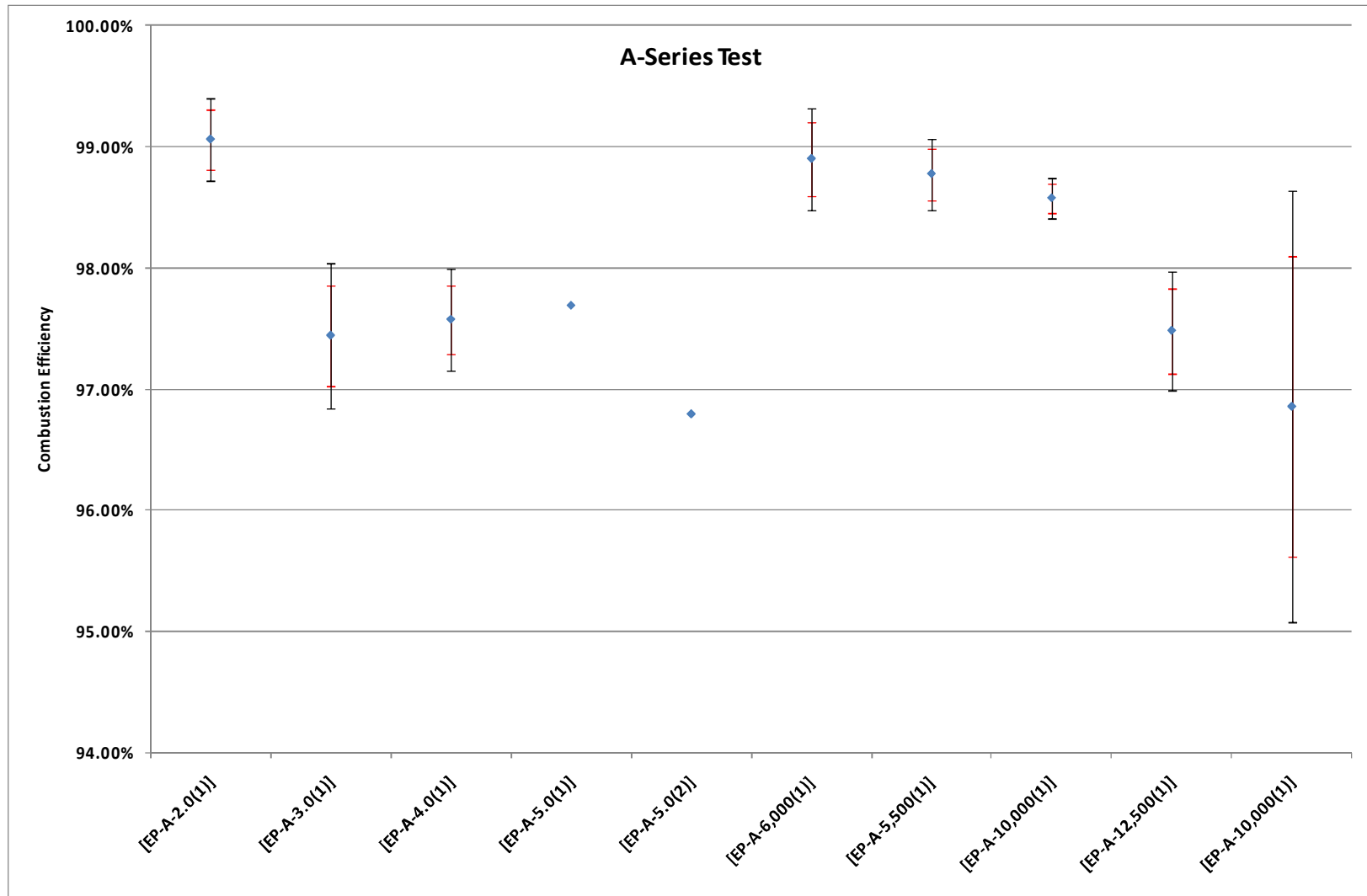


Figure 2.3.3-1. Series A Test Data Variability

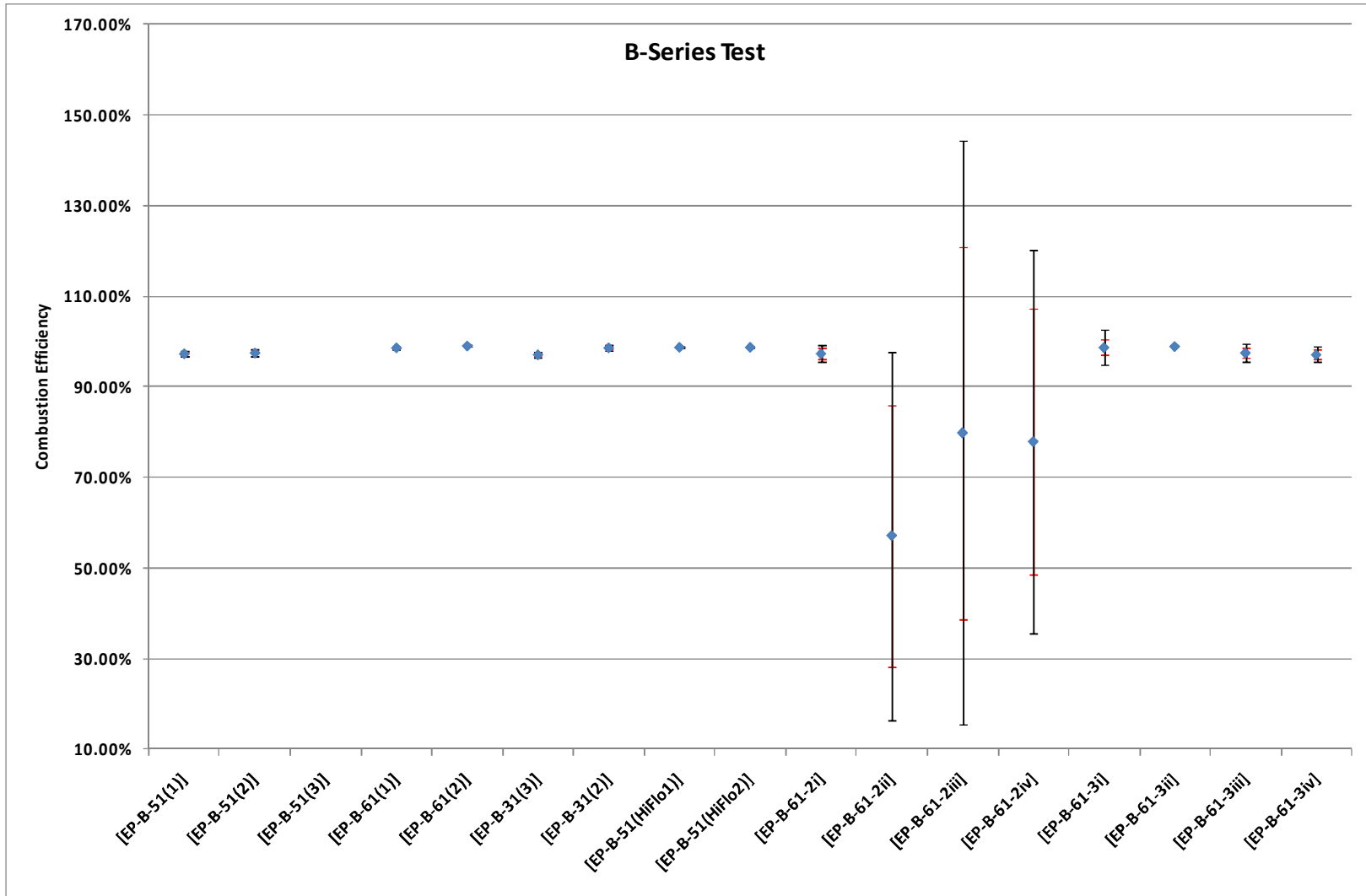


Figure 2.3.3-2. Series B Test Data Variability

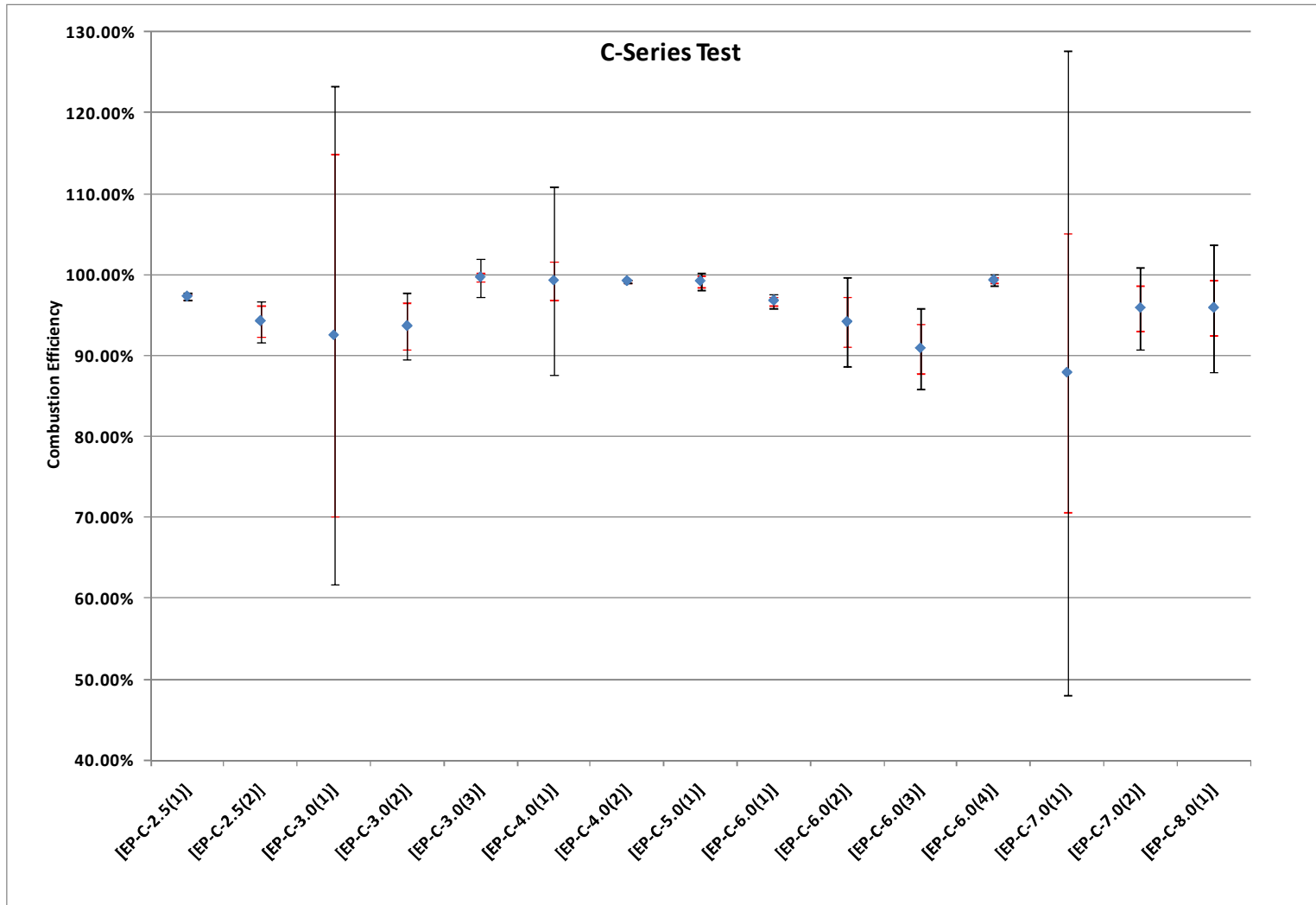


Figure 2.3.3-3. Series C Test Data Variability

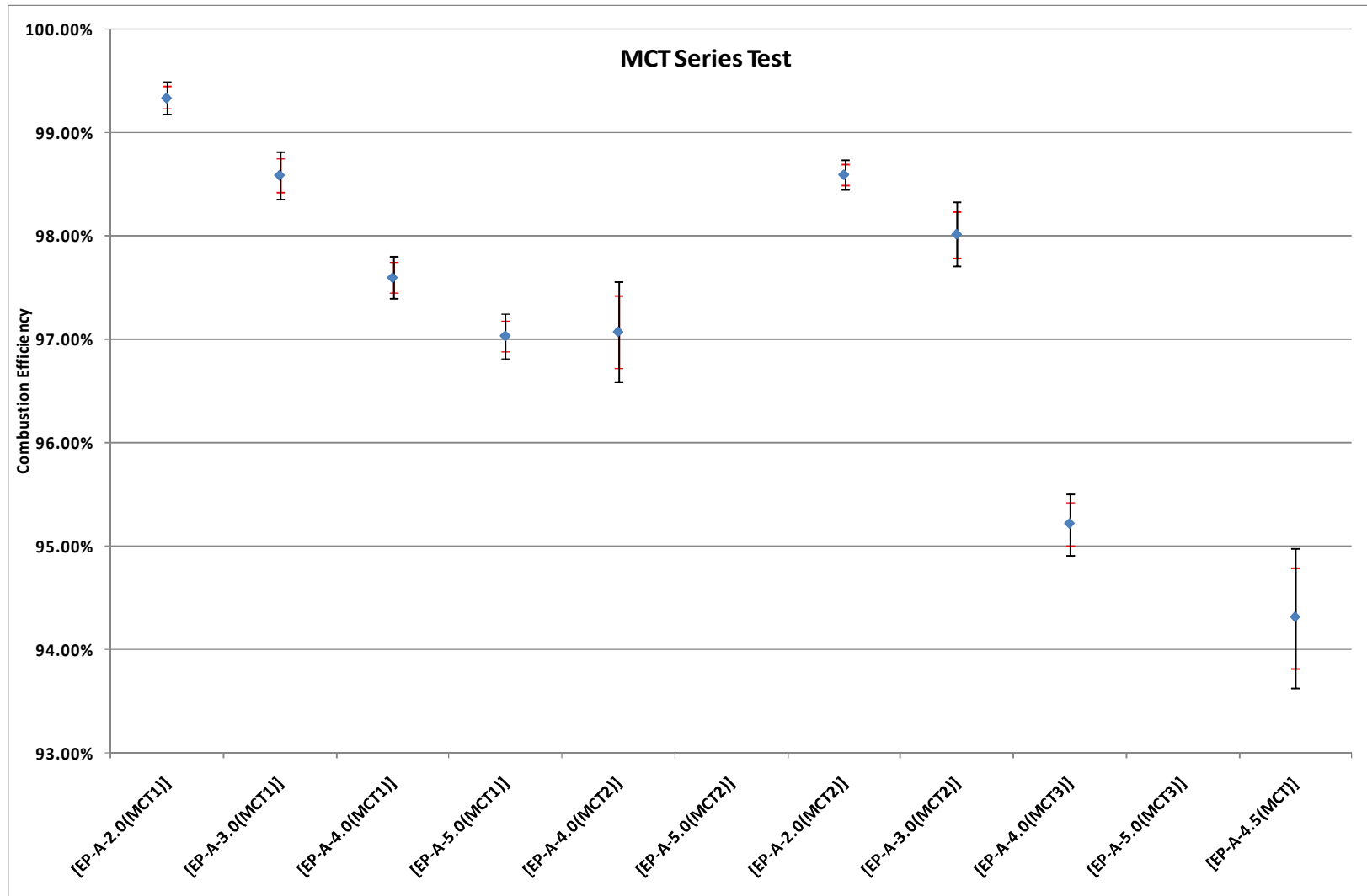


Figure 2.3.3-4. Series D Test Data Variability

Table 2.3.3-1. Series A Test Data Variability

Test Date	Test Run	Average Combustion Efficiency	95% Confidence Limit	99% Confidence Limit	Sample Size	Standard Deviation
3-29, 13:30-14:23	[EP-A-2.0(1)] *	99.06%	± 0.24%	± 0.34%	13	0.40%
3-29, 11:37-12:20	[EP-A-3.0(1)] *	97.44%	± 0.41%	± 0.59%	10	0.58%
3-29, 12:21:12:51	[EP-A-4.0(1)] *	97.57%	± 0.28%	± 0.41%	8	0.34%
3-29, 13:10-13:15	[EP-A-5.0(1)] *	97.69%	NA	NA	1	NA
3-29, 13:16-13:22	[EP-A-5.0(2)] *	96.79%	NA	NA	1	NA
4-13, 9:30-10:04	[EP-A-6,000(1)] *	98.90%	± 0.3%	± 0.41%	16	0.57%
4-13, 10:07-10:39	[EP-A-5,500(1)] *	98.77%	± 0.21%	± 0.29%	15	0.39%
4-13, 10:51-11:22	[EP-A-10,000(1)] *	98.57%	± 0.11%	± 0.16%	16	0.22%
4-13, 11:32-12:03	[EP-A-12,500(1)] *	97.48%	± 0.35%	± 0.48%	16	0.66%
4-13, 12:51-13:11	[EP-A-10,000(1)]	96.85%	± 1.24%	± 1.78%	10	1.73%

\* Vent gas flow was adjusted for this test. See discussion in Section 2.3.1.

Table 2.3.3-2. Series B Test Data Variability

Test Date	Test Run	Average Combustion Efficiency	95% Confidence Limit	99% Confidence Limit	Sample Size	Standard Deviation
3-30, 9:55-10:38	[EP-B-51(1)]	97.30%	± 0.45%	± 0.61%	18	0.91%
3-30, 10:40-11:30	[EP-B-51(2)]	97.51%	± 0.62%	± 0.86%	18	1.26%
4/1 08:48- 09:16	[EP-B-61(1)] *	98.63%	± 0.21%	± 0.3%	13	0.36%
4/1 09:17- 09:46	[EP-B-61(2)] *	99.04%	± 0.16%	± 0.22%	15	0.30%
4/1 10:17- 10:50	[EP-B-31(3)] *	97.11%	± 0.46%	± 0.64%	16	0.87%
4/1 10:51- 11:28	[EP-B-31(2)] *	98.62%	± 0.46%	± 0.63%	19	0.96%
4/1 12:32- 13:16	[EP-B-51(HiFlo1)] *	98.77%	± 0.09%	± 0.12%	22	0.21%
4/1 13:17- 13:53	[EP-B-51(HiFlo2)] *	98.76%	± 0.08%	± 0.11%	18	0.16%
4-6, 10:00-10:16	[EP-B-61-2i]	97.35%	± 1.23%	± 1.82%	8	1.47%
4-6,10:17-10:42	[EP-B-61-2ii]	57.08%	± 28.94%	± 40.58%	13	47.90%
4-6, 10:43-10:53	[EP-B-61-2iii]	79.83%	± 41.05%	± 64.4%	6	39.12%
4-6, 10:54-11:14	[EP-B-61-2iv]	77.89%	± 29.37%	± 42.19%	10	41.06%
4-6, 11:16-11:24	[EP-B-61-3i]	98.71%	± 1.68%	± 3.88%	3	0.68%
4-6, 11:32-11:49	[EP-B-61-3ii]	98.92%	NA	NA	1	NA
4-6, 11:50-11:58	[EP-B-61-3iii]	97.53%	± 1.15%	± 2.11%	4	0.72%
4-6, 11:59-12:09	[EP-B-61-3iv]	97.12%	± 1.01%	± 1.68%	5	0.82%

\* Vent gas flow was adjusted for this test. See discussion in Section 2.3.1.

Table 2.3.3-3 Series C Test Data Variability

Test Date	Test Run	Average Combustion Efficiency	95% Confidence Limit	99% Confidence Limit	Sample Size	Standard Deviation
3-22, 17:14-17:38	[EP-C-2.5(1)]	97.29%	± 0.32%	± 0.47%	9	0.28%
3-22, 17:39-19:16	[EP-C-2.5(2)]	94.25%	± 1.87%	± 2.53%	28	0.77%
3-22, 19:17-20:08	[EP-C-3.0(1)]	92.49%	± 22.44%	± 30.83%	18	22.81%
3-22, 20:09-20:39	[EP-C-3.0(2)]	93.63%	± 2.86%	± 4.16%	9	1.01%
3-24, 14:08-14:18	[EP-C-3.0(3)]	99.67%	± 0.47%	± 2.38%	2	0.05%
3-24, 14:26-14:35	[EP-C-4.0(1)]	99.27%	± 2.31%	± 11.6%	2	0.26%
3-25, 15:55-16:16	[EP-C-4.0(2)]	99.21%	± 0.12%	± 0.2%	5	0.10%
3-24.16:01-16:11	[EP-C-5.0(1)]	99.19%	± 0.63%	± 1.05%	5	0.46%
3-24.15:47-15:58	[EP-C-6.0(1)]	96.78%	± 0.52%	± 0.86%	5	0.60%
3-24, 16:20-16:31	[EP-C-6.0(2)]	94.15%	± 3.02%	± 5.55%	4	1.90%
3-24, 16:41-16:52	[EP-C-6.0(3)]	90.88%	± 3.03%	± 5.03%	5	2.44%
3-24, 16:56-17:07	[EP-C-6.0(4)]	99.33%	± 0.29%	± 0.67%	3	0.12%
3-25, 10:02-10:16	[EP-C-7.0(1)]	87.86%	± 17.26%	± 39.83%	3	6.95%
3-25, 10:20-10:32	[EP-C-7.0(2)]	95.88%	± 2.73%	± 5.02%	4	1.72%
3-25, 11:28-11:37	[EP-C-8.0(1)]	95.90%	± 3.41%	± 7.86%	3	0.79%

Table 2.3.3-4 Series D Test Data Variability

Test Date	Test Run	Average Combustion Efficiency	95% Confidence Limit	99% Confidence Limit	Sample Size	Standard Deviation
4-15, 12:44 -13:15	[EP-D-2.0(MCT1)]	99.34%	± 0.1%	± 0.15%	14	0.19%
4-15, 10:28 -10:59	[EP-D-3.0(MCT1)]	98.59%	± 0.16%	± 0.22%	14	0.28%
4-15, 11:09-11:39	[EP-D-4.0(MCT1)]	97.60%	± 0.14%	± 0.2%	14	0.25%
4-15, 11:46-12:17	[EP-D-5.0(MCT1)]	97.03%	± 0.15%	± 0.2%	14	0.26%
4-15, 13:34-14:05	[EP-D-4.0(MCT2)]	97.07%	± 0.35%	± 0.48%	15	0.63%
4-16, 10:28-11:01	[EP-D-2.0(MCT2)]	98.60%	± 0.1%	± 0.14%	16	0.20%
4-16, 11:09-11:46	[EP-D-3.0(MCT2)]	98.02%	± 0.22%	± 0.3%	18	0.45%
4-16, 11:58-12:29	[EP-D-4.0(MCT3)]	95.22%	± 0.21%	± 0.29%	15	0.39%
4-16, 13:43-14:20	[EP-D-4.5(MCT)]	94.31%	± 0.48%	± 0.67%	15	0.88%

### 2.3.4 PFTIR Component Errors

IMACC provided an error value for each species detected by the PFTIR. This error is the residual error calculated when the observed spectra obtained during the test is fit to the reference spectra using a Classical Least Squares (CLS) fitting routine. This error represents the “goodness of fit” of the observed data to the reference spectra. As such, it represents the minimum error in the measurement, not the actual error of the measurement. Other sources of

error potentially exist in selecting the reference spectra, determining the sky radiance spectrum, plume transmittance, etc. These types of systematic error can produce additional bias and uncertainty in the observed values on top of the component error present in fitting the radiance spectrum. The potential bias introduced by the aforementioned background radiance measurements is difficult to quantify, but can be significantly reduced by using the hot cell calibration method employed in this study. Any bias introduced by the determination of the background radiance should be detected during the hot cell calibration and the appropriate adjustments made as a result.

As the PFTIR data represent the mass of each component along the line of sight of the instrument, conversion to a concentration requires that a plume length be estimated. In strong winds, there can be considerable error in this value due to bending of the plume. While these effects generally will cancel out in CE calculations (e.g. same relative error in concentration determination exists in both the numerator and the denominator), the error in data expressed as a concentration can be significant due to poor path length assumptions. Consequently, the errors in data expressed as concentrations can be considerably larger than errors in data expressed as CE values.

### 2.3.5 PFTIR Hot Cell Calibration

After recent PFTIR flare testing studies, IMACC tested the PFTIR instrument in the laboratory by placing a hot cell of known path length and containing known gas composition in the PFTIR path. This method was used as a check on procedures utilized to develop the background radiance spectra. For the testing done at the Deer Park EPF, hot cell calibrations were done in the field each day as an additional check on the PFTIR data measurement protocols. In all cases, IMACC determined correction factors for each species detected from these hot cell calibrations. In most cases the results obtained from these hot cell calibrations were well within the normal EPA QA/QC acceptance protocols (e.g. 70% - 130% of the known value). However, these correction factors were applied to all spectra collected each day (e.g. applied to values within normal acceptance criteria as well as those outside the 70-130% window). This hot cell calibration step is an additional step utilized to minimize any bias and uncertainty associated with determining the background radiance parameters utilized to process the PFTIR data. A more detailed description of the hot cell calibration is available in Appendix 5.1.

### 2.3.6 Validation of Online Gas Composition Analyzers

Throughout all the test series, the online vent gas analyzers were checked by taking hourly composite vent gas samples into evacuated summa canisters. SDP had the canisters analyzed by an offsite laboratory. Analytical results for these canisters are presented in Appendix 5.3, along with the Chain of Custody documentation for these samples.

In all, SDP collected 27 summa canisters samples during the test period. Table 2.3.6-1 illustrates the agreement between the hourly composite samples analyzed at an outside laboratory and the hourly average data from the online analyzers for the same period. In all cases a small amount of air was drawn into the evacuated summa canisters, as evidenced by the bias in the oxygen and nitrogen values between the online analyzers to that of the summa canisters. In 20 of the 27 canisters, the amount of air leakage was calculated to be less than 5% of the sample. All the summa canister hydrocarbon concentration data in Table 2.3.6-1 were adjusted upward to account for the dilution of the small amount of air that was drawn into the canister. Conversely, the nitrogen and oxygen values were adjusted downward to account for the air that was drawn into the canister. For the major components ( $H_2$ ,  $N_2$ , and  $CH_4$ ) the agreement of the data was well within standard EPA QA/QC acceptance protocols (e.g. relative

difference less than  $\pm 20\%$ ) and, in fact, in most cases was much better than this. The relative difference for some of the minor components was at times somewhat greater, but these differences would have only minor impact on the combustion properties of the vent gas. Given the agreement between the online analyzers and the summa canister data, the vent gas composition data obtained from the online analyzers was used exclusively when vent gas composition data was needed.

Table 2.3.6-1. Comparison of Online Vent Gas Composition Analyzers to Summa Canister Samples

Component	Units	SPL			SPL			SPL			SPL			EPF 4345			EPF 4165			EPF 4315		
		EPF EQ2	HRVOC	Relative	EPF 4163 SN	HRVOC	Relative	EPF 3862	HRVOC	Relative	EPF 4166	HRVOC	Relative	EPF 4345	HRVOC	Relative	EPF 4165	HRVOC	Relative	EPF 4315	HRVOC	Relative
		03/22/10	03/22/10	@08:00-09:00	03/24/10	03/24/10	@14:07-15:07	03/24/10	03/24/10	@15:07-16:07	03/24/10	03/24/10	@16:07-17:07	03/25/10	03/25/10	@10:02-11:02	03/25/10	03/25/10	@11:02-12:02	03/25/10	03/25/10	@12:02-13:02
Hydrogen	MOLE%	41.53	43.65	4.86	41.53	43.65	4.86	41.20	44.37	7.15	41.66	44.47	6.32	45.43	48.56	6.43	48.62	51.52	5.63	34.93	37.96	7.99
Oxygen	MOLE%	0.04	0.04	-0.77	0.04	0.04	-0.77	0.04	0.04	-1.82	0.04	0.04	-2.13	0.02	0.02	-1.20	0.01	0.01	-0.97	0.02	0.01	-1.34
Nitrogen	MOLE%	12.25	11.27	-8.72	12.25	11.27	-8.72	12.89	11.22	-14.91	12.27	10.58	-16.02	22.13	20.92	-5.78	14.92	13.89	-7.36	41.33	38.58	-7.12
Methane	MOLE%	31.99	30.34	-5.45	31.99	30.34	-5.45	33.03	30.54	-8.15	31.32	29.75	-5.30	19.55	17.84	-9.54	22.49	20.80	-8.17	12.98	12.24	-6.03
Ethylene	MOLE%	NIL	0.00		NIL	0.00		NIL	0.00		NIL	0.00		NIL	0.00		NIL	0.00	-	NIL	0.00	
Ethane	MOLE%	3.10	2.98	-4.36	3.10	2.98	-4.36	3.14	3.07	-2.36	3.30	3.19	-3.35	3.68	3.45	-6.50	4.45	4.19	-6.08	3.73	3.62	-2.96
Acetylene	MOLE%	0.00	0.00		0.00	0.00	100.00	0.00	0.00		0.00	0.00		0.00	0.00		0.00	0.00		0.00	0.00	
Propylene	MOLE%	0.08	0.07		0.08	0.07	-13.72	0.05	0.05	-6.55	0.07	0.08	15.03	0.05	0.05	-0.21	0.05	0.05	10.70	0.02	0.03	43.38
Propane	MOLE%	2.36	2.27	-3.99	2.36	2.27	-3.99	2.04	2.33	12.22	2.29	2.51	8.62	1.94	2.10	7.76	1.96	2.15	8.81	1.72	1.94	11.29
Butene1&Isobutane	MOLE%	0.00	0.11	100.00	0.00	0.11	100.00	0.00	0.09	100.00	0.00	0.15	100.00	0.00	0.03	100.00	0.00	0.03	100.00	0.00	0.02	100.00
Trans2Butene	MOLE%	0.00	0.05		0.00	0.05	100.00	0.00	0.05	100.00	0.00	0.08	100.00	0.00	0.00		0.00	0.00		0.00	0.00	
Cis2Butene	MOLE%	0.00	0.04		0.00	0.04	100.00	0.00	0.04	100.00	0.00	0.07	100.00	0.00	0.00		0.00	0.00		0.00	0.00	
13BD	MOLE%	0.00	0.00		0.00	0.00		0.00	0.00		0.00	0.00		0.00	0.00		0.00	0.00		0.00	0.00	
IsoButane	MOLE%	1.22	1.10	-11.41	1.22	1.10	-11.41	1.04	1.11	5.77	1.22	1.26	3.24	1.00	1.02	2.28	1.00	1.02	2.04	0.77	0.82	6.15
Butane	MOLE%	0.00	0.90	100.00	0.00	0.90	100.00	0.00	0.93	100.00	0.00	1.06	100.00	0.00	0.87	100.00	0.00	0.88	100.00	0.00	0.73	100.00
C5+	MOLE%	0.00	3.92	100.00	0.00	3.92	100.00	0.00	2.73	100.00	0.00	3.01	100.00	0.00	3.01	100.00	0.00	3.34	100.00	0.00	2.41	100.00
Hydrogen Sulfide	MOLE%	2.41	1.71	-40.86	2.41	1.71	-40.86	2.37	1.74	-36.52	2.89	2.11	-37.16	2.50	1.58	-58.62	2.66	1.56	-70.76	1.61	1.20	-34.78
Water	MOLE%	0.00	0.00		0.00	0.00	100.00	0.00	0.00		0.00	0.00		0.00	0.00		0.00	0.00		0.00	0.00	
Carbon Dioxide	MOLE%	1.23	1.17	-5.35	1.23	1.17	-5.35	1.25	1.16	-7.06	1.17	1.08	-7.50	0.59	0.56	-5.87	0.59	0.56	-5.09	0.44	0.43	-3.49
Carbon Monoxide	MOLE%	0.00	0.00		0.00	0.00	100.00	0.00	0.00		0.00	0.00		0.00	0.00		0.00	0.00		0.00	0.00	
Benzene	MOLE%	0.53	0.35		0.53	0.35	-51.52	0.36	0.35	-2.06	0.45	0.35	-27.79	0.44	0.36	-22.44	0.45	0.35	-28.40	0.40	0.32	-26.36
Toluene	MOLE%	0.11	0.14		0.11	0.14	19.30	0.07	0.14	49.12	0.10	0.15	31.27	0.09	0.12	29.44	0.10	0.15	32.54	0.07	0.12	41.63
Ethylbenzene	MOLE%	0.01	0.01		0.01	0.01	54.36	0.00	0.01	73.67	0.00	0.01	67.99	0.00	0.01	64.00	0.00	0.01	67.79	0.00	0.01	66.93
Xylene's	MOLE%	0.02	0.01		0.02	0.01	-52.18	0.01	0.01	10.17	0.02	0.02	-14.65	0.01	0.02	6.23	0.02	0.02	-12.00	0.01	0.01	8.09
Air Ingress	v%		30.6%			0.8%			1.8%			2.1%			1.2%			1.0%			1.3%	

Table 2.3.6-1. Comparison of Online Vent Gas Composition Analyzers to Summa Canister Samples (cont'd)

Component	Units	SPL			SPL			SPL			SPL			SPL			SPL			SPL		
		EPF 4402		Relative	EPF 3861		Relative	EPF 1144		Relative	EPF 3621		Relative	EPF 1149		Relative	EPF 1143		Relative	EPF 3622		Relative
		HRVOC	HRVOC		HRVOC	HRVOC		HRVOC	HRVOC		HRVOC	HRVOC		HRVOC	HRVOC		HRVOC	HRVOC		HRVOC	HRVOC	
		03/25/10	03/25/10	@ 09:29-	03/30/10	03/30/10	@ 09:29-	03/30/10	03/30/10	@ 09:12-	04/01/10	04/01/10	@ 09:12-	04/01/10	04/01/10	@ 10:17-	04/01/10	04/01/10	@ 12:42-	04/01/10	04/01/10	@ 09:45-
		14:50	14:50	accuracy	10:29	10:29	accuracy	11:42	11:42	accuracy	09:45	09:45	precision	11:27	11:27	precision	13:40	@ 12:42-	precision	10:45	10:45	precision
Hydrogen	MOLE%	21.93	24.02	8.72	50.45	57.18	11.77	51.78	57.12	9.34	51.53	61.77	16.58	31.42	36.31	13.48	45.28	51.11	11.41	53.56	61.10	12.34
Oxygen	MOLE%	0.01	0.01	-1.63	0.05	0.05	-4.72	0.07	0.07	-3.35	0.01	0.01	-13.99	0.02	0.02	-1.27	0.02	0.02	-2.45	0.04	0.04	-1.89
Nitrogen	MOLE%	53.00	50.30	-5.37	15.19	13.67	-11.11	15.09	13.28	-13.67	23.78	12.96	-83.56	49.59	46.33	-7.04	35.33	32.54	-8.58	16.35	14.70	-11.23
Methane	MOLE%	17.87	17.57	-1.70	12.83	10.87	-18.04	11.81	10.90	-8.38	10.94	11.59	5.58	7.08	6.79	-4.39	6.22	5.48	-13.44	11.90	10.59	-12.45
Ethylene	MOLE%	NIL	0.00	-	0.08	0.00	-21441.66	0.07	0.00	-9384.82	0.09	0.00	-17420.07	0.81	0.00	-68927.29	1.13	0.00	-70995.90	0.98	0.00	-23971.33
Ethane	MOLE%	1.82	1.89	3.81	4.02	3.94	-2.04	4.02	3.87	-3.84	4.14	4.15	0.23	2.32	2.29	-1.40	2.11	2.00	-5.52	3.20	3.10	-3.04
Acetylene	MOLE%	0.00	0.00	-	0.00	0.00	-	0.00	0.00	-	0.00	0.00	-	0.00	0.00	-	0.00	0.00	-	0.00	0.00	-
Propylene	MOLE%	0.02	0.03	28.78	0.06	0.04	-31.03	0.05	0.05	-19.00	0.04	0.04	-14.37	0.30	0.04	-597.62	0.42	0.05	-666.95	0.42	0.06	-646.71
Propane	MOLE%	1.26	1.47	13.88	3.61	3.11	-16.13	3.48	3.12	-11.53	2.94	2.62	-12.02	2.11	1.94	-8.68	2.08	1.84	-12.78	2.42	2.24	-8.09
Butene1&Isobutane	MOLE%	0.00	0.01	100.00	0.00	0.04	100.00	0.00	0.04	100.00	0.00	0.02	100.00	0.00	0.03	100.00	0.00	0.03	100.00	0.00	0.02	100.00
Trans2Butene	MOLE%	0.00	0.00	-	0.00	0.00	-	0.00	0.00	100.00	0.00	0.00	-	0.00	0.00	100.00	0.00	0.00	-	0.00	0.00	-
Cis2Butene	MOLE%	0.00	0.00	-	0.00	0.00	-	0.00	0.00	-	0.00	0.00	-	0.00	0.00	-	0.00	0.00	-	0.00	0.00	-
13BD	MOLE%	0.00	0.00	-	0.00	0.00	-	0.00	0.00	-	0.00	0.00	-	0.00	0.00	-	0.00	0.00	-	0.00	0.00	-
IsoButane	MOLE%	0.53	0.59	9.82	1.77	1.49	-19.00	1.71	1.42	-20.30	0.80	0.75	-6.86	0.82	0.70	-16.21	0.87	0.72	-19.82	1.12	0.84	-32.91
Butane	MOLE%	0.00	0.53	100.00	0.00	1.33	100.00	0.00	1.29	100.00	0.00	0.69	100.00	0.00	0.67	100.00	0.00	0.56	100.00	0.00	0.76	100.00
C5+	MOLE%	0.00	2.07	100.00	0.00	4.86	100.00	0.00	5.48	100.00	0.00	2.96	100.00	0.00	2.85	100.00	0.00	3.64	100.00	0.00	2.94	100.00
Hydrogen Sulfide	MOLE%	0.97	0.93	-5.16	5.05	2.54	-98.69	5.34	2.49	-114.03	1.68	1.81	7.26	1.85	1.51	-22.58	2.61	1.53	-71.05	5.30	2.53	-109.98
Water	MOLE%	0.00	0.00	-	0.00	0.00	-	0.00	0.00	-	0.00	0.03	100.00	0.00	0.00	-	0.00	0.00	-	0.00	0.02	100.00
Carbon Dioxide	MOLE%	0.57	0.56	-1.81	0.90	0.87	-3.48	0.93	0.87	-7.28	0.50	0.61	17.67	0.50	0.48	-3.45	0.46	0.44	-4.58	1.05	1.02	-3.10
Carbon Monoxide	MOLE%	0.00	0.00	-	0.00	0.00	-	0.00	0.00	-	0.00	0.00	-	0.00	0.00	-	0.00	0.00	-	0.00	0.00	-
Benzene	MOLE%	0.37	0.30	-23.62	0.78	0.73	-7.28	0.70	0.79	10.55	0.60	0.61	2.97	0.56	0.65	14.00	0.55	0.60	8.27	0.60	0.67	9.42
Toluene	MOLE%	0.07	0.10	30.16	0.17	0.27	38.43	0.13	0.29	55.77	0.16	0.27	42.29	0.11	0.26	56.15	0.18	0.27	32.30	0.09	0.19	51.57
Ethylbenzene	MOLE%	0.00	0.01	63.02	0.02	0.03	44.30	0.01	0.03	63.93	0.04	0.05	15.79	0.02	0.00	-	0.04	0.04	10.54	0.02	0.04	53.94
Xylene's	MOLE%	0.01	0.01	-17.87	0.08	0.00	-	0.00	0.00	-	0.22	0.00	-	0.10	0.00	-	0.06	0.00	-	0.08	0.00	-
Air Ingress	v%		1.6%	-		4.5%	-		0.03	-		12.3%	-		0.01	-		2.4%	-		0.02	-

Table 2.3.6-1. Comparison of Online Vent Gas Composition Analyzers to Summa Canister Samples (cont'd)

Component	Units	SPL			SPL			SPL			SPL			SPL			SPL			SPL		
		EPF 3857	HRVOC	Relative	EPF EQ-16	HRVOC	Relative	EPF EQ-12	HRVOC	Relative	EPF EQ-22	HRVOC	relative	EPF EQ-4	HRVOC	Relative	EPF EQ 20	HRVOC	Relative	EPF EQ9	HRVOC	Relative
		04/06/10	04/06/10		04/07/10	04/07/10		04/07/10	04/07/10		04/07/10	04/07/10		04/07/10	04/07/10		04/07/10	04/07/10		04/07/10	04/13/10	
Hydrogen	MOLE%	54.37	60.97	10.83	7.16	25.03	71.41	24.99	28.33	11.80	27.27	28.33	3.76	9.53	39.81	76.06	33.94	36.33	6.58	22.08	25.06	11.91
Oxygen	MOLE%	0.05	0.05	-4.56	0.02	0.02	-14.48	0.02	0.02	-3.45	0.02	0.02	-0.49	0.03	0.02	-47.85	0.01	0.01	-6.74	0.01	0.01	-1.40
Nitrogen	MOLE%	17.10	14.66	-16.64	64.35	32.28	-99.34	48.43	44.69	-8.38	44.56	44.69	0.30	53.94	36.54	-47.60	34.64	32.70	-5.91	54.40	50.17	-8.42
Methane	MOLE%	11.30	10.58	-6.77	16.70	15.29	-9.22	18.75	18.85	0.53	18.46	18.85	2.07	15.94	14.36	-10.96	21.28	20.91	-1.77	17.29	17.62	1.87
Ethylene	MOLE%	0.03	0.00	-695.60	0.00	0.00		0.00	0.00		0.06	0.00		0.00	0.00	100.00	NIL	0.01		NIL	0.00	
Ethane	MOLE%	3.27	3.09	-5.77	0.59	1.85	68.20	1.86	2.06	9.78	2.60	2.06	-26.07	3.34	2.55	-31.22	3.18	3.23	1.47	1.61	1.96	18.08
Acetylene	MOLE%	0.00	0.00		0.00	0.00		0.00	0.00		0.00	0.00		0.00	0.00		0.00	0.00		0.00	0.00	
Propylene	MOLE%	0.05	0.06	11.49	0.03	0.02	-48.69	0.02	0.02	2.32	0.29	0.02	-1201.30	0.08	0.04	-115.68	0.02	0.02	7.98	0.02	0.03	17.97
Propane	MOLE%	2.45	2.25	-8.65	1.38	1.27	-8.19	1.41	1.62	12.67	1.81	1.62	-11.67	2.49	1.96	-27.45	2.35	2.56	7.94	1.34	1.65	18.69
Butene1&Isobutane	MOLE%	0.00	0.02	100.00	0.00	0.01	100.00	0.00	0.01	100.00	0.00	0.01	100.00	0.00	0.01	100.00	0.00	0.01	100.00	0.00	0.00	100.00
Trans2Butene	MOLE%	0.00	0.00		0.00	0.00		0.00	0.00		0.00	0.00		0.00	0.00		0.00	0.00		0.00	0.00	
Cis2Butene	MOLE%	0.00	0.00		0.00	0.00		0.00	0.00		0.00	0.00		0.00	0.00		0.00	0.00		0.00	0.00	
13BD	MOLE%	0.00	0.00		0.00	0.00		0.00	0.00		0.00	0.00		0.00	0.00		0.00	0.00		0.00	0.00	
IsoButane	MOLE%	1.11	0.85	-31.40	0.53	0.46	-15.32	0.57	0.59	3.39	0.59	0.59	-0.47	0.89	0.66	-35.18	0.66	0.63	-3.64	0.46	0.47	2.59
Butane	MOLE%	0.00	0.76	100.00	0.00	0.39	100.00	0.00	0.55	100.00	0.00	0.55	100.00	0.00	0.59	100.00	0.00	0.55	100.00	0.00	0.36	100.00
CS+	MOLE%	0.00	3.11	100.00	0.00	1.17	100.00	0.00	1.29	100.00	0.00	1.29	100.00	0.00	1.51	100.00	0.00	1.06	100.00	0.00	0.90	100.00
Hydrogen Sulfide	MOLE%	5.41	2.48	-117.79	1.37	0.97	-41.34	1.27	1.10	-14.79	1.49	1.10	-34.81	1.53	1.28	-19.55	1.40	1.19	-17.32	0.78	1.01	22.36
Water	MOLE%	0.00	0.02	100.00	0.00	0.12	100.00	0.00	0.21	100.00	0.00	0.21	100.00	0.00	0.13	100.00	0.00	0.11	100.00	0.00	0.14	100.00
Carbon Dioxide	MOLE%	1.10	1.05	-5.35	6.49	0.50	-1187.95	0.64	0.63	-0.86	0.62	0.63	2.18	8.60	0.51	-1579.69	0.69	0.68	-2.17	0.61	0.61	0.39
Carbon Monoxide	MOLE%	0.00	0.00		0.00	0.00		0.00	0.00		0.00	0.00		0.00	0.00		0.00	0.00		0.00	0.00	
Benzene	MOLE%	0.68	0.71	3.56	0.17	0.00		0.39	0.00		0.39	0.00		0.45	0.00		0.29	0.41	28.49	0.33	0.34	3.34
Toluene	MOLE%	0.11	0.21	46.23	0.02	0.00		0.06	0.00		0.11	0.00		0.10	0.00		0.09	0.17	48.15	0.04	0.09	59.93
Ethylbenzene	MOLE%	0.02	0.04	44.90	0.00	0.00		0.01	0.00		0.01	0.00		0.04	0.00		0.01	0.05	83.32	0.01	0.05	86.62
Xylene's	MOLE%	0.11	0.00		0.03	0.00		0.04	0.00		0.09	0.00		0.23	0.00		0.05	0.00		0.03	0.00	
Air Ingress	v%		0.04			0.13			0.03			0.00			0.32			0.06			0.01	

Table 2.3.6-1. Comparison of Online Vent Gas Composition Analyzers to Summa Canister Samples (cont'd)

Component	Units	SPL EPF EQ 23			SPL EPF 2912			SPL DPEPF 3864			SPL DPEPF EQ12			SPL DPEPF 1143			SPL DPEPF 3861		
		HRVOC	HRVOC	relative	HRVOC	HRVOC	Relative	HRVOC	HRVOC	Relative	HRVOC	HRVOC	Relative	HRVOC	HRVOC	relative	HRVOC	HRVOC	Relative
		04/13/10	04/13/10	precision	04/13/10	04/13/10	precision	04/16/10	04/16/10	precision									
		10:37-	10:37-		11:32-	11:32-	@ 10:48-	@ 10:48-		@ 11:58-	@ 11:58-		@ 12:59-	@ 12:59-		@ 13:40-	@ 13:40-		
		11:29	11:29		12:30	12:30	11:46	11:46	precision	12:58	12:58	precision	13:36	13:36	precision	14:27	14:27	precision	
Hydrogen	MOLE%	18.77	21.24	11.60	19.35	24.87	22.18	49.41	54.50	9.34	48.61	55.52	12.44	49.38	54.56	9.50	49.02	55.15	11.11
Oxygen	MOLE%	0.03	0.03	-10.31	0.01	0.01	-1.08	0.04	0.04	-3.33	0.03	0.03	-1.27	0.04	0.04	-11.87	0.03	0.03	-1.25
Nitrogen	MOLE%	50.01	49.18	-1.69	45.96	36.23	-26.87	23.83	23.01	-3.56	25.36	22.40	-13.21	26.40	22.73	-16.14	25.13	22.41	-12.14
Methane	MOLE%	25.18	23.84	-5.62	26.04	32.15	19.01	9.61	8.78	-9.53	9.07	8.91	-1.88	9.15	8.90	-2.74	9.35	9.15	-2.21
Ethylene	MOLE%	0.08	0.00		2.19	0.00		NIL	0.00		0.06	0.00		NIL	0.00		0.04	0.00	
Ethane	MOLE%	1.30	1.35	4.26	1.38	1.58	12.56	3.26	3.03	-7.51	3.07	3.18	3.62	3.10	3.19	2.75	3.28	3.25	-0.77
Acetylene	MOLE%	0.00	0.00		0.00	0.00		0.00	0.00		0.00	0.00		0.00	0.00		0.00	0.00	
Propylene	MOLE%	0.39	0.01	-2822.03	0.81	0.01	-15914.81	NIL	0.10		0.12	0.01	-778.24	NIL	0.01		0.03	0.01	-154.70
Propane	MOLE%	0.95	1.05	9.58	0.94	1.13	16.74	2.40	2.63	8.70	2.86	2.26	-26.64	3.40	3.02	-12.71	2.52	2.26	-11.57
Butene1&Isobutane	MOLE%	0.00	0.00		0.00	0.00		0.00	0.00		0.00	0.00		0.00	0.00		0.00	0.00	
Trans2Butene	MOLE%	0.00	0.00		0.00	0.00		0.00	0.00		0.00	0.00		0.00	0.00		0.00	0.00	
Cis2Butene	MOLE%	0.00	0.00		0.00	0.00		0.00	0.00		0.00	0.00		0.00	0.00		0.00	0.00	
13BD	MOLE%	0.00	0.00		0.00	0.00		0.00	0.00		0.00	0.00		0.00	0.00		0.00	0.00	
IsoButane	MOLE%	0.41	0.41	-0.06	0.40	0.48	16.10	1.04	0.93	-11.77	1.08	0.93	-17.20	1.04	0.91	-14.18	1.06	0.91	-16.00
Butane	MOLE%	0.00	0.29	100.00	0.00	0.33	100.00	0.00	0.65	100.00	0.00	0.65	100.00	0.00	0.63	100.00	0.00	0.63	100.00
C5+	MOLE%	0.00	0.89	100.00	0.00	1.05	100.00	0.00	2.38	100.00	0.00	2.28	100.00	0.00	2.09	100.00	0.00	2.13	100.00
Hydrogen Sulfide	MOLE%	0.80	0.92	13.40	0.86	1.12	23.60	6.08	2.89	-110.09	5.10	2.79	-82.85	3.17	2.85	-11.19	5.19	3.03	-71.34
Water	MOLE%	0.00	0.06	100.00	0.00	0.14	100.00	0.00	0.00		0.00	0.00		0.00	0.00		0.00	0.00	
Carbon Dioxide	MOLE%	0.72	0.70	-1.86	0.73	0.92	20.33	1.04	1.06	2.23	1.07	1.04	-2.62	1.09	1.06	-2.44	1.07	1.04	-2.96
Carbon Monoxide	MOLE%	0.00	0.00		0.00	0.00		0.00	0.00		0.00	0.00		0.00	0.00		0.00	0.00	
Benzene	MOLE%	0.31	0.35	11.55	0.34	0.40	13.13	0.70	0.71	2.31	0.81	0.72	-13.29	0.79	0.70	-13.44	0.72	0.67	-6.70
Toluene	MOLE%	0.04	0.07	50.13	0.04	0.09	60.09	0.09	0.17	45.39	0.10	0.18	44.48	0.08	0.18	53.79	0.09	0.17	47.55
Ethylbenzene	MOLE%	0.01	0.02	75.79	0.01	0.02	68.35	0.02	0.04	48.55	0.02	0.04	53.85	0.01	0.04	60.59	0.02	0.04	53.91
Xylene's	MOLE%	0.03	0.00		0.03	0.00		0.09	0.00		0.08	0.00		0.07	0.00		0.08	0.00	
Air Ingress	v%		0.09			0.01			0.03			0.01			0.11			0.01	

### 2.3.7 Potential Impacts of Integrated Sampling

Previous studies conducted to assess flare CEs have cited the need to sample the entire plume envelope, both radially and axially, in order to obtain representative CE values.<sup>4,5</sup> The PFTIR instrumentation does not sample the entire flare plume, but instead analyzes only one small section of the plume at a time. However, because the flare flame is turbulent and subject to interactions with the wind, the PFTIR is randomly sampling different areas of the hot plume on a continuous basis. The inhomogeneous nature of the flare plume may be more apparent near the flame envelope and perhaps less apparent at greater distances from the flame (e.g. opportunity for burn out increases). However, at greater distances from the flame, lower temperatures can also increase the variability of the observed results due to the lower IR signal strength. A comprehensive treatment of this issue is beyond the scope of this investigation and might be addressed in the future in more controlled test environments to assess the optimal distance from the flame tip to aim the PFTIR telescope, such that the signal strength can be maximized but artifacts due to flame heterogeneity can be minimized.

### 2.3.8 Accuracy of Combustion Efficiency Measurements at Unstable Combustion Conditions

During several of the test runs at high S/VG ratio, when the EPF was approaching unstable operation (e.g. pulsating both visually and audibly), unexpectedly high CEs (90- 97%) were observed from the PFTIR instrumentation. The Testing Team hypothesized that the PFTIR data collection algorithm might be leading to unrepresentatively high CEs under these conditions.

The PFTIR instrument collects a spectrum every second. If the instrument QA/QC parameters for that scan are acceptable (signal to noise ratio, signal strength, etc.), the spectrum is recorded. If an invalid spectrum is obtained, it is discarded. This continues until 82 valid spectra are recorded. When the flare starts to pulse, valid spectra can be recorded when combustible packets of vent gas are present, but no data is recorded when an incombustible packet is present. Data is not recorded under these conditions because no usable signal is received by the PFTIR instrument and the instrument QA/QC parameters are not met.

This pulsing can be seen in the GasFindIR video recorded under these conditions. A combustible packet is characterized by a bright flash from the heat signature of the combusting gas. This flash disappears completely or almost completely when an incombustible packet of gas appears at the flare tip. Because IMACC does not collect data on the number of valid spectra recorded per the number of spectra attempted, there was no way to recover data on the frequency and duration of invalid spectra.

There are reasons other than the presence of incombustible gas that could cause a spectrum to fail the QA/QC protocol. However, it is conceivable that if the frequency and duration of incombustible gas packets was consistent and persistent, the PFTIR instrument could have

---

<sup>4</sup> Pohl, J.H., R. Payne and J. Lee, "Evaluation of the Efficiency of Industrial Flares: Test Result," United States Environmental Protection Agency, Office of Air Quality Planning and Standards, EPA-600/2-84-095, May 1984.

<sup>5</sup> M. McDaniel, US EPA/600-2-83-052, Flare Efficiency Study. Engineering-Science, Inc., July 1983.

recorded a high CE based upon the limited data that passed the spectral QA/QC protocols, even if these data represented only a smaller percentage of all spectral scans attempted. It is possible that the greater degree of variability observed at high S/VG ratios is a function of the PFTIR being unable to adequately integrate these low combustion periods into the results.

## 2.4 Conclusions

The EPF vent gas typically contains large quantities of hydrogen, low molecular weight paraffinic hydrocarbons, nitrogen, and low concentrations of aromatic hydrocarbons. No visible emissions were detected during the testing.

High CEs were observed over a wide range of S/VG ratios. CEs in excess of 98.0% were obtained up to S/VG ratios approaching 6 lb steam/lb vent gas. However, due to the large variation in vent gas composition observed at the EPF, CEs below 98.0% were occasionally observed at S/VG ratios of less than 1.0 lb steam/lb vent gas (i.e. test conditions with nitrogen concentrations in excess of 30 v%).  $NHV_{czg}$  exhibited a more consistent relationship with CE than either S/VG ratio or vent gas composition alone.  $NHV_{czg}$  is calculated as the volumetric dilution of all process gases going to the flare tip (e.g. vent gas, steam, and pilot gas).

Based upon the detector comparison work during this study, the greater sensitivity of the InSb detector for hydrocarbons, and the ability of the MCT detector to estimate plume temperature via fitting  $CO_2$  concentrations in multiple spectral regions; it may be advantageous during future PFTIR flare work to have a beam splitter that would allow the simultaneous use of both the InSb and MCT detector.

### **3. PFTIR Testing Methods and Procedures**

#### **3.1 Description and Principles of Passive FTIR Measurements**

The gas composition data presented in this report was generated by measuring flare radiances with a PFTIR instrument. PFTIR analysis operates on the principle of spectral analysis of thermal radiation emitted by hot gases.

In normal absorption spectroscopy, light is passed through a region containing gas to be analyzed, and the transmitted light is spread out into a spectrum using an interferometer (FTIR) or a spectrometer. In this spectrum, the presence of specific compounds can be determined from the patterns of light absorbed while the compound's concentrations can be measured from the intensity of the patterns. The low energy of infrared light is absorbed by molecular species causing them to vibrate and rotate faster. Because each molecule consists of a unique structure of bound atoms, the patterns of infrared wavelengths (IR colors) absorbed by a molecule are also unique. These molecular "finger prints" are used in the infrared analysis of gases.

In PFTIR analysis, there is no "active" infrared light source, as used in standard absorption infrared spectroscopy. Instead the hot gases of the flare are the infrared source. The spectrometer is a receiver only. This approach is possible because the infrared radiation emitted by hot gases has the same patterns or fingerprints as the absorption spectra for those gases. Consequently, like absorption spectroscopy, observing a flare with a passive infrared instrument allows for identification and quantification of species through emission spectroscopy. However, there is one main difference: the signature arising from a hot gas is proportional to the gas' concentration and to its temperature. Therefore, to accurately take emission or radiance measurements, the temperature must be deduced in addition to the gas concentrations. A detailed explanation of the temperature determination method utilized for this testing is presented in Appendix 5.1.

Consequently, unlike absorption spectroscopy, the PFTIR signal must be calibrated in absolute units of radiance. This requires that the instrument be calibrated utilizing an IR source of known spectral radiance. This calibration is accomplished with a commercial black body calibrator. This calibrator produces a known radiance IR distribution as predicted by the Planck function. Details of this calibration are provided in Appendix 5.1.

Dr. Curtis Laush of IMACC conducted the PFTIR operation and data analysis for this test program. IMACC developed the PFTIR instrument and the analytical software used in this study.

#### **3.2 PFTIR Siting Configuration**

The PFTIR telescope was sited about 115 meters and 5-10 degrees above horizon for the flare and 115 meters at 0-3 degrees below horizon for the calibration cells. Figure 3.2-1 illustrates a plot plan of the site with the location of the PFTIR telescope, the flare, and the tent housing the black body source, cold source, and the hot cell calibration equipment. Also identified is the position of the video equipment used during the tests (e.g. visible video and GasFindIR video camera positions).

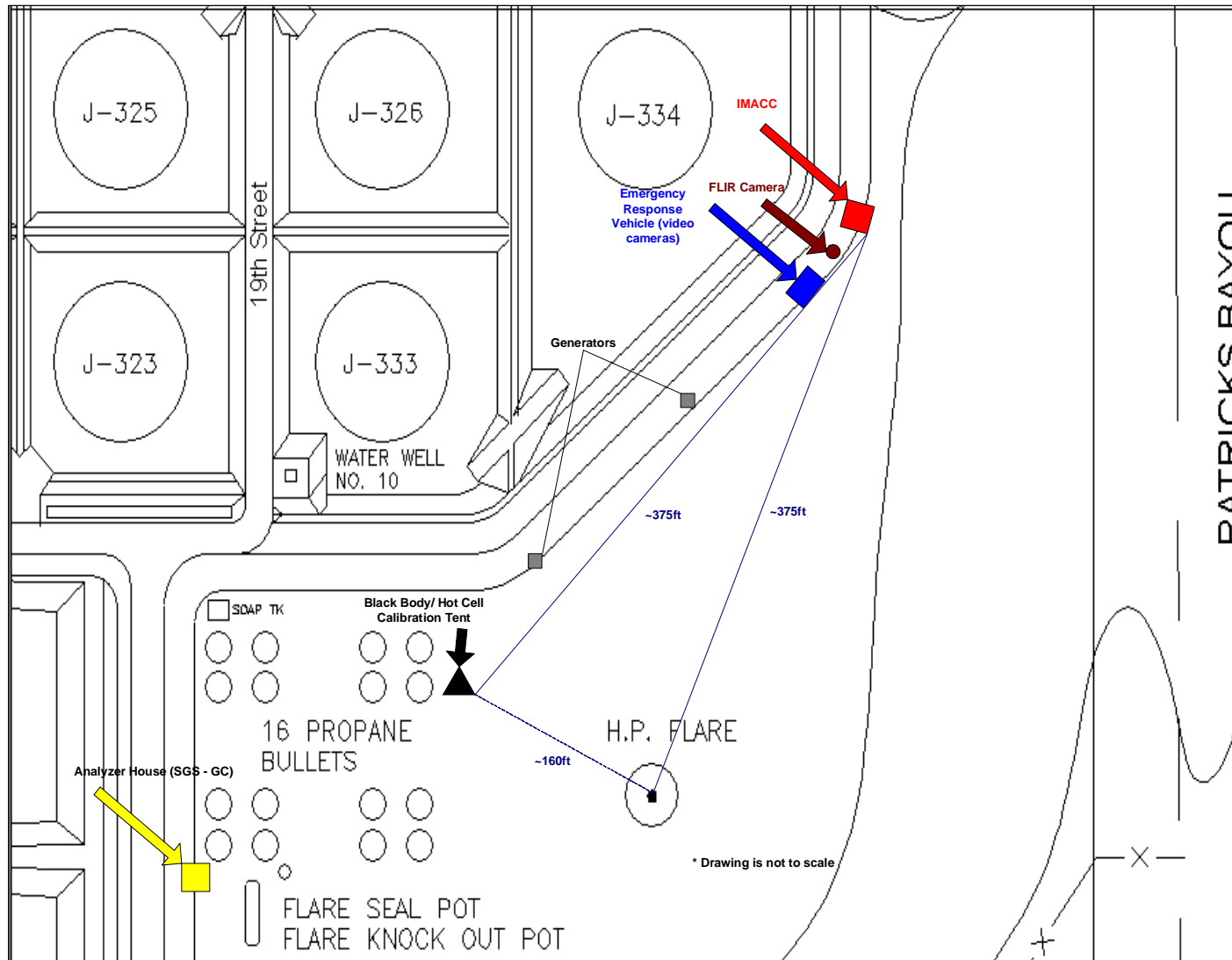


Figure 3.2-1. Plot Plan of East Property Flare and PFTIR Test Equipment

### **3.3 PFTIR Operation**

The PFTIR instrument was located at about 115 meters from the flare. It was housed in and operated from a trailer.

The equipment was calibrated twice a day. Calibration was completed in the morning prior to commencement of testing and again at the end of the day after testing was completed to validate the data collected that particular day. The calibrations were implemented in the quantitative analysis routines immediately prior to when field sample spectra were recorded.

The calibration of this equipment required three different calibration sources: a cold source, IR source and a black body source. Calibration sources were located under a tent on the ground adjacent to the base of the flare. The location was chosen so the distance between the PFTIR and the calibration equipment was approximately the same as the ground distance between the PFTIR and the flare.

After calibration was completed, the equipment was ready to start testing. A sky background was taken to be used in later analysis to subtract background radiance. A new sky background was taken as sky conditions changed during the testing. In PFTIR testing, it is important to adjust collected spectra with representative sky backgrounds. The calibration log for these tests is included in Appendix 5.4.

For collection of spectral data from the hot gas plume of the flare, the field of view of the PFTIR telescope was aimed at a position approximately one flame length from the tip of the visible flame. This was deemed to be a point sufficiently away from the active flame for combustion reactions to have been completed and to avoid the high heat signature of the flare, which would complicate data reduction.

### **3.4 PFTIR Data Reduction**

The raw PFTIR data must be processed to obtain the individual flare plume component concentrations. Dr. Curtis Laush from IMACC processed data and compiled it at approximately two minute intervals. IMACC took a spectral scan every second and recorded scans which met spectral QA/QC criteria. When 82 valid scans were recorded these scans were averaged. Constituents in the hot flare plume were determined by a Classical Least Squares curve fitting of the averaged spectral data.

The total radiance measured by the PFTIR is comprised of four components as shown in Figure 3.4-1. The four components are: (1) the background radiance altered by its transmission through the flare plume and the atmosphere, (2) the flare radiance altered by its transmission through the atmosphere, (3) the atmosphere radiance of the air, and (4) the radiance from the PFTIR instrument itself.

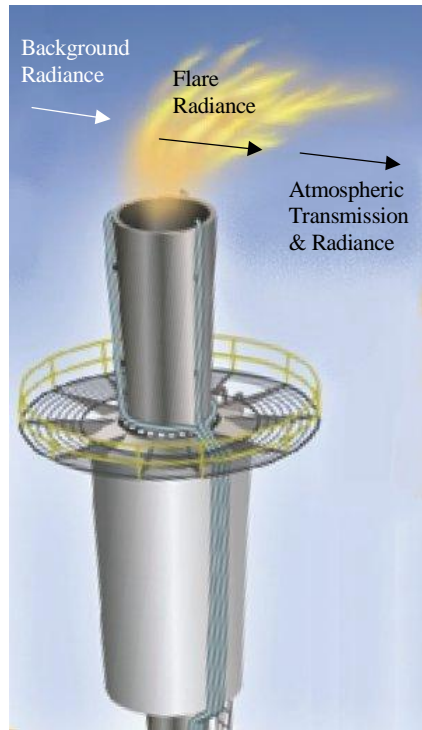


Figure 3.4-1 Contributions to the measured flare radiance

The total radiant signal received can be represented by:

$$N_{total} = N_{bkg} * \tau_{flr} * \tau_{atm} + N_{flr} * \tau_{atm} + N_{atm} + N_f \quad \text{Equation 1}$$

Where

- $N_{total}$  = total radiance
- $N_{bkg}$  = background sky radiance
- $\tau_{flr}$  = flare transmissivity
- $\tau_{atm}$  = atmospheric transmissivity
- $N_{flr}$  = flare radiance
- $N_{atm}$  = atmospheric radiance
- $N_f$  = radiance of the FTIR instrument itself

The data analysis procedure is comprised of four steps. First, the raw interferogram is converted to a single-beam spectrum using a Fourier Transform process. Second, the flare transmissivity is isolated from the other interferences as listed above. Third, the isolated flare transmissivity spectrum is converted to an absorbance spectrum so it can be further analyzed with standard spectroscopic techniques. Finally, the concentrations of individual components of the flare plume are determined from the absorbance spectrum.

Each of these steps are described briefly below:

*Step 1 – Convert the raw interferogram to a radiance spectrum*

The raw data from the PFTIR are in the form of an interferogram which is radiance as a function of FTIR scan position. The Fourier Transform (FT) process converts this data into a radiance spectrum, which is radiance as a function of wavelength or, in this case, wavenumber. The result is what is referred to as a “single beam” radiance spectrum. The FT process is a standard spectroscopic procedure and is not discussed in detail in this report.

*Step 2 – Isolate the flare transmission spectrum*

Once the radiance spectrum has been generated, the flare transmission must be isolated from all the interferants that the PFTIR also “sees.” In order to accomplish this, each term in Equation 1 above must be determined. This is done as follows:

*Background radiance (N<sub>bkg</sub>)* – At least once each day, the PFTIR was aimed at an unobstructed part of the sky. Since the background radiance is affected by conditions such as sun position and cloud cover, this procedure was repeated whenever a significant change in background was observed.

*Flare transmissivity (τ<sub>flr</sub>)* – This is the value sought and is the result when all competing factors are removed. This value appears two places: 1) in transmitting the sky background through the flare to the PFTIR and 2) in the radiance term for the flare itself. Therefore, the flare transmission must be extracted from the complex mixture of signals received by the PFTIR. This task is accomplished by the IMACC software.

*Atmospheric transmissivity (τ<sub>atm</sub>)* – This value is determined by aiming the PFTIR at an IR source and taking the ratio of the value obtained (minus the atmospheric radiance) to a “synthetic background” spectrum. This synthetic background (referred to as I<sub>0</sub>) represents the shape of the radiance spectrum that would be generated by the PFTIR in the absence of all gases. For this project the IR source was a SiC source operated at a temperature of 1250 K. This is a standard source used in most active FTIR systems. This source has sufficient signal throughout the infrared to allow for a transmission spectrum to be determined over the range of wavenumbers needed.

*Flare plume radiance (N<sub>flr</sub>)* – Plume radiance is (1 – plume transmission) times the Planck function (evaluated at the temperature of the plume). The radiance is what is measured by the PFTIR, but it is mixed in with other signals and so must be corrected with respect to this interference.

*Atmospheric radiance (N<sub>atm</sub>)* – This value is determined by aiming the PFTIR at a very cold source in the calibration telescope located at the same distance from the PFTIR as the flare. Any radiance observed will then be due to the intervening atmosphere plus any radiance from the PFTIR instrument itself. This measured value is referred to as M<sub>n</sub>. For this project, the cold source was an aluminum bar immersed in liquid nitrogen.

*PFTIR radiance (N<sub>f</sub>)* – PFTIR radiance is the emissions of the instrument itself. It is measured together with atmospheric radiance and is part of the M<sub>n</sub> measurement.

Once these values are known, they are applied to the total radiance spectrum by IMACC proprietary software to isolate the flare transmission spectrum.

*Step 3 – Convert the transmission spectrum to an absorption spectrum*

Once the flare transmission spectrum has been isolated, it must be converted to an absorbance spectrum so that standard spectroscopic techniques can be used for further analysis. Transmission and absorbance are related by the Beer-Lambert law through the following equation.

$$\tau_{\text{plume}} = e^{-K(\nu) \cdot c \cdot l} \quad \text{Equation 2}$$

Essentially, absorbance is the negative log of transmission, thus:

$$\text{Absorbance}(\nu) = (0.434)K(\nu) * c * l \quad \text{Equation 3}$$

This conversion is a standard spectroscopic procedure.

*Step 4 – Determine the concentrations of individual components in the flare plume*

Once the absorbance spectrum has been generated, there are several analytical techniques that may be used to estimate individual component concentrations. For this project, a modified Classical Least Squares (CLS) analysis was used. IMACC proprietary software was used for this step of the data analysis. The modifications to standard CLS include algorithms for linearizing the absorbance for each analyte with concentration, corrections for spectral baseline shifts, corrections for any spectral line shifts observed, and algorithms for dynamic reference spectra selection based upon observed concentrations of each compound.

The CLS technique compares measured spectra to reference spectra of known concentration and interfering compounds and matches the absorbance of the data and the references to determine gas concentration. This process is performed for all components present to account for all spectral features present.

After fitting, CLS also determines the difference or residual between the measured and scaled references. The fitting process minimizes the residuals in each analysis region. The software used for this project uses dynamic reference selection to select reference spectra based upon measured gas concentrations. In most cases, this means different reference spectra will be chosen for each analyte in the measured spectrum. This process will be repeated up to four times to optimize all spectra compared to the measured data.

A flow chart of the PFTIR data analysis process is shown in Figure 3.4-2.

### PFTIR Data Analysis Progression

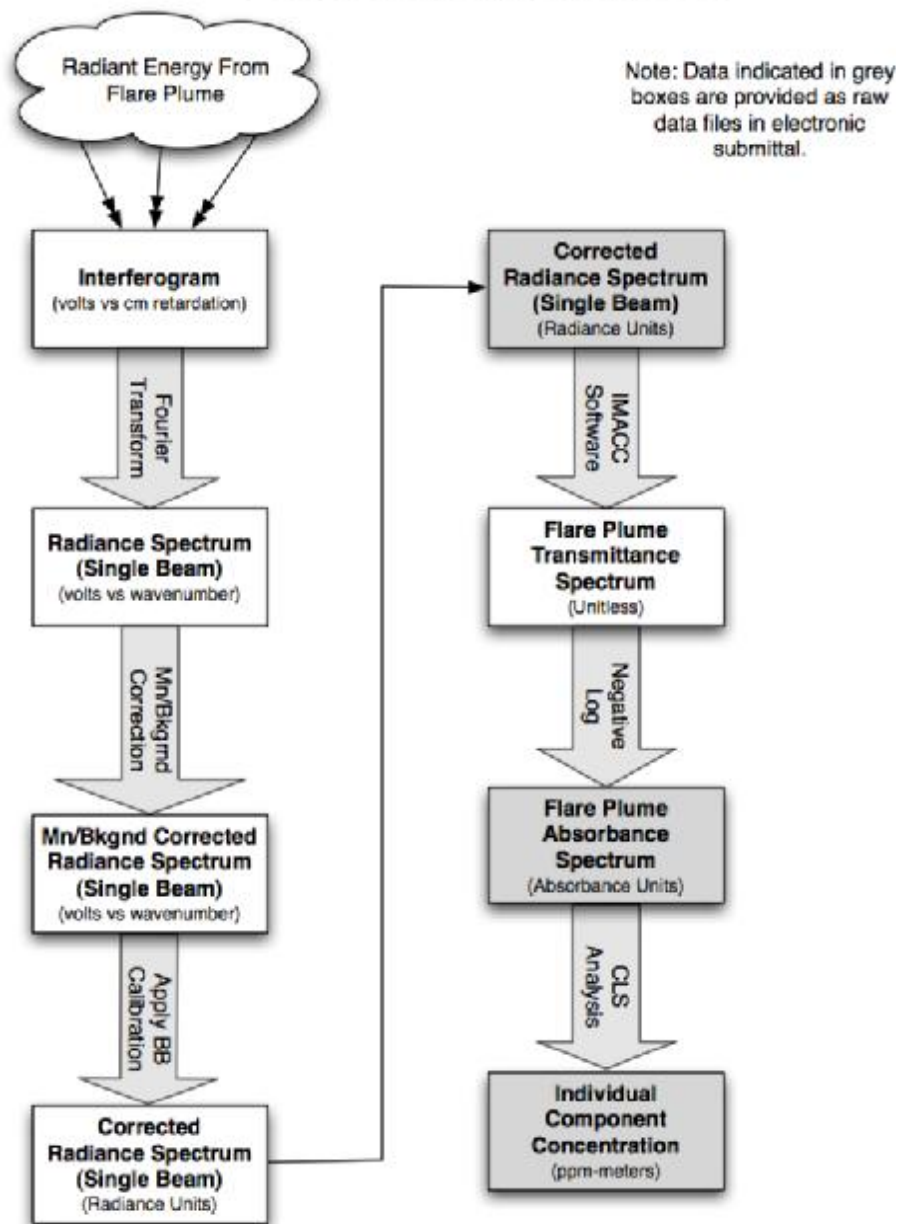


Figure 3.4-2 PFTIR Data Analysis Progression

## **4. Data Tables and Files**

### **4.1 Data Tables**

The test data are provided electronically in the Master Data Workbook. See Appendix 5.5. The test data consists of one minute plant data from the SDP Distributed Control System: vent and steam flow data, vent gas online GC data, and online BTEX data. SDP imported the IMACC PFTIR data from the flare hot gas plume into the plant data spreadsheet for analysis. Each test run is identified in the data file by the EPA test ID number and is color coded to facilitate location of individual test runs.

### **4.2 Visible Video Files**

All of the tests were recorded with a video camera. These electronic data files are attached as Appendix 5.6. The video data files were not cataloged by Run ID, but rather were collected and labeled by date and time stamp. Therefore, the date, start, and stop times from the test data tables must be used to access the appropriate video file.

### **4.3 GasFindIR Video Files**

All the tests were also recorded using a FLIR GasFindIR Model 25147-200 IR video camera. This camera captures both a thermal image of the flare and, further afield of the flame, a visible image of unburned hydrocarbon escaping the flame. These electronic data files are attached as Appendix 5.7. These files were also cataloged by date and time stamp in a similar fashion as the visible video files.

**5. Appendices**

**5.1 PFTIR Test Protocol (IMACC)**

**5.2 Weather Data**

**5.3 Summa Canister Sample Results**

**5.4 PFTIR Calibration Log**

**5.5 Master Data Workbook**

**5.6 Flare Testing Video Files**

**5.7 Flare Testing GasFindIR Video Files**